Westinghouse Non-Proprietary Class 3

WCAP-16996-NP
Revision 0

November 2010

Realistic LOCA Evaluation Methodology Applied to the Full Spectrum of Break Sizes (FULL SPECTRUM LOCA Methodology)

Volume II, Part 1
WCOBRA/TRAC-TF2 Assessment

Westinghouse

WCAP-16996-NP
Revision 0

Realistic LOCA Evaluation Methodology Applied to the Full Spectrum of Break Sizes (FULL SPECTRUM LOCA Methodology)

Author's Name	Author's Department
Dr. Cesare Frepoli*	LOCA Integrated Services
Dr. Katsuhiro Ohkawa*	LOCA Integrated Services
Dr. Liping Cao*	LOCA Integrated Services
Aaron M. Everhard*	LOCA Integrated Services
Jeffrey R. Kobelak*	LOCA Integrated Services
Dr. Jun Liao*	LOCA Integrated Services
Nikolay P. Petkov*	LOCA Integrated Services
Michael A. Shockling*	LOCA Integrated Services

November 2010

Reviewer: Mitchell E. Nissley*
Safety Analysis and Licensing

Approved: Amy J. Colussy*, Manager
LOCA Integrated Services

*Electronically approved records are authenticated in the electronic document management system.

Westinghouse Electric Company LLC
1000 Westinghouse Drive
Cranberry Township, PA 16066, USA

ACKNOWLEDGMENTS

The development of the FULL SPECTRUM™ LOCA methodology and this report has been a true team effort.

The principal contributors throughout the project were, in alphabetical order: John Besspiata, Dr. Liping Cao, Aaron Everhard, Randy Fittante, Dr. Cesare Frepoli, Robert Kemper, Jeff Kobelak, Dr. Vefa Kucukboyaci, Dr. Jun Liao, Mitch Nissley, Nikolay Petkov, Dr. Katsuhiro Ohkawa and Mike Shockling.

The development of this product span over a period of several years and individuals outside Westinghouse organization also contributed at various stages. Preliminary functional requirements benefited from the external reviewer of experts in the field such as Prof. Larry Hochreiter from the Penn State University and Dr. Tom Larson from the Idaho National Laboratory (INL). Marv Thurgood supported code activities as consultant while Prof. Satish Iyengar from the University of Pittsburgh was instrumental during the development of the statistical procedures utilized in the uncertainty methodology.

Carly Belovesick supported the first part of the development program as project manager and DFSS tools were implemented during the definition of the functional requirements by Dr. Luca Oriani as part of his CFL training.

Erin McGrew managed the second half of the project and led the completion of this report. Her project management skills were essential to the developers' team to navigate during the challenging phase of product integration and documentation and to ensure that a final quality product could be submitted for NRC review and approval on an expedited schedule.

The report benefited from the expertise of the Design Review Team which included Lou Grobmyer, Brian Ising, John Blaisdell, Naugab Lee, Andy Gagnon, Josh Hartz, Rich Schoff, Mike Young, Dr. Bob Perdue, Ray Tajc, Jason Eisenhauer, Yixing Sung, Bill Slagle and Dick Morrison. Ken Frederick from FENOC and Lou Cartin from SCE&G were also part of the Design Review Team. Moreover the support provided by Ken and Lou and their organizations represent the true motivation and driver behind this effort.

An extensive consistency review of the three volumes that comprises this topical report was performed by Meghan Leslie, therefore ensuring the various sections have been properly integrated from a technical standpoint.

Additional support provided by Doug Atkins, Fatih Aydogan, Kevin Barber, Hugo DaSilva, Dave DiBasilio, Ruben Espinosa, Dan Golden, Brian Ising, Molly McKain, Prudence Moon, Ajal Parikh and Bradley Slezak are also acknowledged.

Preparation of this report placed stringent demands on Technical and Online Publishing Services, particularly Jamie Hart and Carla Hamilton. The support of Dave Scherf for technical help for the preparation of this report and all the associated supporting documentation and calculation notes is deeply appreciated.

Finally, the authors would like to acknowledge the overall support provided by the Westinghouse organization management in general, particularly the LOCA Integrated Services groups which during the duration of the development program was led by Mike Corletti, then Cathy Sherbine and Amy Colussy (for LIS-I) and Chuck Boyd (for LIS-II).

TABLE OF CONTENTS

TABLE OF CONTENTS (cont.)

TABLE OF CONTENTS (cont.)

TABLE OF CONTENTS (cont.)

TABLE OF CONTENTS (cont.)

TABLE OF CONTENTS (cont.)

TABLE OF CONTENTS (cont.)

VOLUME 2

TABLE OF CONTENTS (cont.)

TABLE OF CONTENTS (cont.)

TABLE OF CONTENTS (cont.)

TABLE OF CONTENTS (cont.)

TABLE OF CONTENTS (cont.)

TABLE OF CONTENTS (cont.)

TABLE OF CONTENTS (cont.)

TABLE OF CONTENTS (cont.)

TABLE OF CONTENTS (cont.)

TABLE OF CONTENTS (cont.)

TABLE OF CONTENTS (cont.)

LIST OF TABLES

VOLUME 1

LIST OF TABLES (cont.)

LIST OF TABLES (cont.)

VOLUME 2

LIST OF TABLES (cont.)

LIST OF TABLES (cont.)

LIST OF TABLES (cont.)

LIST OF TABLES (cont.)

LIST OF TABLES (cont.)

LIST OF TABLES (cont.)

LIST OF TABLES (cont.)

LIST OF FIGURES

VOLUME 1

LIST OF FIGURES (cont.)

LIST OF FIGURES (cont.)

LIST OF FIGURES (cont.)

LIST OF FIGURES (cont.)

LIST OF FIGURES (cont.)

LIST OF FIGURES (cont.)

LIST OF FIGURES (cont.)

LIST OF FIGURES (cont.)

LIST OF FIGURES (cont.)

LIST OF FIGURES (cont.)

LIST OF FIGURES (cont.)

LIST OF FIGURES (cont.)

LIST OF FIGURES (cont.)

LIST OF FIGURES (cont.)

LIST OF FIGURES (cont.)

LIST OF FIGURES (cont.)

LIST OF FIGURES (cont.)

LIST OF FIGURES (cont.)

LIST OF FIGURES (cont.)

LIST OF FIGURES (cont.)

LIST OF FIGURES (cont.)

LIST OF FIGURES (cont.)

LIST OF FIGURES (cont.)

LIST OF FIGURES (cont.)

LIST OF FIGURES (cont.)

LIST OF FIGURES (cont.)

LIST OF FIGURES (cont.)

LIST OF FIGURES (cont.)

LIST OF FIGURES (cont.)

LIST OF FIGURES (cont.)

LIST OF FIGURES (cont.)

LIST OF FIGURES (cont.)

LIST OF FIGURES (cont.)

LIST OF FIGURES (cont.)

LIST OF FIGURES (cont.)

LIST OF FIGURES (cont.)

LIST OF FIGURES (cont.)

LIST OF FIGURES (cont.)

LIST OF FIGURES (cont.)

LIST OF FIGURES (cont.)

LIST OF FIGURES (cont.)

LIST OF FIGURES (cont.)

LIST OF FIGURES (cont.)

LIST OF FIGURES (cont.)

LIST OF FIGURES (cont.)

LIST OF FIGURES (cont.)

LIST OF FIGURES (cont.)

LIST OF FIGURES (cont.)

LIST OF FIGURES (cont.)

LIST OF FIGURES (cont.)

LIST OF FIGURES (cont.)

LIST OF FIGURES (cont.)

LIST OF FIGURES (cont.)

LIST OF FIGURES (cont.)

LIST OF FIGURES (cont.)

LIST OF FIGURES (cont.)

LIST OF FIGURES (cont.)

LIST OF FIGURES (cont.)

LIST OF FIGURES (cont.)

LIST OF FIGURES (cont.)

LIST OF FIGURES (cont.)

LIST OF FIGURES (cont.)

LIST OF FIGURES (cont.)

LIST OF FIGURES (cont.)

LIST OF FIGURES (cont.)

LIST OF FIGURES (cont.)

LIST OF FIGURES (cont.)

LIST OF FIGURES (cont.)

LIST OF FIGURES (cont.)

LIST OF FIGURES (cont.)

LIST OF FIGURES (cont.)

LIST OF FIGURES (cont.)

LIST OF FIGURES (cont.)

LIST OF FIGURES (cont.)

LIST OF FIGURES (cont.)

LIST OF FIGURES (cont.)

LIST OF FIGURES (cont.)

LIST OF FIGURES (cont.)

LIST OF FIGURES (cont.)

LIST OF FIGURES (cont.)

LIST OF FIGURES (cont.)

LIST OF FIGURES (cont.)

LIST OF FIGURES (cont.)

LIST OF FIGURES (cont.)

LIST OF FIGURES (cont.)

LIST OF FIGURES (cont.)

LIST OF FIGURES (cont.)

LIST OF FIGURES (cont.)

LIST OF FIGURES (cont.)

LIST OF FIGURES (cont.)

LIST OF FIGURES (cont.)

LIST OF FIGURES (cont.)

LIST OF FIGURES (cont.)

LIST OF FIGURES (cont.)

LIST OF FIGURES (cont.)

LIST OF FIGURES (cont.)

LIST OF FIGURES (cont.)

LIST OF FIGURES (cont.)

LIST OF FIGURES (cont.)

LIST OF FIGURES (cont.)

LIST OF FIGURES (cont.)

LIST OF FIGURES (cont.)

LIST OF FIGURES (cont.)

LIST OF FIGURES (cont.)

LIST OF FIGURES (cont.)

LIST OF FIGURES (cont.)

LIST OF FIGURES (cont.)

LIST OF FIGURES (cont.)

LIST OF FIGURES (cont.)

LIST OF FIGURES (cont.)

LIST OF FIGURES (cont.)

LIST OF FIGURES (cont.)

LIST OF FIGURES (cont.)

LIST OF FIGURES (cont.)

LIST OF FIGURES (cont.)

EXECUTIVE SUMMARY

Westinghouse's previously approved best-estimate Large Break loss-of-coolant accident (LBLOCA) methodology (or Evaluation Model (EM)) is described in WCAP-16009-P-A (Nissley et al., 2005). The methodology is referred to as the Automated Statistical Treatment of Uncertainty Method (ASTRUM) and is applicable to Westinghouse designed 3- and 4-loop plants with emergency core cooling system (ECCS) injection into the cold legs, Westinghouse designed 2-loop plants with upper plenum injection (UPI) and Combustion Engineering designs. The ASTRUM EM is based on the use of WCOBRA/TRAC as the system code. The ASTRUM EM was also submitted as part of the AP1000™[1] Design Control Document (APP-GW-GL-700, Rev. 17).

The ASTRUM EM addressed Large Break LOCA scenarios with a minimum size of 1.0 ft^2. In this report the applicability of the Westinghouse best-estimate LOCA EM was extended to consider smaller break size, therefore including what traditionally are defined as Small and Intermediate Break LOCA scenarios. The new realistic LOCA EM is called FULL SPECTRUM™[1] LOCA (FSLOCA™[1]) methodology. The term 'Full Spectrum' specifies that the new EM is intended to resolve the full spectrum of LOCA scenarios which result from a postulated break in the cold leg of a PWR (While this EM is also applicable for analysis of breaks at other loop locations, such as the hot leg, these breaks are not limiting compared with the cold leg break). The break sizes considered in the Westinghouse FULL SPECTRUM LOCA include any break size in which break flow is beyond the capacity of the normal charging pumps, up to and including a double ended guillotine (DEG) rupture with a break flow area equal to two times the pipe area.

As in previous EMs, the FULL SPECTRUM LOCA methodology was patterned after the Code Scaling, Applicability, and Uncertainty (CSAU) methodology developed under the guidance of the U.S. Nuclear Regulatory Commission (NRC) (Boyack et al., 1989). The development roadmap is consistent with Regulatory Guide 1.203.

For the FULL SPECTRUM LOCA methodology WCOBRA/TRAC was modified by replacing the 1D Module (based on TRAC-PD2) with the TRAC-PF1/MOD2 code and adding a few improvements to the 3D module (based on Westinghouse modified COBRA-TF). One of the major changes is the addition of an explicit non-condensable gas transport equation within the 3D module. The replacement of TRAC-PD2 with TRAC-PF1/MOD2 allows the extension of a two-fluid, six-equation formulation of the two-phase flow to the 1D loop components. This new code has been named WCOBRA/TRAC-TF2 where "TF2" is an identifier that reflects the use of a three-field (TF) formulation of the 3D module derived by COBRA-TF and a two-fluid (TF) formulation of the 1D module based on TRAC-PF1/MOD2.

With the exception of the additional tracking of a non-condensable gas field, and few minor upgrades needed to address Small Break LOCA scenarios, the Vessel model is equivalent to the Vessel model of the approved version of WCOBRA/TRAC. Requests for additional information (RAIs) identified during the early review of the code that led to the approval of the original CQD (Bajorek et al., 1998) and

1. FULL SPECTRUM™, FSLOCA™, AP1000™, and ZIRLO™ are trademarks or registered trademarks in the United States of Westinghouse Electric Company LLC, its subsidiaries and/or its affiliates. These marks may be used and/or registered in other countries throughout the world. All rights reserved. Unauthorized use is strictly prohibited. Other names may be trademarks of their respective owners.

subsequent ASTRUM EM (Nissley et al., 2005), and associated responses should still be applicable. In a few instances, as in the downcomer region, a more refined noding scheme has been adopted to improve accuracy or provide more consistency across the various test facilities. Such noding choices have been justified by assessing the model against large and full scale experiments.

The FULL SPECTRUM LOCA EM is intended to be applicable to all PWR fuel designs with Zirconium alloy cladding. Most of the data considered in the methodology is based on Zircaloy-4 and ZIRLO™[1]. [

]^{a,c}

The uncertainty methodology is based on a direct Monte Carlo sampling of the uncertainty attributes. The overall uncertainty is bounded using a non-parametric statistical method similar to the ASTRUM EM. However, sample size is increased to reduce the variability of the estimator. The break size spectrum is divided in two regions. Region-I provides coverage of what typically are defined as Small Break LOCA scenarios and stretch into Intermediate Break LOCA. Region-II starts from Intermediate Break size and include what typically are defined Large Break LOCA scenarios. A 95/95 joint-probability statement is developed for the key parameters that are needed to demonstrate compliance with 10 CFR 50.46 acceptance criteria.

The code models, their assessment, and conclusions on model biases and uncertainties are aimed to be generic and applicable to the same class of plants covered by the ASTRUM EM. When modeling aspects are specific to a particular PWR design, the choice was made to focus attention on the Westinghouse 3-loop PWR with cold leg ECCS injection. Therefore, the demonstration plant analysis is limited to such a design.

1. FULL SPECTRUM™, FSLOCA™, AP1000™, and ZIRLO™ are trademarks or registered trademarks in the United States of Westinghouse Electric Company LLC, its subsidiaries and/or its affiliates. These marks may be used and/or registered in other countries throughout the world. All rights reserved. Unauthorized use is strictly prohibited. Other names may be trademarks of their respective owners.

12 ASSESSMENT OF BREAK FLOW MODEL

12.1 INTRODUCTION

During a LOCA, the break flow rate determines the depressurization rate as well as the mass inventory of the primary system of a PWR. These parameters in turn influence the timing of various engineered safeguard system responses, such as reactor trip and safety injection, and the degree of core uncovery which is the major parameter determining the subsequent heatup and clad temperature. Although the size, location, and shape of the break are not known for the postulated LOCA, the best-estimate code needs to predict consistent responses given the break size and location over a range of pressure, subcooling, and upstream fluid states expected in LOCA.

In this section, an assessment is made of the critical flow model in the WCOBRA/TRAC-TF2 version described in Section 5.12.2, Volume 1, of this document. This section presents the following assessment results.

12.1.1 Critical Flow in LOCA (Relation to LOCA PIRT)

A fluid system contained in a reactor vessel with a pipe break is in communication with the containment atmosphere, which is at a lower pressure through the break flow path. Under critical flow conditions, the discharge flow rate from the high pressure system becomes independent of the containment conditions, which are at the lower pressure.

Since the break flow rate determines the depressurization and inventory and mass distribution in the vessel, it is easy to justify a high ranking of this phenomenon as discussed in Section 2. For Small Break LOCA, because the Reactor Coolant System (RCS) pressure remains high enough to cause the break flow critical [

]a,c

Early in a LOCA, the fluid condition upstream of the break location is subcooled. This results in a high discharge flow rate and a fast depressurization. As the pressure drops to the saturation pressure corresponding to the coolant liquid temperature upstream of the break, the discharge becomes two-phase and a relatively low discharge rate and a slow depressurization result. As the system mass depletes and the flow in the main pipe stratifies, the break location begins to uncover. The break quality under the stratified upstream is determined by the offtake phenomena and is the subject of Section 12.7.

12.1.2 Assessment Objective

In this section, the break flow model in WCOBRA/TRAC-TF2 is assessed relative to the following effects on the break flow in addition to the accuracy relative to data:

- Break path length
- Break flow area variation
- Upstream pressure variation
- Variation in degree of subcooling during liquid discharge
- Upstream void fraction/quality variation
- Break entrance geometry
- Non-condensable gas concentration in the Vapor phase

The critical flow model's bias and uncertainty will be determined by comparing the critical flow model prediction implemented in WCOBRA/TRAC-TF2 with selected data from the qualified break flow dataset. A selection of the model assessment dataset is described in the subsequent section.

12.2 CRITICAL FLOW DATA NEEDS FOR PWR LOCA MODEL VALIDATION

The requirements of a critical flow data base which would be suitable for use in validating critical flow models for the range of conditions occurring during PWR LOCAs is discussed in this section. The range of geometrical, and physical conditions, and the criteria for defining the necessary quality of the data were discussed by Holmes and Allen (1998).

Holmes and Allen (1998) identified the range of parameters, both geometrical and physical, which would cover the perceived need for the analytical model validation used in LOCA analyses as shown in Tables 12.2-1 through 12.2-3.

In LOCA scenarios, the worst break is postulated to occur in the cold leg of the primary coolant system. For bounding purposes, the size of the break is assumed to be as large as the full cross section of the primary loop pipes, and as small as the break size of ~0.5in^2 below which the coolant makeup system is able to maintain the reactor coolant inventory by matching the injection to the leak rate from the break. Thus the scale requirement for the critical flow data for the purpose of PWR LOCA analyses is 0.5 in^2 to ~4.15 ft^2. The data requirement for the break upstream fluid conditions may be determined by examining LOCA experiment measurements/analyses and PWR LOCA simulations. Figures 12.2-1 and 12.2-2 show respectively the predicted temperature-pressure and the quality-pressure trajectories for LBLOCA transients and a 5% small break tests. The blue line shows the predicted trajectory for the largest Double Ended Guillotine Break in a typical 3 loop PWR. The green line shows the predicted trajectory for the smallest (~1ft^2 break area) LBLOCA of a 3 loop PWR which could be considered an largest Intermediate Break (IB) LOCA. The red line shows the predicted trajectory of SB-CL-05, a 5% cold leg break simulation performed at ROSA facility. Trajectory for IB and LB LOCA shows a rapid depressurization to saturation from the operating condition to saturation at around 1000~1200 psia where the initially subcooled liquid reaches saturation and the upstream of the break turns two-phase. The predicted SB-CL-05 small break trajectory reaches saturation at around 1200 psia and transitions from all liquid to all vapor due to loop-seal clearing. The upstream quality remains at or near 1.0 until accumulator injection at around 600 psia at which time the break becomes subcritical. The desired critical flow data should cover the range of fluid condition indicated in these figures.

Table 12.2-1 Range of Geometrical Configurations[1]	
Component	**Ranges**
Straight Pipe	Diameter ≤ 0.7 m, 1 ≤ L/D ≤ 10 (This range of L/D is for large break LOCAs in PWRs, i.e., e. pipe length of 0.5 m-7 m, small break LOCAs will require a correspondingly wider range of L/D)
Elbows	45°-90°, diameter ≤ 0.7 m, 1 ≤ r/d ≤ 4
Tees	Angle of offtake 45°-90°, diameter ≤ 0.7 m, 0.3 ≤ L/D ≤ 10, round/square entry
Pumps	Pump Specific Geometry
Valves	All valve data
Orifices, flow meters, etc.	Where available

Note:
1. Holmes and Allen, 1998.

Table 12.2-2 Break Configuration[1]	
Break Configuration	**Ranges**
Guillotine Breaks	Varying degree of off-set
Holes	10^{-4} m^2 ≤ Break Area ≤ 0.1 m^2
Splits	Horizontal/Circumferential, ~10^{-4} m^2 ≤ Break Area ≤ 1.0 m^2
Reactor Coolant Pump seal Geometry	Pump design specific

Note:
1. Holmes and Allen, 1998.

Table 12.2-3 Range of Physical Conditions Upstream of Discharge[1]		
Pressure (MPa)	**Temperature**	**Flow Condition**
0.1 – 20	~ Saturation	Single-phase steam/two-phase
0.1 – 15	≤ 200K subcooled/saturation	Single-phase liquid/two-phase
-	-	Single-phase vapor/two-phase with Non-condensable gas

Note:
1. Holmes and Allen, 1998.

a,c

Figure 12.2-1 Upstream P-T in Small and Large Break LOCAs

a,c

Figure 12.2-2 Upstream Quality in Small and Large Break LOCAs

12.3 ASSESSMENT TEST MATRIX AND BASIS FOR SELECTION

The critical flow dataset compiled by V. Illic (1986) was further examined for the purpose of the critical flow model validation and the bias/uncertainty evaluation in a similar screening discussed in Elias and Lellouche (1994), and Holmes and Allen (1998). Data without well defined or stagnation condition or upstream condition were excluded for assessment. Dataset generated by Cruver (1963), Fauske (1962), Henry (1990), Isbin (1957) and Zaloudek (1964) do not report stagnation pressure. Dataset generated by Guizovarn (1975) contains superheated liquid upstream of the nozzle, which is contrary to the description in V. Illic (1986) which states subcooled inlet condition. Dataset generated by Bryers and Hsieh (1966) contains highly subcooled stagnation condition contrary to the description. The dataset generated by Ogasawara (1969) did not contain the reservoir temperature or the quality. Datasets generated by Danforth (1941) and Schrock (1977) are suspect with regard to achieving the critical condition according to Illic. Dataset generated by Morrison (1977) appears to be inconsistent with other similar data.

The dataset mentioned above need to be further investigated for the use in the model bias and uncertainty study since as-reported upstream condition is suspect. These subsections were discarded in much the same reasons as the previous work (pp. 117, Elias and Lellouche, 1994). The database was further expanded by including four additional sources. Marviken (1982) test data were added since this set is the only critical flow data for diameters above 200 mm and can be considered a full scale. While this is a transient experiment, necessary upstream conditions were reported at 1 second interval which could be used to define the inlet condition. The offtake dataset taken at TPFL (Anderson and Benedetti, 1986) was added which contains fluid condition measurements upstream of the break nozzle where the flow was critical. Amos and Schrock's (1983) data covers the pressure and subcooling range comparable to the PWR's operating condition. Celata's (1988) subcooled data were included for the subsequent validation of the non-condensable gas capability. Table 12.4-1 is a summary of all selected datasets for this assessment. The subsection number in the table was assigned prior to the selection process. This is the reason why the dataset number seen in the table is not contiguous. The dataset represents 3199 points from 53 geometries containing data from 13 to 2500 psia. The geometry ranges from $0 < L < 2300$ mm, $0.464 \text{ mm} < D_H < 500$ mm.

Additionally, Celata's non-condensable gas data was selected for the validation of non-condensable gas effects as seen in Table 12.4-3.

Table 12.4-3, is the complete list of database in the assessment test matrix used to evaluate the accuracy of the WCOBRA-TRAC-TF2 break flow model; it describes in detail all 53 nozzle geometries and orientations. Comment section describes Diameter, D, as a function of axial distance, z.

Table 12.4-1 Selected Dataset and Input Variables					
Reference	**Pressure (psia)**	**Upstream Condition**	**No. of Data Points**	**Length (mm)**	**Dhyd (mm)**
Ardron (1978)	22-55	Subcooled	32	1015	26.3
Boivin (1979)	200-1500	Subcooled	21	500-1830	12-50
Fincke (1981)	13-45	Subcooled	92	79.72	18.28
Jeandey (1981)	100-2100	Subcooled	88	463	20.13
Neusen (1962)	100-600	Saturated to X=0.23	37	Orifice (1 mm)	6.4-11.125
Reocreux (1974)	30-50	Subcooled	28	2335	20
Seynhaeve (1980)	40-150	Subcooled	57	221-306	12.5
Sozzi & Sutherland(1975)	400-1100	Subcool and Saturated	667	4.7-1822.5	12.7
Amos (1983)	500-2300	Subcooled	44	63.5	0.464, 0.748
Anderson (1985)	500-900	Saturated Liquid up to Saturated Vapor	109	54	16.2
Marviken (1982)	400-750	Subcooled and Saturated	1927	166-1809	200-509
Celata (1988)	72-218	Subcooled to Saturated,	97	1500	4.6
	13-2300	Subcooled Liquid to Saturated Vapor	3199	0-2335	0.418-509

Table 12.4-2 Additional Dataset for Non-condensable Gas Model Validation and Input Variables					
Reference	**Pressure (psia)**	**Upstream Condition**	**No. of Data Points**	**Length (mm)**	**Dhyd (mm)**
Celata (1988)	72-218	Data-41 with Non-C (Volume %): 0-80.	96	1500	4.6

Table 12.4-3 Critical Flow Data Considered for Model Evaluation

Reference	L (mm)	D (mm)	cosθ	N-Data	Comments
Ardron, K. H. & Ackerman, M. C. (1978)	1015	26.3	0	33	One superheated upstream condition was not used
Boivin (1979)	500	12	0	10	D=50 (z<0); 0<z<50 rounded entrance; D=12 (50<z<500); D=12+19(z-500) (500<z<700); D=50 (z>700 mm)
Boivin (1979)	1600	30	0	5	D=150 (z<0); 0<z<130 rounded entrance; D=30 (130<z<1730); D=30+0.12(z-1730) (1730<z<2305); D=100 (z>2305 mm)
Boivin (1979)	1700	50	0	6	D=150 (z<0); 0<z<130 rounded entrance; D=50 (130<z<1830); D=50+0.12(z-1830) (1830<z<2240); D=100 (z>2240 mm)
Fincke & Collins (1981)	25	18.3	0	92	D=18.28 (54.7<z<79.7); D=18.28+0.12(z-79.7), (z<215.9 mm)
Jeandey et al. (1981)	463	20	1	15	D=66.7-0.54z (0<z<86.9); D=20.1 (z>86.9 mm)
Jeandey et al. (1981)	463	20	1	73	see Appendix C.7.1 for (z<100); D=20.13 (100<z<463); D=20.13+0.12(z-463) (z<900); D=737 (z>900 mm)
Neusen (1962)	0	11	0	25	D=11.12 mm at throat; D=11.12+0.425z (0<z<35.91 mm)
Neusen (1962)	0	6	0	12	D=16.4 mm at throat; D=6.4+0.425z (0<z<59.81 mm)
Reocreux (1974)	2335	20	1	28	D=20 (0<z<2335); D=20+0.12(z-2335) (z<2662 mm)
Seynhaeve (1980)	306	13	1	26	D=12.5 (0<z<306); D=12.5+0.245(z-306) (z>541); D=70 (z>541 mm)
Seynhaeve (1980)	306	13	1	31	D=12.5 (0<z<221); D=12.5+0.245(z-221) (z>541); D=70 (z>541 mm)
Sozzi & Sutherland (1975)	45	12.7	0	129	D=43.2 (z=0); rounded convergent (0<z<44.5); D=12.7+0.105(z-44.5) (z<158.5 mm) (Nozzle 1)
Sozzi & Sutherland (1975)	45	12.7	0	13	D=43.2 (z=0); rounded convergent (0<z<44.5 mm) (Nozzle 2)
Sozzi & Sutherland (1975)	57	12.7	0	47	D=43.2 (z=0); rounded convergent (0<z<44.5 mm) (Nozzle 2)
Sozzi & Sutherland (1975)	362	12.7	0	19	D=43.2 (z=0); rounded convergent (0<z<44.5 mm) (Nozzle 2)

Table 12.4-3 Critical Flow Data Considered for Model Evaluation (cont.)

Reference	L (mm)	D (mm)	cosθ	N-Data	Comments
Sozzi & Sutherland (1975)	83	12.7	0	17	D=43.2 (z=0); rounded convergent (0<z<44.5 mm) (Nozzle 2)
Sozzi & Sutherland (1975)	553	12.7	0	13	D=43.2 (z=0); rounded convergent (0<z<44.5 mm) (Nozzle 2)
Sozzi & Sutherland (1975)	108	12.7	0	23	D=43.2 (z=0); rounded convergent (0<z<44.5 mm) (Nozzle 2)
Sozzi & Sutherland (1975)	679	12.7	0	96	D=43.2 (z=0); rounded convergent (0<z<44.5 mm) (Nozzle 2)
Sozzi & Sutherland (1975)	159	12.7	0	15	D=43.2 (z=0); rounded convergent (0<z<44.5 mm) (Nozzle 2)
Sozzi & Sutherland (1975)	1823	12.7	0	81	D=43.2 (z=0); rounded convergent (0<z<44.5 mm) (Nozzle 2)
Sozzi & Sutherland (1975)	235	12.7	0	12	D=43.2 (z=0); rounded convergent (0<z<44.5 mm) (Nozzle 2)
Sozzi & Sutherland (1975)	273	12.7	0	22	D=43.2 (z=0); rounded convergent (0<z<44.5 mm) (Nozzle 2)
Sozzi & Sutherland (1975)	5	12.7	0	58	Nozzle No. 3 (Sharp entrance)
Sozzi & Sutherland (1975)	322	12.7	0	24	Nozzle No. 3 (Sharp entrance)
Sozzi & Sutherland (1975)	513	12.7	0	24	Nozzle No. 3 (Sharp entrance)
Sozzi & Sutherland (1975)	640	12.7	0	17	Nozzle No. 3 (Sharp entrance)
Sozzi & Sutherland (1975)	195	12.7	0	23	Nozzle No. 3 (Sharp entrance)
Sozzi & Sutherland (1975)	45	19	0	23	D=43.2 (z=0); rounded convergent (0<z<44.5 mm)
Sozzi & Sutherland (1975)	732	54	0	4	D=260-0.39(z-202) (202<z<732); D=54+0.263(z-732) (z<1112 mm)
Sozzi & Sutherland (1975)	696	76	0	3	D=260-0.39(z-223) (223<z<696); D=54+0.263(z-696) (z<1076 mm)
Sozzi & Sutherland (1975)	63	28	0	5	D=72.6 (z=0); rounded elliptical sec. (0<z<63.5); D=28+0.246(z-63.5) (z<228.5)
Amos & Schrock (1983)	63.5	0.747	-1	18	Rec. Slit 0.381x63.5 mm with known entrance losses

Table 12.4-3 Critical Flow Data Considered for Model Evaluation (cont.)

Reference	L (mm)	D (mm)	cosθ	N-Data	Comments
Amos & Schrock (1983)	63.5	0.418	-1	26	Rec. Slit 0.254x63.5 mm with known entrance losses
Anderson & Benedetti (1986)	31.9	16.2	0	109	Rounded entrance (at 500, 640 and 900 psia)
Marviken Test 1 (1982)	300	300	-1	97	Rounded entrance, Nozzle I, Type III
Marviken Test 2 (1982)	300	300	-1	91	Rounded entrance, Nozzle II, Type II Exp.
Marviken Test 3 (1982)	150	500	-1	40	Rounded entrance
Marviken Test 4 (1982)	150	500	-1	39	Rounded entrance
Marviken Test 5 (1982)	300	300	-1	43	Rounded entrance
Marviken Test 6 (1982)	300	300	-1	85	Rounded entrance
Marviken Test 7 (1982)	150	500	-1	84	Rounded entrance
Marviken Test 8 (1982)	150	500	-1	40	Rounded entrance
Marviken Test 9 (1982)	150	500	-1	58	Rounded entrance
Marviken Test 10 (1982)	150	500	-1	57	Rounded entrance
Marviken Test 11 (1982)	150	500	-1	41	Rounded entrance
Marviken Test 12 (1982)	150	500	-1	121	Rounded entrance
Marviken Test 13 (1982)	150	500	-1	139	Rounded entrance
Marviken Test 14 (1982)	150	500	-1	144	Rounded entrance
Marviken Test 15 (1982)	1809	500	-1	45	Rounded entrance
Marviken Test 16 (1982) 590200-1146	1809	500	-1	40	Rounded entrance
Marviken Test 17 (1982) 590200-1146	1110	300	-1	90	Rounded entrance
Marviken Test 18 (1982) 590200-1146	1110	300	-1	69	Rounded entrance
Marviken Test 19 (1982) 590200-1146	1110	300	-1	85	Rounded entrance
Marviken Test 20 (1982) 590200-1146	730	500	-1	50	Rounded entrance
Marviken Test 21 (1982) 590200-1146	730	500	-1	50	Rounded entrance
Marviken Test 22 (1982) 590200-1146	730	500	-1	37	Rounded entrance

Table 12.4-3 Critical Flow Data Considered for Model Evaluation (cont.)

Reference	L (mm)	D (mm)	cosθ	N-Data	Comments
Marviken Test 23 (1982)	166	500	-1	61	Rounded entrance
Marviken Test 24 (1982)	166	500	-1	44	Rounded entrance
Marviken Test 25 (1982) 590200-1146	510	300	-1	84	Rounded entrance
Marviken Test 26 (1982) 590200-1146	510	300	-1	134	Rounded entrance
Marviken Test 27 (1982) 590200-1146	730	500	-1	59	Rounded entrance
Celata (1988)	1500	4.6	-1	97	Entrance loss calibrated using one single-phase flow test.

12.4 DESCRIPTION OF DATASETS

The stagnation condition of each dataset such as Pressure/Temperature and Pressure/Quality are shown graphically in the following figures. The Pressure/Temperature trajectories of the primary system of LOFT 2.5% cold leg break and ROSA 5% cold break while the break is choked during small break LOCA experiments along with the saturation line are shown for comparison.

12.4.1 Ardron and Ackerman

Ardron and Ackerman conducted critical flow experiments by discharging subcooled water from a pressure vessel through a horizontal test section. The test section consisted of a straight cylindrical pipe 0.0263 m in diameter and 1.015 m long. Instrumentation included measurement of stagnation pressure and temperature with reported uncertainties of 7.0 kPa and 0.1°C, respectively, mass flux with uncertainty of 200 kg/m^2-s, and differential pressure measurements, the roughness of pipe was estimated to be 2.5E-06 m. As seen in Figures 12.4-1a and 12.4-1b, the range of stagnation pressure tested was from 150 to 370 kPa (21.8 to 53.7 psia) with subcooling from 0 to 7°C (quality of 0 to $-6x10^{-6}$). All tests were conducted with de-mineralized and degassed water.

a,c

Figure 12.4-1a Upstream P-T in Ardron-Ackerman

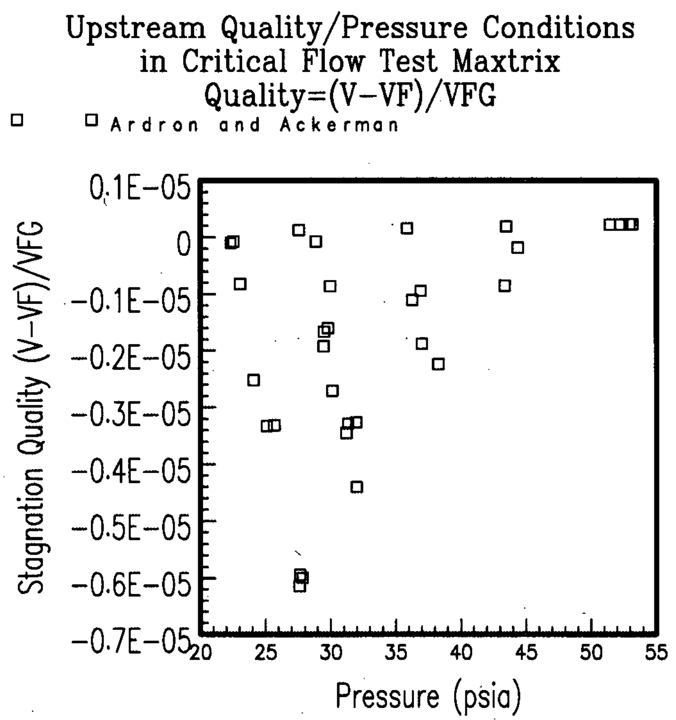

Figure 12.4-1b Upstream Quality in Ardron-Ackerman

12.4.2 Boivin

Boivin conducted critical flow experiments by discharging water through long, horizontal nozzles. Three nozzles were tested. Each nozzle had a rounded inlet, a long cylindrical smooth pipe, and a diffuser having a small expanding angle. In the three cases, the L/D ratio is greater than 30 to minimize 2D effects. The first nozzle had a pipe diameter of 0.012 m, 0.45 m long with a diffuser angle of 11 degrees. The second nozzle had a pipe diameter of 0.030 m, 1.6 m long with a 7 degree diffuser. The diameter of the third nozzle was 0.050 m, 1.7 m long with a diffuser of 7.7 degree.

Measurements reported include inlet (stagnation) pressure and temperature, mass flux, and throat pressure. No measurement uncertainties were reported. Stagnation pressure conditions ranged from 1960 to 10100 kPa (284.3 to 1464.9 psia) with inlet water somewhat subcooled.

The upstream conditions in Pressure/Temperature and Pressure/Quality planes, along with (P, T) trajectories observed in LOFT and ROSA small break tests, are shown in Figures 12.4-2a and 12.4-2b.

a,c

Figure 12.4-2a Upstream P-T in Boivin

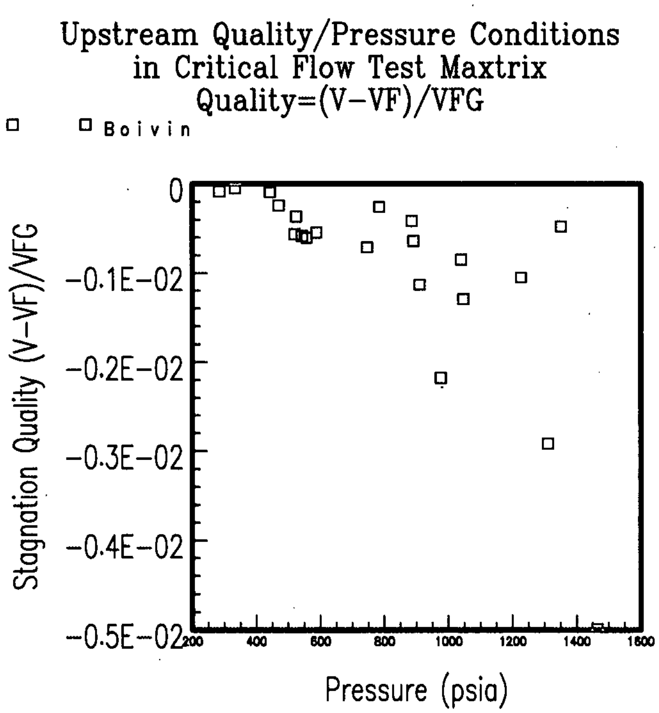

Figure 12.4-2b Upstream Quality in Boivin

12.4.3 Fincke and Collins

Fincke and Collins performed critical flow experiments by flowing subcooled water through a loop and test section. Mass flow rate was controlled by a flow control valve upstream of the test section and back pressure was controlled by a valve downstream of the test section. The test section consisted of a 1.8 m long, 0.0444 m diameter Lexan cylindrical tube followed by a convergent-divergent Lexan nozzle with a minimum diameter of 0.01828 m. Degassed water was used for all experiments. Instrumentation included upstream temperature (reported uncertainty of 0.1°C), volumetric flow rate (uncertainty of 0.1 l/s), pressure just upstream of the nozzle (no uncertainty given), and differential pressure measurements along the nozzle (uncertainty ranging from 0.5 to 2.5 kPa). The differential pressure measurements were used to determine the throat pressure that is included in this data base. The upstream pressure ranged from 90 to 300 kPa (13.1 to 43.5 psia), inlet temperatures were 5° to 40°C subcooled (quality of $-3x10^{-6}$ to $-7x10^{-5}$).

The upstream conditions in Pressure/Temperature and Pressure/Quality planes, along with (P, T) trajectories from LOFT and ROSA small break tests are shown in Figures 12.4-3a and 12.4-3b.

a,c

Figure 12.4-3a Upstream P-T in Fincke-Collins

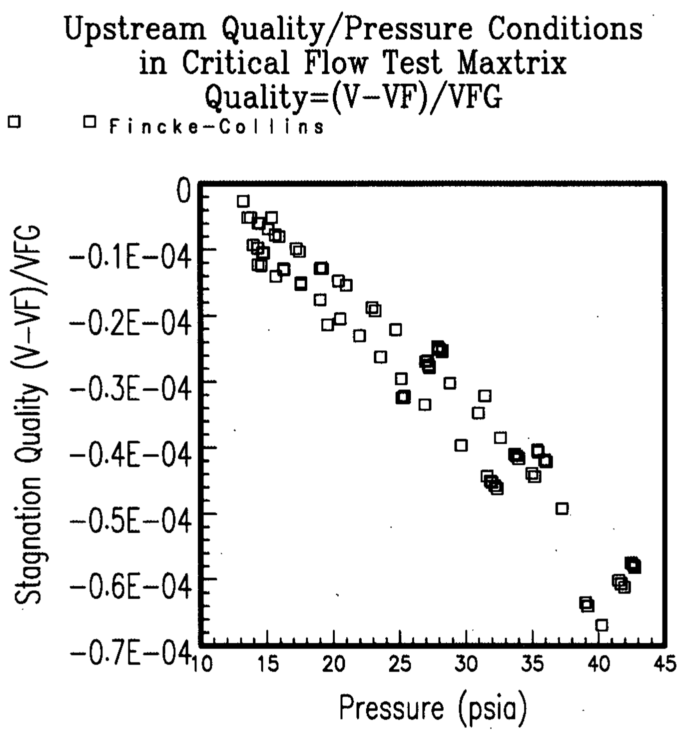

Figure 12.4-3b Upstream Quality in Fincke-Collins

12.4.4 Jeandey

Jeandey performed critical flow experiments by flowing subcooled, demineralized and degassed water through a vertical test section. The test section consisted of a smoothly convergent entrance followed by a straight cylindrical pipe 0.02013 m in diameter followed by a diverging section with a divergent angle of 7 degrees. Flow was vertically upward for all the experiments. Stagnation conditions ranged from pressures of 900 to 14000 kPa (130.5 to 2030.5 psia) and temperatures of 148.5 to 324.6 C (quality of 0 to -0.01). The resulting critical mass fluxes ranged from 14500 to 62000 kg/m^2-s.

The throat pressure was measured along with many other pressures along the test section. In addition, for 21 of the experiments, axial and radial void fraction profiles were obtained using an X-ray densitometer.

The upstream conditions in Pressure/Temperature and Pressure/Quality planes, along with (P, T) trajectories observed in LOFT and ROSA small break tests, are shown in Figures 12.4-4a and 12.4-4b.

a,c

Figure 12.4-4a Upstream P-T in Jeandey

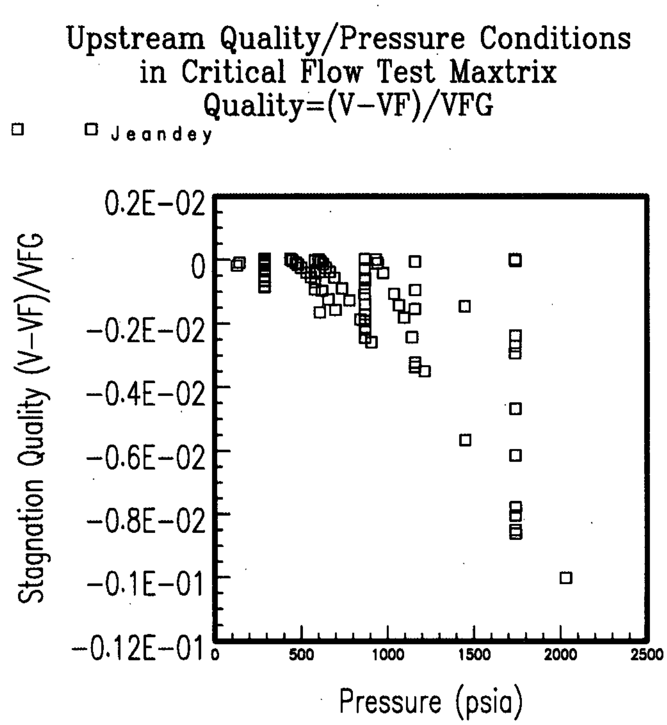

Figure 12.4-4b Upstream Quality in Jeandey

12.4.5 Neusen

Neusen performed experiments to determine design criteria for convergent-divergent nozzles. Critical flow occurred during these experiments, and the data are included in this data base. Neusen ran the saturated water through two convergent-divergent nozzles with minimum diameters of 0.0064 and 0.011 m. Reported stagnation conditions ranged from pressures of 841 to 6516 kPa (122 to 945 psia) and qualities of 0.0028 and 0.228.

Stagnation conditions for these experiments were determined by measuring subcooled temperature and pressure upstream of a throttling valve. The throttling process was assumed to be isentropic, and pressure was measured downstream of the throttling valve (reported uncertainty of 1%). Reported uncertainties for mass flux and calculated enthalpy were less than 2.5% and 0.5%, respectively.

The upstream conditions in Pressure/Temperature and Pressure/Quality planes, along with (P, T) trajectories observed in LOFT and ROSA small breaks, are shown in Figures 12.4-5a and 12.4-5b.

a,c

Figure 12.4-5a Upstream P-T in Neusen

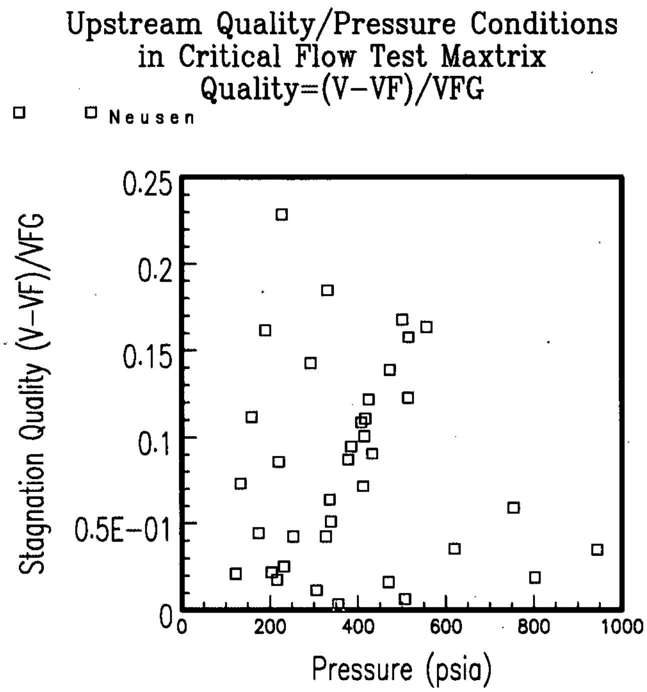

Figure 12.4-5b Upstream Quality in Neusen

12.4.6 Reocreux

Reocreux performed critical flow experiments by flowing subcooled degassed, demineralized water upwards through a vertical test section. The test section consisted of a straight, cylindrical section 2.335 m long and 0.020 m in diameter, followed by a divergent section 0.327 m long. Stagnation pressures ranged from 212 to 340 kPa (30.7 to 49.3 psia), and stagnation temperatures ranged from 115.9 to 121.8 C (quality of $-5x10^{-6}$ to $-3.5x10^{-5}$). Pressures were measured along the test section at many locations, most concentrated near the choking point (at the entrance to the divergent section). The critical or throat pressures were determined from these measurements. In addition, the void fraction at the choking point was measured for most of the tests using X-ray attenuation method.

The upstream conditions in Pressure/Temperature and Pressure/Quality planes, along with (P, T) trajectories observed in LOFT and ROSA small break tests, are shown in Figures 12.4-6a and 12.4-6b.

a,c

Figure 12.4-6a Upstream P-T in Reocreux

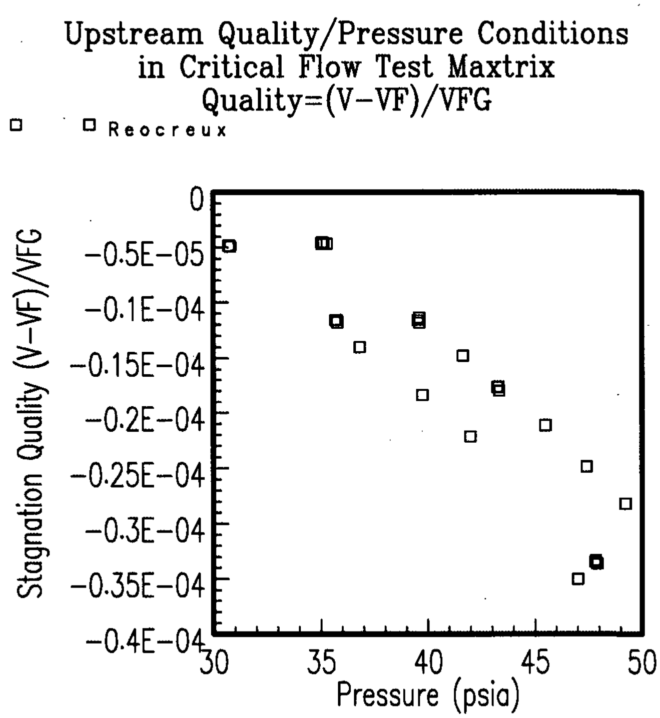

Figure 12.4-6b Upstream Quality in Reocruex

12.4.7 Seynhaeve

Seynhaeve performed critical flow experiments by flowing subcooled, demineralized water upwards in vertical test sections. Two test sections were employed. Each section consisted of a straight, cylindrical pipe 0.0125 m in diameter followed by a divergent section. One section had the straight pipe 0.306 m long, and the other 0.221 m long. Stagnation conditions for these experiments range from 280 to 1015 kPa (40.6 to 147.2 psia) in pressure and 111 to 166.8 C in temperature (quality of $-9\text{x}10^{-6}$ to $-8.9\text{x}10^{-5}$). Critical pressure was measured near the choking plane. Measurement uncertainties are not known.

The upstream conditions in Pressure/Temperature and Pressure/Quality planes, along with (P, T) trajectories observed in LOFT and ROSA small break tests, are shown in Figures 12.4-7a and 12.4-7b.

a,c

Figure 12.4-7a Upstream P-T in Seynhaeve

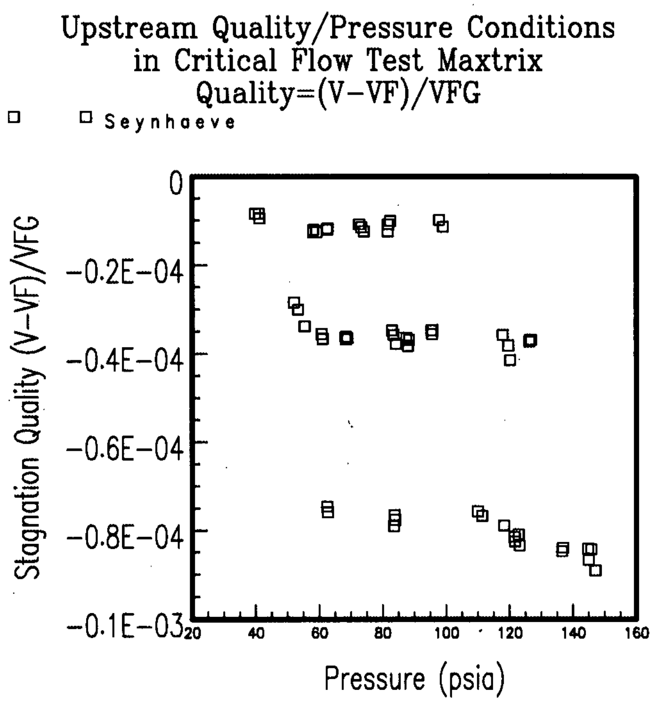

Figure 12.4-7b Upstream Quality in Seynhaeve

12.4.8 Sozzi and Sutherland

Sozzi and Sutherland conducted a series of critical flow experiments with subcooled and low quality water. The water for each experiment was demineralized and degassed. Water from a large vessel was blown down through test nozzles. Data from 21 different nozzle shapes and configurations have been taken with more than 650 individual data points. Stagnation pressure ranged from 3000 to 7000 kPa (435 to 1015.3 psia), and stagnation qualities ranged from approximately -0.006 to 0.01 (based on the specific volume).

The upstream conditions in Pressure/Temperature and Pressure/Quality planes, along with (P, T) trajectories observed in LOFT and ROSA small break tests, are shown in Figures 12.4-8a and 12.4-8b.

a,c

Figure 12.4-8a Upstream P-T in Sozzi-Sutherland

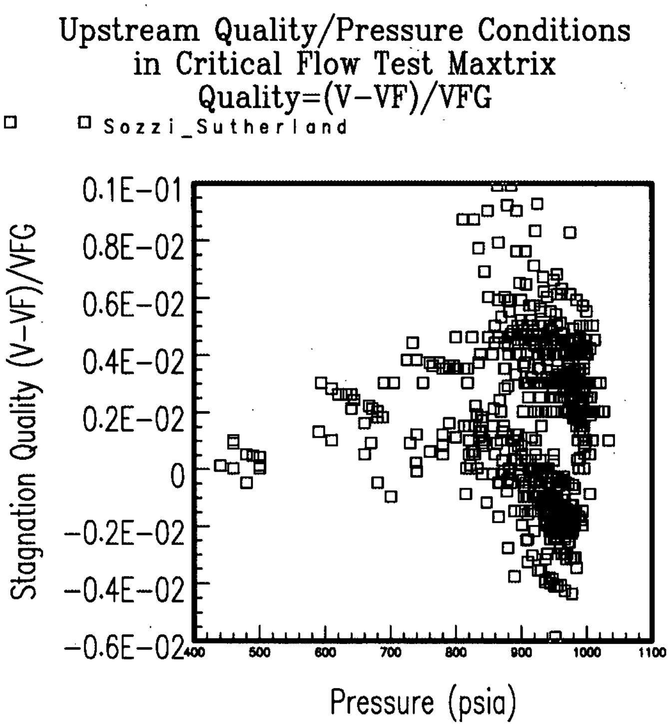

Figure 12.4-8b Upstream Quality in Sozzi-Sutherland

12.4.9 Marviken Tests 1 through 27

Marviken tests provide very large diameter downflow data typically considered full scale. The Marviken facility was used for full-scale critical flow tests between mid-1977 and December 1979. During this time, 27 tests were conducted by a downward discharge of water and steam mixtures from a full-sized reactor vessel through a large diameter vertical discharge pipe that supplied the flow to a test nozzle. There were 9 nozzles tested; all had rounded entrances followed by a nominal 20, 30 and 50 cm constant diameter straight section. Table 12.4-4 shows the characteristic dimensions for the tests. As seen in the table, the entire test series (Tests 1 through 27) were selected for the model validation.

The discharge pipe that connects the vessel to the nozzle is 6283 mm long and is geometrically complex. It is made up of several pieces: nozzle, permanently attached to the vessel with a 752 mm diameter, a 1980 mm long drift tube of the same diameter, a 1778 mm long global valve with a 780 mm diameter and a 1000 mm long with 752 mm diameter section to which the nozzle is attached. Besides these there were two 120 mm long instrument rings inserted on either end of the 1980 mm drift tube. It is quite clear that with this degree of geometric complexity, the question of establishing a consistent set of complete inlet conditions is not simple.

For assessment, only the nozzle is modeled by the critical flow model. Thus the inlet condition to the nozzle was taken from 004M109 for pressure (0.7 m upstream of the nozzle entrance) ranging from 2580 to 5160 kPa (374 to 748 psia) and 003M404 for temperature (2.8 m upstream of the nozzle entrance) ranging from 469 to 535 K (quality of -0.0036 to 0.004).

Probable measurement error is stated as: Pressure – 7 kPa, Temperature – 0.6°C.

The upstream conditions in Pressure/Temperature and Pressure/Quality planes, along with (P, T) trajectories observed in LOFT and ROSA small break tests, are shown in Figures 12.4-9a and 12.4-9b.

Table 12.4-4 Marviken Test Nozzles (from pp. 51, MXC-101, EPRI/NP-2370)			
Nozzle Number	**Diameter (mm)**	**Length (mm)**	**Used in Tests**
1	200	590	13, 14
2	300	290	6, 7
3	300	511	25, 26
4	300	895	1, 2, 12
5	300	1116	17, 18, 19
6	500	166	23, 24
7	500	730	20, 21, 22, 27
8	500	1809	15, 16
9	509	1589	3, 4, 5, 8, 9, 10, 11

a,c

Figure 12.4-9a Upstream P-T in Marviken Tests 1 through 27

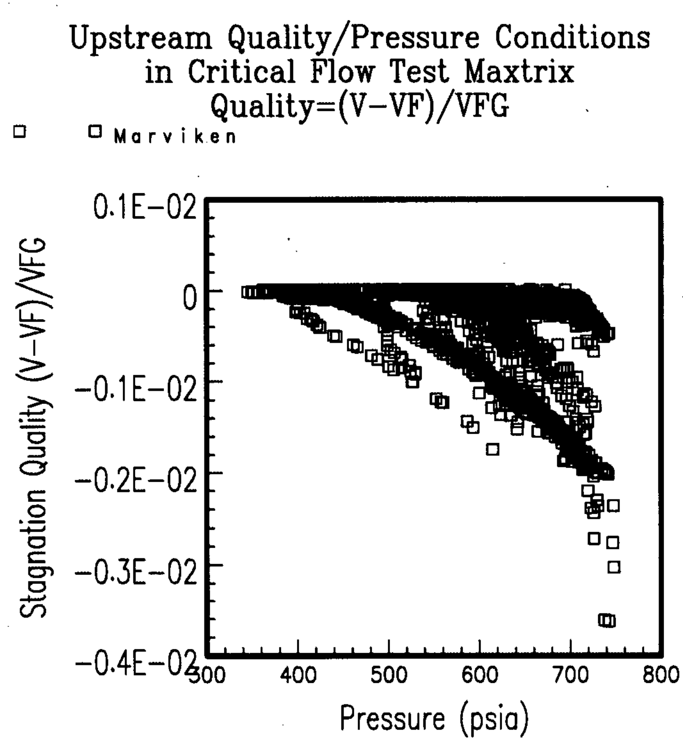

Figure 12.4-9b Upstream Quality in Marviken Tests 1 through 27

12.4.10 Amos and Schrock

Amos and Schrock's break flow data cover a wide range of pressure from 4000 to 15500 kPa (580 to 2248 psia), and subcooling from 0 to 60°C (quality of $8x10^{-6}$ to -0.043) which is suited for evaluating a performance of the break model for small break LOCA analyses. The configuration of the break is thin rectangular slit with the nominal width of 0.381 and 0.254 mm. These set of tests are two of larger slit size of the three of their experiments. Although the break flow area is rectangular and small (equivalent hydraulic diameter = 0.748 and 0.464 mm), the data is valuable since the phenomena which governs the critical condition appeared to be the same for breaks of all sizes. This may be why the 1D flow model is sufficiently accurate to describe the break flows.

The upstream conditions in Pressure/Temperature and Pressure/Quality planes, along with (P, T) trajectories observed in LOFT and ROSA small break tests, are shown in Figures 12.4-10a and 12.4-10b.

a,c

Figure 12.4-10a Upstream P-T in Amos-Schrock

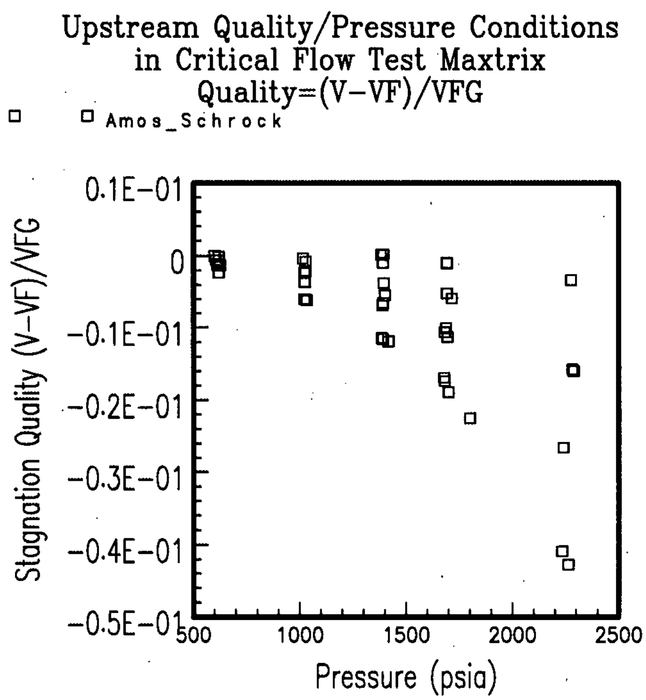

Figure 12.4-10b Upstream Quality in Amos-Schrock

12.4.11 Anderson and Benedetti (TPFL)

Anderson and Benedetti conducted critical flow tests at the Two Phase Flow Loop (TPFL) located in INEL, for purpose of investigating the entrainment at the break off the stratified upstream flow under saturated condition. A two-phase mixture of known phasic mass flow rate flowed through a branch line pipe of 1.63 m long, 34 mm diameter attached to a simulated cold leg pipe, to the nozzle which is 54 mm long and has a diameter of 16.2 mm. The pressure just upstream of the rounded entrance nozzle as well as the void fraction was measured by a gamma attenuation method. Their experiments are well instrumented critical flow tests with saturated upstream conditions at 900, 640 and 500 psia. The flow qualities in the tests were varied from 0 to 1 at all three pressures.

The upstream conditions in Pressure/Temperature and Pressure/Quality planes, along with (P, T) trajectories observed in LOFT and ROSA small break tests, are shown in Figures 12.4-11a and 12.4-11b.

a,c

Figure 12.4-11a Upstream P-T in TPFL

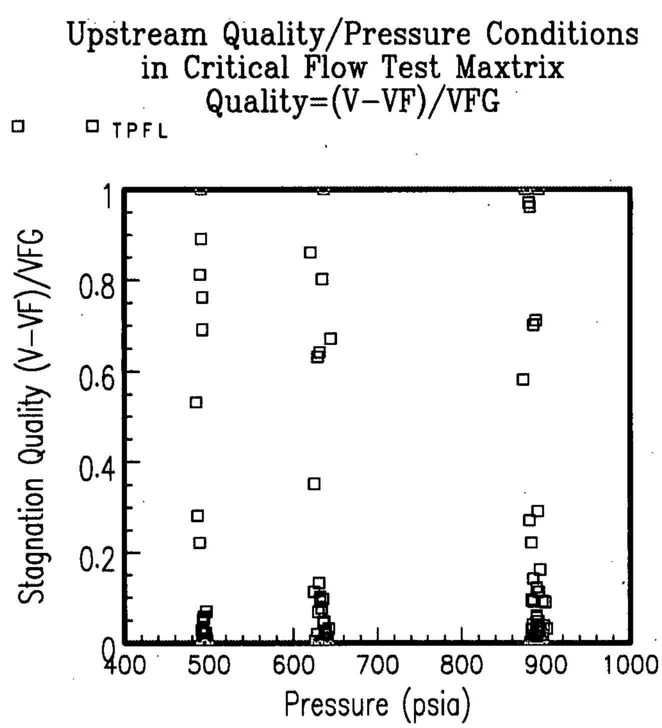

Figure 12.4-11b Upstream Quality in TPFL

12.4.12 Celata (1988)

Celata et al. (1988) conducted a set of flow rate critical flow experiments with and without non-condensable using a 1.5 m long 4.6 mm id vertical downward pipe. The experiments were conducted at the pressure of 0.5, 1.0, and 1.5 MPa, and the subcooling of 0, 20, 40, and 60°C ($-5.5x10^{-5}$ to $-6.3x10^{-4}$). Figure 12.4-12a shows the stagnation pressure and the inlet subcooling of Celata's data. As seen in the figure data were taken at three roughly discrete pressures, namely 0.5 MPa (72.5 psia), 1.0 MPa (145 psia), and 1.5 MPa (217.5 psia). They have reported the un-reliability and a lack of reproducibility associated with the saturated water data. Figure 12.4-12b shows the measured critical mass flux vs. subcooling at all three pressures. It is noted that the critical mass flux data near saturation are higher than that at the higher subcooling condition which is inconsistent and is due to difficulty with this particular set of data as stated by Celata et al. Therefore the validation will use Celata's subcooled dataset (subcooling greater than 10°C). This represents 97 out of 132 test runs.

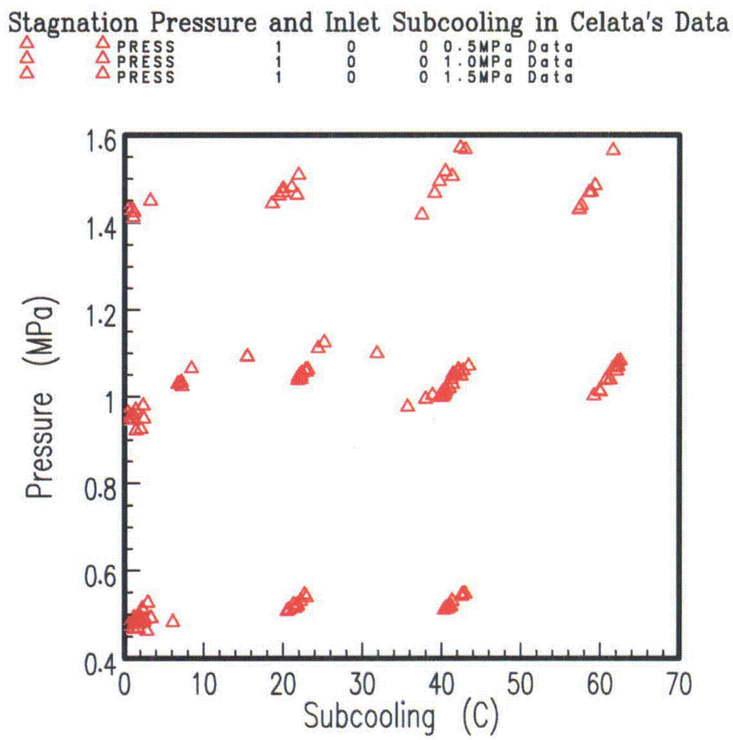

Figure 12.4-12a Stagnation (P,DTsub) in Celata (1988) data

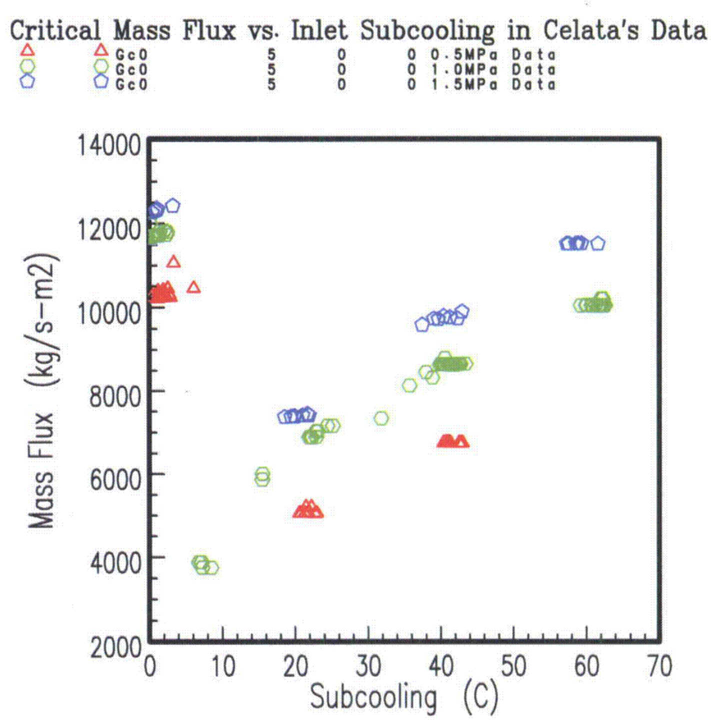

Figure 12.4-12b Critical Mass Flux in Celata's data

For each test point, two paired runs were made, i.e., a reference run without non-condensable gas and with non-condensable gas, and following data were recorded,

- Stagnation pressure, P_0 (MPa),
- Temperature, T_0 (°C),
- Inlet subcooling, $\Delta T_{süb}$ (°C)
- Outlet critical pressure, P_c (MPa)
- Reference Critical Mass Flux without non-condensable gas, G_{c0} (kg/s-m^2)
- Critical Mass Flux with non-condensable gas, G_c (kg/s-m^2)
- Air Mass Flux, G_a (kg/s-m^2)
- Ratio of Critical Mass Flux with non-condensable gas to the reference Critical Mass Flux, G_c/G_{c0}

In addition to the above data, pressure and temperature were measured at 6 locations in the test section for selected test runs.

a,c

Figure 12.4-12c Upstream P-T in Celata

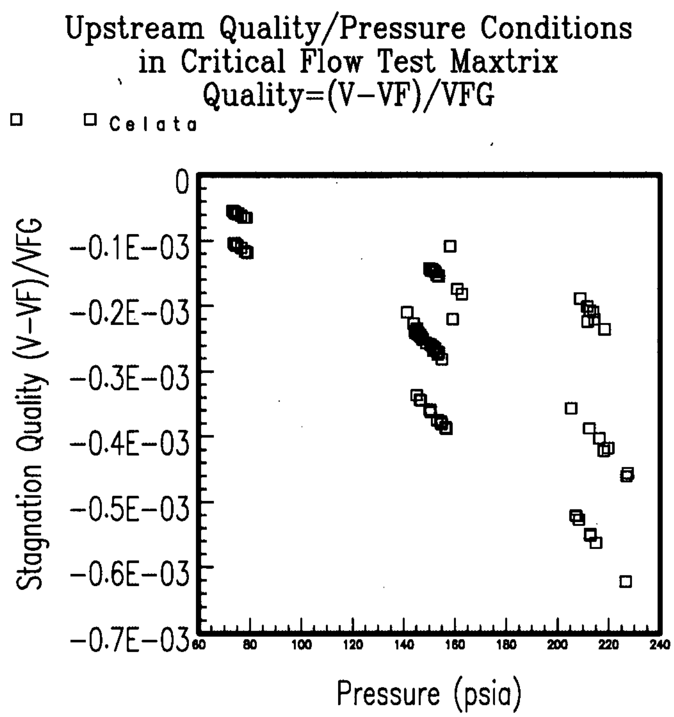

Figure 12.4-12d Upstream Quality in Celata

12.4.13 Overall

The test matrix selected covers from 13 psia to 2300 psia, and quality of -0.0429 to 1.0. The coverage of upstream condition is graphically shown in Figure 12.4-13a and Figure 12.4-13b below. Figures show the upstream fluid condition found in the critical flow database for the validation as well as the predicted trajectories of temperature-pressure and quality-pressure for small and large break LOCAs. It is noted that while more dataset with the two-phase inlet condition and high pressure-high subcooling are desirable, the validation database adequately covers the range of upstream conditions expected during PWR LOCAs.

a,c

Figure 12.4-13a Upstream Condition in Test Matrix

a,c

Figure 12.4-13b Upstream Condition in Test Matrix

12.5 ASSESSMENT RESULTS

12.5.1 Assessment Method

A stand-alone model of the WCOBRA/TRAC-TF2 critical flow module was used for the prediction-data comparison. The consistency between the stand-alone code results and the WCOBRA/TRAC-TF2 results was confirmed by comparing the prediction for subset of critical flow data points in Section 12.5.4.1.

12.5.1.1 CALCULATION

As described in Section 5.12.2 of this document, the inlet flow is iterated until the exit pressure gradient becomes [ ]^{a,c}. At this point the pressure along the break path becomes what is shown in Figure 12.5-1. The figure shows the pressure along the break path with the measured pressures for Celata's Run 020 data.

[ ]^{a,c} and compared to the measured critical mass flux, G_c value.

a,c

Figure 12-5-1 Pressure Profile along the Break Path

12.5.2 DATA COMPARISON

The critical mass flux prediction is compared with the measured critical mass flux. This comparison is performed for a total of 3199 data points with no non-condensable gas and 96 data points with non-condensable gas.

12.5.2.1 Bias and Uncertainty Results

A total of 3199 data points from 53 nozzle geometries were used for the determination of bias and uncertainty associated with the critical flow model prediction used in WCOBRA/TRAC-TF2. The prediction error was calculated as, $\varepsilon = \frac{G_{meas} - G_{pred}}{G_{preds}}$. This is not a usual definition of the deviation from the measurement, $\frac{G_{pred} - G_{meas}}{G_{meas}}$, but the one convenient for the purpose of ranging the break flow for the statistical sampling process since the quantity $(1 + \varepsilon)$ can be used as the multiplier to the model prediction (or C_D, the discharge coefficient) to recover the measured value.

The following results were obtained through the comparison to data. Note that since uncertainty associated with many of the measurement were unknown. Others have the reported uncertainty. The reported uncertainty was much smaller than the prediction error and thus the contribution of measurement error on the prediction error is neglected.

A valid range of the bias and uncertainty estimate given here is based on selected experimental data. A comparison was made for 0 (Orifice) < L ≤ 2335 mm, and $0.418 \leq D_H \leq 500$ mm.

Overall (-0.0429 ≤ Quality ≤ 1.0)

Predictions for all selected data are shown in Table 12.5-1. Appendix-A contains all output and the comparison of predicted and measured critical mass flux for all individual test series.

The mean error (or the bias) for the entire dataset,

$$\bar{\varepsilon} = \frac{\sum_{i}^{N}\left(\frac{G_{meas} - G_{pred}}{G_{preds}}\right)}{N}$$ was found to be [ ]^{a,c},

and the standard deviation,

$$\sigma(\varepsilon) = \sqrt{\frac{\sum_{i}^{N}(\varepsilon_i - \bar{\varepsilon})}{N-1}}$$ was found to be [ ]^{a,c}.

The bias and standard deviation based on the upstream fluid state are;

- For Subcooled Liquid Region ($-0.043 \leq$ Quality ≤ 0)
  - Bias = [ ]^{a,c}
  - Standard Deviation = [ ]^{a,c}
- For Saturated Flow rate including Single Phase Vapor Region ($0 <$ Quality ≤ 1.0)
  - Bias = [ ]^{a,c}
  - Standard Deviation = [ ]^{a,c}

Table 12.5-1 Critical Flow Data Comparison for WCOBRA/TRAC Critical Flow Model

Reference	L (mm)	D (mm)	cosθ	N-Data	Mean Error ε (%) $(\frac{G_{meas} - G_{calc}}{G_{meas}})$	σ(ε) (%)
Andron, K. H. & Ackerman, M. C. (1978)	1015	26.3	0	32		
Boivin (1979)	500	12	0	10		
Boivin (1979)	1600	30	0	5		
Boivin (1979)	1700	50	0	6		
Fincke & Collins (1981)	13	44	0	92		
Jeandey et al. (1981)	463	20	1	15		
Jeandey et al. (1981)	463	20	1	73		
Neusen (1962)	0	11	0	25		
Neusen (1962)	0	6	0	12		
Reocreux (1974)	2335	20	1	28		
Seybhaeve (1980)	306	13	1	26		
Seybhaeve (1980)	306	13	1	31		
Sozzi & Sutherland (1975)	45	12.7	0	128		
Sozzi & Sutherland (1975)	45	12.7	0	13		
Sozzi & Sutherland (1975)	57	12.7	0	47		
Sozzi & Sutherland (1975)	362	12.7	0	19		
Sozzi & Sutherland (1975)	83	12.7	0	17		
Sozzi & Sutherland (1975)	553	12.7	0	13		
Sozzi & Sutherland (1975)	108	12.7	0	23		
Sozzi & Sutherland (1975)	679	12.7	0	96		
Sozzi & Sutherland (1975)	159	12.7	0	15		
Sozzi & Sutherland (1975)	1823	12.7	0	81		
Sozzi & Sutherland (1975)	235	12.7	0	12		
Sozzi & Sutherland (1975)	273	12.7	0	22		
Sozzi & Sutherland (1975)	5	12.7	0	58		
Sozzi & Sutherland (1975)	322	12.7	0	24		
Sozzi & Sutherland (1975)	513	12.7	0	24		
Sozzi & Sutherland (1975)	640	12.7	0	17		

a,c

Table 12.5-1 Critical Flow Data Comparison for WCOBRA/TRAC Critical Flow Model (cont.)

Reference	L (mm)	D (mm)	cosθ	N-Data	Mean Error ε (%) $(\frac{G_{meas} - G_{calc}}{G_{meas}})$	σ(ε) (%)
Sozzi & Sutherland (1975)	195	12.7	0	23		
Sozzi & Sutherland (1975)	45	19	0	23		
Sozzi & Sutherland (1975)	732	54	0	4		
Sozzi & Sutherland (1975)	696	76	0	3		
Sozzi & Sutherland (1975)	63	28	0	5		
Amos & Schrock (1983)	63.5	0.748	-1	18		
Amos & Schrock (1983)	63.5	0.464	-1	26		
Anderson & Benedetti (1985)	31.9	16.2	0	109		
Marviken Test 1 (1982)	895	300	-1	97		
Marviken Test 2 (1982)	895	300	-1	91		
Marviken Test 3 (1982)	1589	509	-1	40		
Marviken Test 4 (1982)	1589	509	-1	39		
Marviken Test 5 (1982)	1589	509	-1	43		
Marviken Test 6 (1982)	300	300	-1	85		
Marviken Test 7 (1982)	300	300	-1	84		
Marviken Test 8 (1982)	1589	509	-1	40		
Marviken Test 9 (1982)	1589	509	-1	58		
Marviken Test 10 (1982)	1589	509	-1	57		
Marviken Test 11 (1982)	1589	509	-1	41		
Marviken Test 12 (1982)	895	300	-1	121		
Marviken Test 13 (1982)	590	200	-1	139		
Marviken Test 14 (1982)	590	200	-1	144		
Marviken Test 15 (1982)	1809	500	-1	45		
Marviken Test 16 (1982) 590 200-1146	1809	500	-1	40		
Marviken Test 17 (1982) 590 200-1146	1110	300	-1	90		
Marviken Test 18 (1982) 590 200-1146	1110	300	-1	69		

a,c

Table 12.5-1 Critical Flow Data Comparison for WCOBRA/TRAC Critical Flow Model (cont.)						
Reference	**L (mm)**	**D (mm)**	**cosθ**	**N-Data**	**Mean Error ε (%)** $(\frac{G_{meas} - G_{calc}}{G_{meas}})$	**σ(ε) (%)**
Marviken Test 19 (1982) 590 200-1146	1110	300	-1	85		
Marviken Test 20 (1982) 590 200-1146	730	500	-1	50		
Marviken Test 21 (1982) 590 200-1146	730	500	-1	50		
Marviken Test 22 (1982) 590 200-1146	730	500	-1	37		
Marviken Test 23 (1982)	166	500	-1	61		
Marviken Test 24 (1982)	166	500	-1	44		
Marviken Test 25 (1982) 590 200-1146	510	300	-1	84		
Marviken Test 26 (1982) 590 200-1146	510	300	-1	134		
Marviken Test 27 (1982) 590 200-1146	730	500	-1	59		
Celata (1988)	1500	4.6	-1	97		
Total				3199		

a,c

Figure 12.5-2 below shows the comparison of all points in the test matrix with $\pm 1\sigma$ lines above and below the 45° line.

a,c

Figure 12.5-2 Comparison of Predicted and Measured Critical Flows

12.5.2.2 Non-condensable Effect

Figure 12.5-3a shows the predicted critical flow mass flux vs. the measured critical flow mass flux for cases with non-condensable gas.

To check for a consistency relative to the effect of non-condensable, the ratio of critical mass flux with non-condensable to with no-non-condensable gas cases was reported from the paired experiment by Celata (1980). The predicted ratios were calculated and compared with the measured values. This ratio as a function of the non-condensable gas concentration was examined. Figure 12.5-3b shows the comparison of measured effect of the non-condensable on the critical flow rate and the predicted effect of the non-condensable gas.

Considering the fact that the thermal equilibrium between the non-condensable gas (air) and the steam/water mixture at the inlet was not well established in the experiment, the agreement between the data and the prediction is considered to be adequate. Although there is a tendency to over-predict the impact of Non-condensable as the fraction of non-condensable increases, the deviation is below the saturated two-phase upstream cases. Thus a separate uncertainty value for the two-phase upstream with non-condensable gas would not be applied. The saturated upstream values [ ][a,c] will be used for two-phase regardless of the presence of non-condensable.

a,c

Figure 12.5-3a Comparison of Predicted and Measured Critical Mass Flux with Non-condensable Gas

a,c

Figure 12.5-3b Comparison of Predicted and Measured effect of Non-condensable Gas on Critical Mass Flux

12.5.3 PARAMETRIC TREND OF PREDICTION

This section examines the presence of bias in the major parameters such as pressure, quality, break area and break path length. For the purpose of examining the model trend in this subsection, the error is defined in the usual way, (as the deviation from the measurement), $\frac{G_{pred} - G_{meas}}{G_{meas}}$.

12.5.3.1 Trend with Respect to Pressure Variation

In this section, a possible model trend with respect to the upstream pressure is examined. Figure 12.5-4 below shows the error vs. pressure of all data points. The figure does not show global trend relative to the upstream pressure, although it does show that there is a larger spread in the lower pressure points ($p < 1000$ psia).

a,c

Figure 12.5-4 Prediction Trend in Pressure Variation

12.5.3.2 Trend with Respect to Quality Variation

In this section, a possible model trend with respect to the upstream quality is examined. Figure 12.5-5a below show the error vs. quality of all data points. The figure shows global trend relative to the upstream quality. The model [

]^{a,c}

a,c

Figure 12.5-5a Prediction Trend in Quality Variation

a,c

Figure 12.5-5b Prediction Trend Quality Variation

12.5.3.3 Trend with Respect to Channel Length Variation

In this section, a possible model trend with respect to the channel length is examined. Figures 12.5-6a and 12.5-6b below show the error vs. channel length of all data points. The figures [

]a,c

a,c

Figure 12.5-6a Prediction Trend in Channel Length Variation in Linear Scale

a,c

Figure 12.5-6b Prediction Trend in Channel Length Variation in Log Scale

12.5.3.4 Trend with Respect to Hydraulic Diameter Variation

In this section, a possible model trend with respect to the hydraulic diameter is examined. Figure 12.5-7a below shows the error vs. hydraulic diameter of all data points. The figure [

]^{a,c}

a,c

Figure 12.5-7a Prediction Trend in Channel Diameter in Linear Scale

a,c

Figure 12.5-7b Prediction Trend in Channel Diameter in Log Scale

12.5.3.5 Trend with Respect to L/D Variation

In this section, a possible model trend with respect to the break path L/D is examined. Figures 12.5-8a and 12.5-8b show the relative errors vs. L/D of the break path in linear and log scale. [

]a,c

a,c

Figure 12.5-8a Prediction Trend in Channel L/D Variation – Linear Scale

a,c

Figure 12.5-8b Prediction Trend in Channel L/D Variation – Log Scale

12.5.4 Model Performance as Implemented in WCOBRA/TRAC-TF2

12.5.4.1 Impact of Transient

The assessment presented in the previous section was performed with the stand-alone program extracted from WCOBRA/TRAC-TF2. Therefore, the model prediction as an integral part of WCOBRA/TRAC-TF2 was examined by repeating Marviken Test 6 to see the impact of coupling. Figure 12.5-9 shows the noding diagram used for Marviken Test 6 simulation. PIPE-26 models the discharge pipe with the HRM modeling the nozzle. The HRM break model is explicitly shown to be attached to the right most cell of PIPE-26. The input parameters for the nozzle, namely nozzle hydraulic diameter (HRMOFD), nozzle length (HRMOFL), the flow multiplier for single phase liquid (HRM1PM) and two-phase/single phase vapor (HRM2PM) are shown below the noding diagram. These parameters will be discussed in detail in Section 29. Figure 12.5-10 shows the Mass Flow comparison with the stand-alone prediction for Marviken Test 6 given in Appendix A.11.6. Predictions are equivalent. The differences are caused by the sparser boundary condition specification used in the WCOBRA/TRAC-TF2 model compared to the stand-alone input as seen in Figures 12.5-11a (Pressure) and 12.5-11b (Temperature).

a,c

Figure 12.5-9 Test 6 Noding Scheme

a,c

Figure 12.5-10 Test 6 Prediction of WCOBRA/TRAC-TF2 vs. Stand-Alone Model

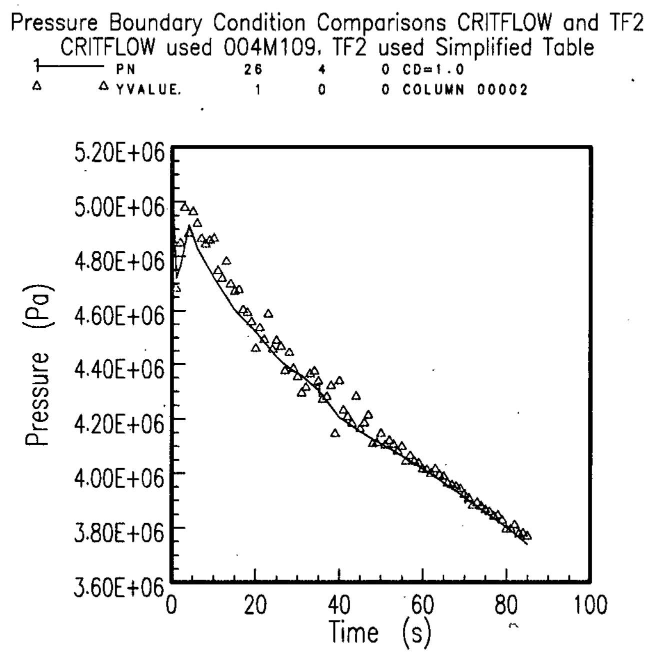

Figure 12.5-11a P(t) BC Comparison

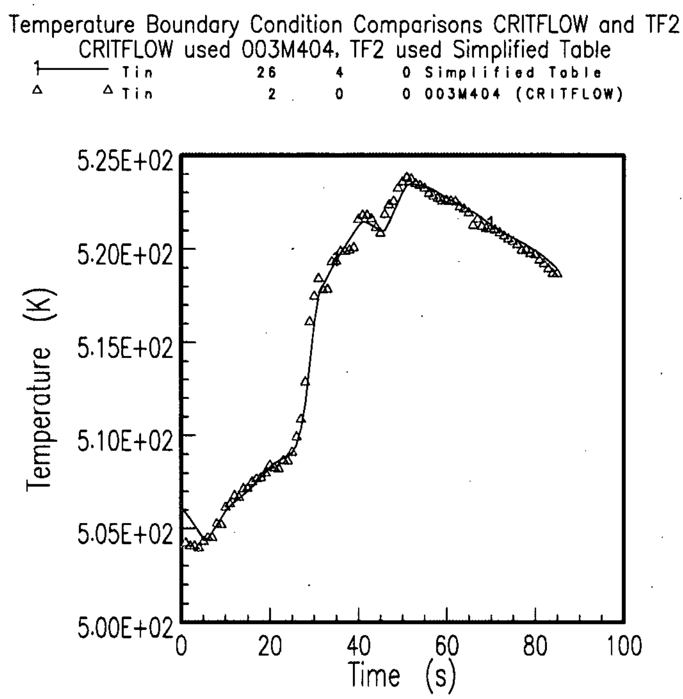

Figure 12.5-11b T(t) BC Comparison

12.5.4.2 Influence of Mesh Size

The model prediction's sensitivity to a number of axial nodes used within the critical flow module, HRM, was investigated using a subset of the validation test cases. The number of axial nodes is set [

]^{a,c}

12.5.4.3 Influence of Friction Factor/Entrance Effect

The entrance and friction factors were found to be very important for predicting the low pressure experiments such as those of Ardron and Ackerman (1978). For very low pressure cases such as these, an inaccurate prediction of entrance and pipe friction pressure loss may cause significant mis-prediction of the pressure in the pipe and subsequent mis-prediction of critical flow rates. This is the reason the reported friction factors were used for simulation of Ardron and Ackerman. For higher pressures where the upstream of the break in PWR LOCAs are expected, the entrance loss and friction factors play an insignificant role.

12.5.4.4 Application of Multiplier (or Discharge Coefficient, CD)

Two sensitivity runs with CD=0.8 and 1.2 were performed to validate the method of applying the discharge coefficient. The results show that the discharge coefficient application via WCOBRA/TRAC-TF2 input parameters, HRM1PM and HRM2PM yields desired break flows as seen in Figure 12.5-9. These input parameters will be discussed in detail in Section 29. Figure 12.5-12a shows the impact of CD on the predicted break flows. Figure 12.5-12b shows the effective multiplier observed in this simulation. They are close to 0.8 and 1.2 but because of the feedback of the flow on the nozzle inlet pressure (Figure 12.5-12c), the multipliers are slightly deviated from CD values, which is expected.

a,c

Figure 12.5-12a Impact of CD on Predicted Flow

a,c

Figure 12.5-12b Observed Effective Multiplier

a,c

Figure 12.5-12c Nozzle Upstream Pressure

12.6 CRITICAL FLOW ASSESSMENT CONCLUSIONS

The critical flow comparisons showed that the present model predicted both small diameter tests such as Amos and Schrock at 0.0295 inch, and Sozzi and Sutherland at 0.5-inch as well as the large diameter (19.7-inch) data obtained in the Marviken tests (EPRI-NP-2370, 1982) with acceptable accuracy.

12.6.1 Scaling Consideration

An observation relative to the scalability of the model is addressed in this section.

12.6.1.1 Pressure, Subcooling, and Quality

For the subcooled break flow model, a pressure range of 13 to 2300 psia and a quality range of -0.0429 to 1.0 were examined. The results indicated that the model is scalable relative to pressure and subcooling with reasonable accuracy. The results showed that the model adequately accounts for the pressure and the quality variations.

12.6.1.2 Break Flow Area

The break flow comparisons showed that the present model predicted both small diameter tests such as Amos and Schrock for 0.0295 inch (Amos and Schrock, 1983), and Sozzi and Sutherland for 0.5-inch (Sozzi and Sutherland, 1975), as well as the large diameter (19.7-inch) data obtained in the Marviken tests

(EPRI-NP-2370, 1982) with adequate accuracy. The WCOBRA/TRAC-TF2 break model was able to simulate both small and large diameter nozzles adequately.

12.6.2 Break Path Geometry and Application to PWR LOCA

The entrance effects, such as the roundness/sharpness of the orifice are accounted for in the present model when they are known and reported for simulation. However, roughness, and sharpness are not known in the PWR LOCA application [

]^{a,c}

12.7 OFFTAKE ENTRAINMENT MODEL

12.7.1 Introduction

During a small break LOCA, the break flow rate determines the depressurization rate as well as the mass inventory of the primary system of a PWR. These parameters in turn influence the timing of various engineered safeguard system responses, such as reactor trip and safety injection.

Early in a small break LOCA, the fluid condition upstream of the break location is subcooled. This results in a high discharge flow rate and a fast depressurization. As the pressure drops to the saturation pressure corresponding to the coolant liquid temperature upstream of the break, the discharge becomes two-phase and a relatively low discharge rate and a slow depressurization result. The flow in the cold leg is expected to be horizontally stratified. Under those conditions the void fraction upstream of the break changes from primarily liquid to primarily vapor as the liquid level in the main pipe decreases. As the stratified surface lowers in the vicinity of the break, the quality at the break is greatly influenced by the entrainment of vapor/liquid off the stratified surface upstream of the break.

Although the size, location, and shape of the break are not known for the postulated small break LOCA, the best-estimate code needs to predict consistent responses relative to experimental data over a range of pressure, subcooling, and upstream fluid states, as well as the break flow area variations, so that accurate sensitivity to small break LOCA responses can be obtained.

12.7.2 Offtake Phenomenon

The vapor pull through and liquid entrainment phenomenon are especially important in the analysis of the small break LOCA accident. For a portion of the small break LOCA accident, one would envision a stratified flow regime in the broken cold leg, where liquid would flow along the bottom of the pipe and vapor flow at the top of the pipe due to the effect of gravity. If the break in the pipe is located in the side of the pipe below the interface, or at the bottom of the pipe, then the quality of the flow through the break will be low. However, certain conditions will lead to a two-phase break flow as opposed to single phase liquid. This phenomenon is known as vapor pull-through, or also as vapor entrainment.

Vapor pull through can occur in the form of vortex or vortex free flow. Figure 12.7.2-1 contains a diagram of each of these flow mechanisms. Vortices tend to be unstable at low flow conditions, and are unable to form at high flow conditions. Vortex flow will also tend to transition into vortex free flow as the distance from the interface to the break decreases. While it is possible for a vortex to form for a break in the side of the pipe, the effect of the pipe wall tends to stunt vortex formation.

Again considering the condition of stratified flow in a pipe, if the break in the pipe is located in the side of the pipe above the interface, or at the top of the pipe, then the quality of the flow through the break will be high. However, certain conditions will lead to a two-phase break flow as opposed to single phase vapor. This phenomenon is known as liquid entrainment. A diagram of the liquid entrainment mechanism is given in Figure 12.7.2-2. The vapor velocity tends to increase near the break due to the Bernoulli effect. As the vapor velocity increases, waves will tend to form at the stratified interface. Some amount of liquid may be entrained from this surface, and carried into the break by the vapor.

Under certain conditions, the size of the wave formed at the break will increase until the wave reaches the top of the pipe. This behavior will propagate through the pipe, and the flow regime will undergo a transition from stratified flow into slug flow. The quality of the break flow will decrease significantly with a transition from a stratified flow regime into a slug flow regime. This transition to slug flow is observed in the experimental data for an upward break orientation presented later in this section. The offtake model is not applicable once transition to slugging occurs.

Some of the key factors which impact the quality of the break flow are the break orientation, flow regime, distance from the interface to the break (for stratified flow), vapor velocity (for liquid entrainment), liquid velocity (for vapor pull through), and the differential pressure across the break.

12.7.3 Relationship to PIRT

The ability of a code to accurately calculate the break flow quality is very important to the analysis of the small break LOCA accident. [

]^{a,c} Since the break flow rate has a significant effect on the system inventory during a SBLOCA, this process is important throughout the entire SBLOCA transient (except for blowdown where the break flow is primarily single-phase liquid).

12.7.4 Section Objectives

In this section, an assessment is made of the offtake model in the WCOBRA/TRAC-TF2 version described in Section 5.13, Volume 1 of this document. The model was validated against test data from the TPFL facility, as well as other additional data as discussed in Section 12.7.6. A description of all the tests performed at the TPFL is given in EPRI NP-4532 (1986).

12.7.5 Two-Phase Flow Loop Offtake Entrainment Tests

12.7.5.1 TPFL Test Facility Description

The tee/critical flow experiments were performed in the TPFL at the INEL Thermal Hydraulics Laboratory (Figure 12.7.5-1). [

]^b The schematic view of the facility is shown in Figure 12.7.5-2.

[

]^b

This facility is the largest scale facility with experimental data which can be used to validate the offtake model within WCOBRA/TRAC-TF2.

12.7.5.2 Test Matrix for TPFL Offtake Simulations

[

]^b Table 12.7.5-1 summarizes the tests selected for simulation using WCOBRA/TRAC-TF2.

[

]^{a,c}

12.7.5.3 Test Procedure for TPFL Offtake Simulations

[

]^b

[

]b

The intent of the test data was to correlate the flow quality in the branch pipe against the mainline liquid level for different pressures and break orientations.

12.7.5.4 WCOBRA/TRAC-TF2 Model for TPFL Offtake Tests

[

]a,c

12.7.5.5 Simulation of TPFL Offtake Tests

[

]b

12.7.5.6 Summary and Conclusions

12.7.5.6.1 Comparison of WCOBRA/TRAC-TF2 Prediction to Horizontal Data

Figure 12.7.5-4 shows the comparison of the WCOBRA/TRAC-TF2 prediction for the branchline quality as a function of the mainline liquid level for the horizontal configuration. [

]a,c

12.7.5.6.2 Comparison of WCOBRA/TRAC-TF2 Prediction to Downward-Vertical Data

Figure 12.7.5-5 shows the comparison of the WCOBRA/TRAC-TF2 prediction and the experimental data of the branchline quality as a function of the mainline liquid level for the downward-vertical configuration. [

]a,c

12.7.6 Additional Offtake Model Validation

The TPFL facility tests address the vertical downward and horizontal break orientations, but provide no data for an upward vertical break. As such, additional validation was performed to ensure that the WCOBRA/TRAC-TF2 code reasonably predicts the offtake phenomenon for an upward oriented break.

Using the TPFL facility geometry, the offtake model was exercised for vertical upward breaks across a range of boundary conditions. The model was exercised at pressures of [

]a,c The code results are compared to [

]a,c to assess the capability of the model.

12.7.6.1 Comparison of WCOBRA/TRAC-TF2 Prediction to Upward-Vertical Data

Figure 12.7.6-1 shows the comparison of the WCOBRA/TRAC-TF2 prediction for the branchline quality as a function of the mainline liquid level divided by the critical height for onset of offtake (hereafter referred to as the level ratio) for the upward-vertical configuration versus experimental data. [

]a,c

[

]a,c

Table 12.7.5-1 Summary of Test Parameters for Two-Phase Flow Loop Offtake Tests

b

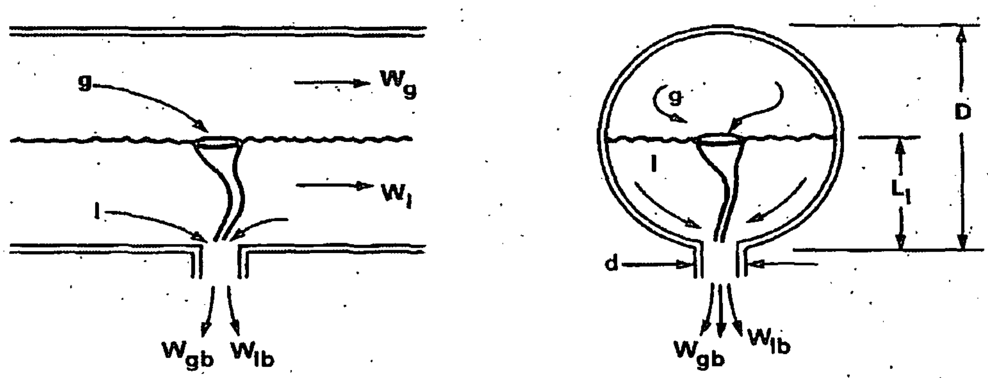

a. Vapor pull-through due to vortex formation

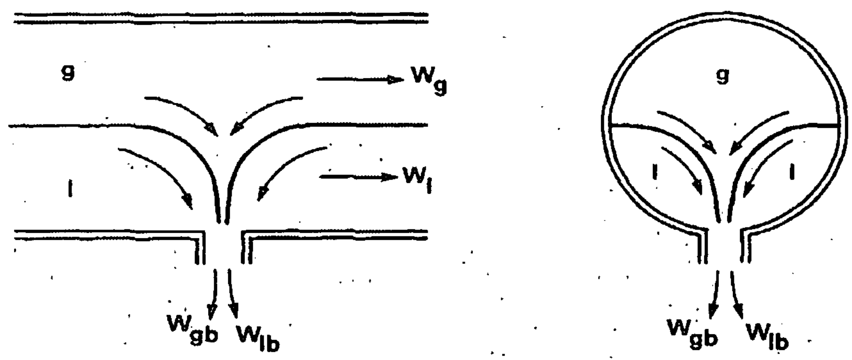

b. Vapor pull-through in vortex-free flow

Figure 12.7.2-1 Vapor Pull Through Mechanisms

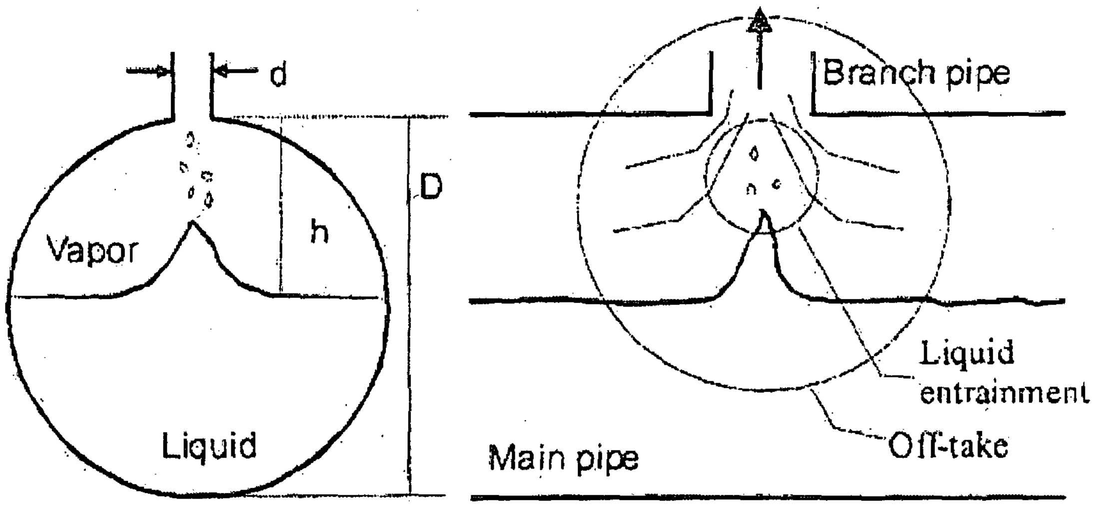

Figure 12.7.2-2 Liquid Entrainment Mechanism

b

Figure 12.7.5-1 Diagram of the Two-Phase Flow Loop Facility

b

Figure 12.7.5-2 Schematic View of the Two-Phase Flow Loop Test Section

a,c

Figure 12.7.5-3 WCOBRA/TRAC-TF2 Noding Diagram of the Two-Phase Flow Loop

a,c

Figure 12.7.5-4 Branchline Quality Versus Mainline Liquid Level for Horizontal Configuration

a,c

Figure 12.7.5-5 Branchline Quality Versus Mainline Liquid Level for Downward-Vertical Configuration

a,c

Figure 12.7.6-1 Branchline Quality Versus Mainline Liquid Level for Upward-Vertical Configuration

a,c

Figure 12.7.6-2 [

]^{a,c}

12.8 REFERENCES

1. Alamgir, M. D. and Lienhard, J. H., 1981, "Correlation of Pressure Undershoot During Hot-Water Depressurization," Trans. ASME, J. Heat Transfer, Vol. 103, pp. 52-55.

2. Amos, C. N. and Schrock, V. E., 1983, "Critical Discharge of Initially Subcooled Water Through Slits," NUREG/CR-3475.

3. Anderson, J. L. and Benedetti, R. L., 1986, "Critical Flow Through Small Pipe Break," EPRI/NP-4532.

4. Ardron, K. H. & Ackerman, M. C., 1978, "Studies of the Critical Flow of Subcooled Water in a Pipe," CEGB Report: RD/B/N4299.

5. Ardron, K. H. and Bryce, W. M., 1990, "Assessment of Horizontal Stratification Entrainment Model in RELAP5/MOD2 by Comparison With Separate Effects Experiment," Nuclear Engineering and Design 122, pp. 263-271.

6. Bajorek, S. M., et al., 1992, "Westinghouse Code Qualification Document for Best Estimate Loss of Coolant Accident Analysis Volume 1: Models and Correlations," WCAP-12945-P-A, Vol. 1, pp. 4-124.

7. Boivin, J. V., 1979, "Two-phase Critical Flow in Long Nozzles," Nuclear Technology, 46, pages 540-545.

8. Bryers, R. W., Hsieh, W. W., Hunter, J. A. & Sieder, E. N., 1966, "Study of Two-phase Metastable Flow," U. S. Department of Interior, Office of Saline Water, R&D Progress Report No. 234, November, 1966.

9. Celata, G. P., Cumo, M., D'Annibale, F., and Farello, G. E., 1988, "THE INFLUENCE OF NON-CONDENSIBLE GAS ON TWO-PHASE CRITICAL FLOW," International Journal of Multiphase Flow, Volume 14, No. 2, pages 175-187.

10. Condie, K. G., 1980, "LOFT LOCE L3-5/L3-5A Results and Analysis." Paper presented at the LOFT Review Group Meeting, Idaho Falls, Idaho.

11. Craya, A., 1949, "Experimental Research on the Flow of Non-homogeneous Fluids," LeHouille Blanche, January-February, pp. 56-64.

12. Cruver, J. E., "Metastable Critical Flow of Steam Water Mixtures, 1963, "Ph.D. Dissertation, Department of Chemical Engineering, University of Washington, (University Microfilms Inc., Ann Arbor, Michigan).

13. Danforth, J. L., 1941, "Flow of Hot Water Through a Rounded Orifice," M. S. Dissertation, Department of Mechanical Engineering, Massachusetts Institute of Technology.

14. Doa, L. T. C and Carpenter, J. M., 1980, "Experiment Data Report for LOFT Nuclear Small-Break Experiment L3-5/L3-5A," NUREG/CR-1695, EGG-2060.

15. Elias, E., and Lellouche, G. S., 1994, "TWO-PHASE CRITICAL," International Journal of Multiphase Flow, Vol. 20, Supplement, pp. 91-168.

16. EPRI/NP-2370, 1982, "The Marviken Full-Scale Critical Flow Tests," Vol. 1, Summary Report.

17. Fauske, H. K., 1962, "Contribution to the Theory of Two-phase, One Component Critical Flow," Argonne National Laboratory Report ANL-6633.

18. Fincke, J. R. & Collins, D. R., "The Correlation of Two-dimension and Non-equilibrium Effects in Subcooled Choked Nozzle Flow," NUREG/CR-1907, EGG-2081.

19. Guizovarn, L., Pinet, B., Barriere, G. & Pietri, D., 1975, "Etude Expermentale des Debits Critiques en Ecoulement Diphasiques eau Vapeur a Faible Titre Dans un Canal Avec Divergent de 7° a des Transports Thermiques," Note TT No. 501.

20. Henry, R. E., 1970, "An Experimental Study of Low Quality, Steam-Water Critical Flow at Moderate Pressures," Argonne National Laboratory Report ANL-7740.

21. Holmes, B. J., and Allen, E. J., 1998, "A REVIEW OF CRITICAL FLOW DATA FOR PRESSURISED WATER REACTOR SAFETY STUDIES," Multiphase Science and Technology, Vol. 10, pp. 141-302.

22. Illic, V., Banerjee S. and Behling S., 1986, "A Qualified Database for the Critical Flow of Water," EPRI-NP-4556, May.

23. Jeandey, C., Gros D'Aillon, L., Bourgin, R. & Barriere, G., "Auto Vaporisation d'Ecoulements Eau/Vapeur," Departement des Reacteurs a Eau Service des Transferts Thermiques (Centre D'Etudes Nucleaires de Grenoble) Report T. T. No. 163, 1981.

24. Jones, O. C., Jr., 1980, "Flashing Inception in Flowing Liquids," Trans. ASME, J. Heat Transfer, Vol. 102, pp. 439-444.

25. Lubin, B. T. and Springer, G. S., 1967, AThe Formation of a Dip on the Surface of a Liquid Draining from a Tank," Journal of Fluid Mechanics, 29, pp. 385-390.

26. Maciaszek, T. and Memponteil, A., 1986, "Experimental Study on Phase Separation in a Tee Junction for Steam-Water Stratified Inlet Flow," Paper C2 presented at European Two-phase Flow Group Meeting, Munich, June 10-13.

27. Moon, Y. M. and No, H. C., 2003, "Offtake and Slug Transition at T-junction of Vertical-up Branch in the Horizontal Pipe," Journal of Nuclear Science and Technology, Vol. 40, No. 5, pp. 317-324.

28. Morrison, A. F., 1977, "Blowdown Flow in the BWR BDHT Test Apparatus," GEAP-21656.

29. Neusen, K. F., 1969, "Optimizing of Flow Parameters for the Expansion of Very Low-quality Steam," University of California, Lawrence Radiation Laboratory, UCRL-6152.

30. Ohkawa, K., "ASSESSMENT OF HOMOGENEOUS NON-EQUILIBRIUM RELAXATION CRITICAL FLOW MODEL," 15th International Conference on Nuclear Engineering, ICONE15-10708, Nagoya, Japan, April 22-26, 2007.

31. Reocreux, M., 1974, "Contribution a l'Etude des Debits Critiques en Econlement Diphasique Eau-Vapeur," Ph.D. Thesis, Universite Scientifique et Medicale de Grenoble, France.

32. Schrock, V. E., et al., 1986, "Small Break Critical Discharge – The Roles of Vapor and Liquid Entrainment in a Stratified Two-phase Region Upstream of the Break," NUREG/CR-4761.

33. Schrock, V. E., Starkman, E. S. & Brown, R. A., 1977, "Flashing Flow of Initially Subcooled Water in Convergent-divergent Nozzles," Journal of Heat Transfer 99 (2).

34. Seynhaeve, J. M., 1980, "Etude Experimentale des Ecoulements Diphasiques Critiques a Faible Titre," Doctoral thesis, Department Thermodynamique et Turbomachines, Universite Catholique de Louvain.

35. Seynhaeve, J. M., et al., 1976, "Non-equilibrium Effects on Critical Flow Rates at Low Qualities," Vol. 2, pp. 672-688, Proceedings of the CSNI Specialist Meeting on Transient Two-phase Flow, Toronto, August 3-4.

36. Smoglie, C. and Reimann, J., 1986, "Two-phase Flow Through Small Branches in a Horizontal Pipe with Stratified Flow," International Journal of Multi-Phase Flow, pp. 609-626.

37. Sozzi, G. L. and Sutherland, W. A., 1975, "Critical Flow of Saturated and Subcooled Water at High Pressure," NEDO-13418.

38. Yonomoto, T. and Tasaka, K., 1988, "New Theoretical Model for Two-phase Flow Discharge from Stratified Two-phase Region Through Small Break," Journal of Nuclear Science and Technology, 25[5], pp. 441-455.

39. Zaloudek, F. R., 1964, "Steam-Water Critical Flow From High Pressure Systems," HW-80535.

40. Zuber, N., 1980, "Problem in Modelling of Small Break LOCA," NUREG-724.

41. Anderson, J. L. and Benedetti, R. L., 1985, "Critical Flow Through Small Pipe Break," EPRI NP-4532.

APPENDIX A
RESULTS OF CRITICAL FLOW ASSESSMENT FOR INDIVIDUAL DATASET

In this appendix, the output for each dataset is given, and comparisons of predicted and measured mass flux for individual test subsection are presented graphically.

A.1 ANDRON & ACKERMAN

a,c

A.2 BOIVIN

a,c

[ ]

A.3 FINCKE & COLLINS

a,c

A.4 JEANDEY

a,c

A.5 NEUSEN

a,c

A.6 REOCREUX

a,c

A.7 SEYNHAEVE

a,c

[ ]

A.8 SOZZI-SUTHERLAND

a,c

A.9 AMOS & SHROCK

a,c

[ ]

A.10 TPFL (ANDERSON & BENEDETTI)

a,c

A.11 MARVIKEN

a,c

A.11.1 MARVIKEN TEST 1

a,c

A.11.2 MARVIKEN TEST 2

a,c

A.11.3 MARVIKEN TEST 3

a,c

A.11.4 MARVIKEN TEST 4

a,c

A.11.5 MARVIKEN TEST 5

a,c

A.11.6 MARVIKEN TEST 6

a,c

A.11.7 MARVIKEN TEST 7

a,c

A.11.8 MARVIKEN TEST 8

a,c

A.11.9 MARVIKEN TEST 9

a,c

A.11.10 MARVIKEN TEST 10

a,c

A.11.11 MARVIKEN TEST 11

a,c

A.11.12 MARVIKEN TEST 12

a,c

A.11.13 MARVIKEN TEST 13

a,c

A.11.14 MARVIKEN TEST 14

a,c

A.11.15 MARVIKEN TEST 15

a,c

A.11.16 MARVIKEN TEST 16

a,c

A.11.17 MARVIKEN TEST 17

a,c

A.11.18 MARVIKEN TEST 18

a,c

A.11.19 MARVIKEN TEST 19

a,c

A.11.20 MARVIKEN TEST 20

a,c

A.11.21 MARVIKEN TEST 21

a,c

A.11.22 MARVIKEN TEST 22

a,c

A.11.23 MARVIKEN TEST 23

a,c

A.11.24 MARVIKEN TEST 24

a,c

A.11.25 MARVIKEN TEST 25

a,c

A.11.26 MARVIKEN TEST 26

a,c

A.11.27 MARVIKEN TEST 27

a,c

A.12 CELATA

a,c

[ ]

13 CORE VOID DISTRIBUTION AND MIXTURE LEVEL SWELL

13.1 INTRODUCTION

Early in a small break LOCA, voids are generated in the primary RCS by flashing and boiling in the core. Because of the small break size, flows in the RCS are primarily gravity-driven. Following the initial rapid depressurization stage of the LOCA, distinct liquid levels are formed at several locations, and most significantly in the core. Below this liquid or two-phase mixture level, the fluid is a low quality two-phase mixture; while above the level, it is primarily single-phase vapor. Liquid levels initially occur in the pressurizer, in the upper head, and in the uphill and downhill steam generator tubing. Eventually, the RCS drains so that the level in the reactor vessel reaches the hot leg. At this point, the rate of system depressurization is low and vapor generation results from boiling in the core, from power produced by decay heat. Because the vapor generation rate resulting from this decay heat can be high, regions in the vessel can achieve a significant void fraction. The two-phase mixture level depends on the interfacial shear exerted by the vapor on the liquid, and as a result, the mixture level can be significantly higher than the collapsed liquid level. The difference between the two-phase mixture level and the collapsed level is a measure of the "mixture level swell," which is defined as:

$$S = \frac{(Z_{2\Phi} - Z_{SAT}) - (Z_{CLL} - Z_{SAT})}{Z_{CLL} - Z_{SAT}} \tag{13-1}$$

where Z_{CLL} is the collapsed liquid level, $Z_{2\Phi}$ is the two-phase mixture level, and Z_{SAT} is the elevation where the liquid reaches the saturation point. Using this definition, a swell of zero corresponds to a two-phase mixture level which is the same as the collapsed liquid level.

Prediction of the mixture level swell and tracking of the mixture level are important [

.]^{a,c} As more liquid is boiled away, the mixture level can eventually drop into the core. While good cooling can be maintained below the mixture level, dryout occurs above the mixture level. Heat transfer above the mixture level is by convection and thermal radiation to steam. These relatively poor modes of heat transfer cause the cladding temperature above the mixture level to increase rapidly. Thus, prediction of the two-phase mixture level in the active core is vital to an accurate prediction of the cladding behavior in a small break or intermediate break LOCA.

13.2 PHYSICAL PROCESSES

As described in Section 13.1, mixture level swell is the process that determines the vertical position of the two-phase interfaces in the system; above the interface the mixture is essentially single-phase vapor. [

]^{a,c}

[

]a,c

Several experimental tests have been run under small or intermediate break LOCA thermal-hydraulic conditions to measure the effects of various parameters on mixture level swell. [

-
-
-]a,c

13.3 WCOBRA/TRAC-TF2 DETERMINATION OF THE MIXTURE LEVEL

The models and correlations for wall and interfacial drag are described in Sections 5.2 through 5.4, Volume 1 of this document. Flow regime transitions are described in Section 4, Volume 1 of this document. These models are used to determine the void fraction distribution within a region. The models and correlations used to determine the critical heat flux elevation are detailed in Section 7.2.3, Volume 1, of this document.

[

]a,c

13.4 ASSESSMENT OF WCOBRA/TRAC-TF2 MIXTURE LEVEL PREDICTIONS

13.4.1 Introduction

There are several separate effects experimental tests that provide data on the mixture level and sometimes mass inventory distribution in a rod bundle under small break LOCA thermal-hydraulic conditions. Four such experimental facilities were modeled with WCOBRA/TRAC-TF2, and several experimental tests were simulated to determine the predictive capability of the code. The tests were as follows:

- The ORNL-THTF Uncovered Bundle Tests by Anklam (Anklam, et al., 1982)
- The Westinghouse G-1 Core Uncovery Tests, WCAP-9764 (WCAP-9764, 1980)

- The Westinghouse G-2 Core Uncovery Tests, EPRI NP-1692 (NP-1692, 1981)
- The JAERI-TPTF Critical Heat Flux Bundle Tests by Guo (Guo, et al., 1993)

Each of these tests, [

]^{a,c} provides information on the cladding heatup elevation; and most provide the mass distribution in a vessel for various thermal-hydraulic conditions. The ORNL-THTF, G-1, and G-2 tests provide mixture level and mass inventories for uncovered rod bundles, and the JAERI-TPTF tests provide critical heat flux elevations for uncovered rod bundles. The following sections discuss each test, the WCOBRA/TRAC-TF2 simulation, and the comparisons between the measured and predicted results.

A comparison of the test conditions versus typical conditions expected in a PWR during the period(s) of interest is presented in Table 13.4.1-1.

The General Electric (GE) Vessel Blowdown Tests by Findlay and Sozzi (Findlay and Sozzi, 1981) provide mass inventory data in a vessel during rapid depressurization. These tests were also simulated with WCOBRA/TRAC-TF2, as described in Section 23.1.1 of this document.

Table 13.4.1-1 Comparison of Test Conditions with Typical PWR Conditions

a,c

13.4.2 ORNL-THTF Small Break Tests

13.4.2.1 Introduction

A series of experimental tests pertinent to WCOBRA/TRAC-TF2 model validation were performed at the ORNL-THTF. Two types of experiments were conducted in the ORNL-THTF. One series consisted of several uncovered bundle heat transfer tests, and the other series consisted of level swell tests. These two different test series are fundamentally the same. In the bundle uncovery tests, the experiment was continued until a steady-state condition was reached in the uncovered part of the bundle and rods were heated to a high temperature. The second type of tests (level swell tests) either did not have bundle uncovery, or only a relatively short portion of the top of the bundle was uncovered. For these tests, a void profile over the entire axial length was obtained.

Additional information on the ORNL-THTF uncovered bundle heat transfer and two-phase mixture level swell tests is contained in NUREG/CR-2456 (Anklam, et al., 1982).

13.4.2.2 ORNL-THTF Facility Description

The ORNL-THTF is a high pressure rod bundle thermal-hydraulics loop. Flow is pumped through the loop via a main coolant pump. After exiting the pump, the flow passes through a turbine meter and then enters the inlet manifold of the test section. The flow does not pass through a downcomer. The flow proceeds upward through the heated bundle and exits through the bundle outlet spool piece. The measurements taken at this spool piece include pressure, temperature, density, and volumetric flow. After leaving the orifice manifold, the flow passes through a heat exchanger and returns to the pump inlet.

The bundle is full height (12 ft) and contains 64 electrically heated rods with internal dimensions typical of a 17x17 PWR fuel bundle. The hydraulic diameter of the test section is consistent with a typical Westinghouse PWR. Figure 13.4.2-1 shows a cross section of the ORNL-THTF test bundle. Four of the rods were unheated to represent control rod guide tubes in a nuclear fuel assembly. Figure 13.4.2-2 shows an axial profile of the ORNL-THTF bundle. The rods have a flat power profile in both the axial and radial directions. The bundle had a heated length of 12 feet (3.66 m) and contained six spacer grids. Thermocouples were located at 25 different axial elevations.

13.4.2.3 Test Matrix for ORNL-THTF Simulations

Simulations of small break LOCAs in PWRs generally show that there are two periods in which the core can possibly be uncovered. The first occurs during the loop seal clearance period. During this uncovery, the primary system pressure [ ]^{a,c} and the two-phased mixture level can drop below the top of the core. The second uncovery occurs if the break flow exceeds the pumped SI flow during the boiloff period. The system pressure during this uncovery is [ ]^{a,c}.

Table 13.4.2-1 lists tests selected for simulation by WCOBRA/TRAC-TF2. As previously discussed there were two different series of tests which were executed at ORNL; one series referred to as the bundle uncovery tests and one as the level swell tests.

Six of the tests are bundle uncovery tests. Three are at relatively low pressure (580 to 650 psia), and three are at high pressure (1010 to 1090 psia). All six had roughly one-half the bundle uncovered. Six other tests are from the level swell test series. Again, three were at low pressure (520 to 590 psia), and three were at high pressure (1090 to 1170 psia). [

]^{a,c}

13.4.2.4 Test Procedure for ORNL-THTF Simulations

All of the experiments in this test series were run within a 24 hour period, which minimized the amount of time required for preheating the facility, and enabled the use of a single instrumentation calibration. The facility was preheated using the accumulating pump heat in the primary flow circuit. Preheating continued until a stable loop temperature of 350°F to 400°F was obtained.

Once the base temperature and pressure were established, the flow was reduced to the pre-determined amount for each experiment. This was accomplished by closing the inlet flooding line and metering the flow through a 1/2 inch flow line.

After the loop was configured for each specific test, the bundle power was applied. Eventually, the test facility settled into a quasi-steady state condition, with the bundle partially uncovered and the inlet liquid mass flow equal to the exiting steam mass flow. The bundle power was then adjusted to produce a peak heater rod temperature of about 1,400°F, and the loop was again allowed to stabilize. Data acquisition was initiated after the loop stabilized, and then the pressure, flow, and power were adjusted for the next test in the series.

13.4.2.5 WCOBRA/TRAC-TF2 Model of the ORNL-THTF

Figure 13.4.2-3 shows the WCOBRA/TRAC-TF2 model of the ORNL-THTF. [

]^{a,c}

13.4.2.6 Simulation of ORNL-THTF Tests

[

]^{a,c}

[

]a,c

13.4.2.7 Summary and Conclusions

[

]a,c

Table 13.4.2-1 ORNL-THTF Test Simulation Matrix				
Test No.	**Pressure(psia)**	**Rod Power (kW/ft)**	**Data Mixture Level (ft)**	**DataCollapsed Liquid Level (ft)**
Bundle uncovery tests				
3.09.10I	650	0.68	8.60	4.39
3.09.10J	610	0.33	8.10	5.31
3.09.10K	580	0.10	6.98	5.31
3.09.10L	1090	0.66	9.02	5.77
3.09.10M	1010	0.31	8.60	6.20
3.09.10N	1030	0.14	6.98	6.10
Level swell tests				
3.09.10AA	590	0.39	11.23	6.56
3.09.10BB	560	0.20	10.85	7.61
3.09.10CC	520	0.10	11.80	9.45
3.09.10DD	1170	0.39	10.61	7.84
3.09.10EE	1120	0.19	11.40	9.35
3.09.10FF	1090	0.098	10.61	9.51

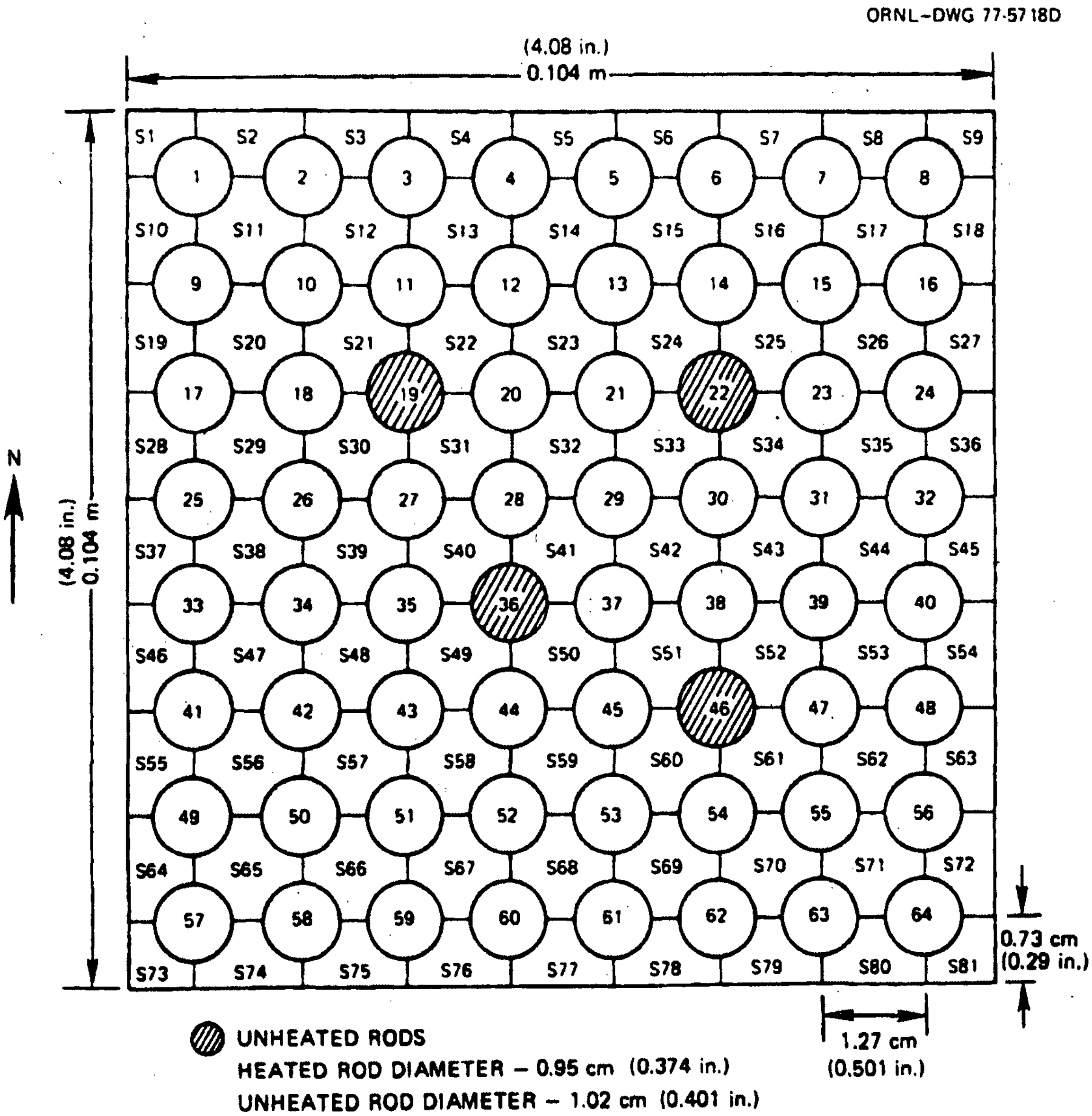

Figure 13.4.2-1 Cross Section of the ORNL-THTF Test Bundle

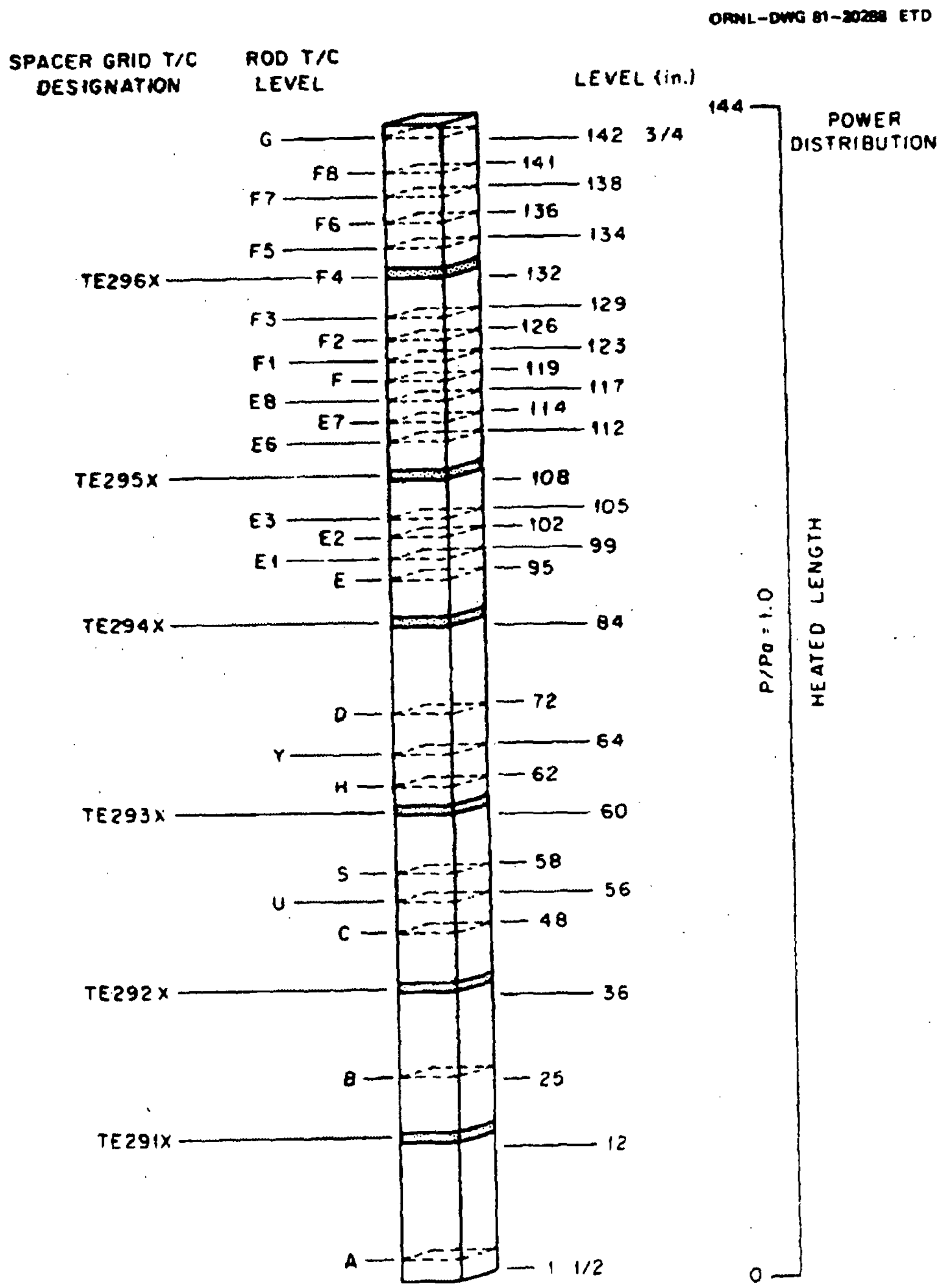

Figure 13.4.2-2 Axial View of the ORNL-THTF Test Bundle

a,c

Figure 13.4.2-3 WCOBRA/TRAC-TF2 Model of the ORNL-THTF

a,c

Figure 13.4.2-4 [

]a,c

a,c

Figure 13.4.2-5 [

]^{a,c}

a,c

Figure 13.4.2-6 [

]a,c

a,c

Figure 13.4.2-7 [

]a,c

a,c

Figure 13.4.2-8 [

]a,c

a,c

Figure 13.4.2-9 [

]a,c

a,c

Figure 13.4.2-10 [

]a,c

a,c

Figure 13.4.2-11 [

]^{a,c}

a,c

Figure 13.4.2-12 [ ]a,c

a,c

Figure 13.4.2-13 [

]a,c

a,c

Figure 13.4.2-14 [ ]a,c

a,c

Figure 13.4.2-15 [

]^{a,c}

a,c

Figure 13.4.2-16 Comparison of Predicted and Measured Void Profiles for YDRAG Sensitivity Study, ORNL – THTF Test 3.09.10I

a,c

Figure 13.4.2-17 **Comparison of Predicted and Measured Void Profiles for YDRAG Sensitivity Study, ORNL – THTF Test 3.09.10J**

a,c

Figure 13.4.2-18 Comparison of Predicted and Measured Void Profiles for YDRAG Sensitivity Study, ORNL – THTF Test 3.09.10K

a,c

Figure 13.4.2-19 Comparison of Predicted and Measured Void Profiles for YDRAG Sensitivity Study, ORNL – THTF Test 3.09.10L

a,c

Figure 13.4.2-20 Comparison of Predicted and Measured Void Profiles for YDRAG Sensitivity Study, ORNL – THTF Test 3.09.10M

a,c

Figure 13.4.2-21 Comparison of Predicted and Measured Void Profiles for YDRAG Sensitivity Study, ORNL – THTF Test 3.09.10N

a,c

Figure 13.4.2-22 Comparison of Predicted and Measured Void Profiles for YDRAG Sensitivity Study, ORNL – THTF Test 3.09.10AA

a,c

Figure 13.4.2-23 Comparison of Predicted and Measured Void Profiles for YDRAG Sensitivity Study, ORNL – THTF Test 3.09.10BB

a,c

Figure 13.4.2-24 Comparison of Predicted and Measured Void Profiles for YDRAG Sensitivity Study, ORNL – THTF Test 3.09.10CC

a,c

Figure 13.4.2-25 Comparison of Predicted and Measured Void Profiles for YDRAG Sensitivity Study, ORNL – THTF Test 3.09.10DD

a,c

Figure 13.4.2-26 Comparison of Predicted and Measured Void Profiles for YDRAG Sensitivity Study, ORNL – THTF Test 3.09.10EE

a,c

Figure 13.4.2-27 Comparison of Predicted and Measured Void Profiles for YDRAG Sensitivity Study, ORNL – THTF Test 3.09.10FF

13.4.3 Simulation of G-1 Core Uncovery Tests

13.4.3.1 Introduction

A series of core uncovery experiments was conducted in the Westinghouse Emergency Core Cooling System (ECCS) High Pressure Test Facility. These tests are pertinent to the validation of the WCOBRA/TRAC-TF2 FULL SPECTRUM LOCA models. [

]^{b}

Additional information on the G-1 Core Uncovery Tests is contained in WCAP-9764 (1980).

13.4.3.2 G-1 Facility Description

[

]^{a,c}

[

]^b

13.4.3.3 Test Matrix for G-1 Uncovery Tests

[

]^b

13.4.3.4 Test Procedure for G-1 Uncovery Tests

[

]b

13.4.3.5 WCOBRA/TRAC-TF2 Model of G-1 Test Facility

[

]a,c

13.4.3.6 Simulation of G-1 Core Uncovery Tests

[

]a,b,c

13.4.3.7 Discussion of Results

[

]a,b,c

[

]a,b,c

13.4.3.8 Summary and Conclusions

[

]a,c

Table 13.4.3-1 Comparison of PWR Rod and G-1 Test Rod Bundle

a,b,c

b

Table 13.4.3-2 G-1 Core Uncovery Test Matrix

Table 13.4.3-3 G-1 Simulation Results Summary at Model Nominal YDRAG

a,b,c

Table 13.4.3-3 G-1 Simulation Results Summary at Model Nominal YDRAG (cont.)

a,b,c

a,b,c

Table 13.4.3-4 YDRAG Values to Match G-1 Level Swell Data

Table 13.4.3-4 YDRAG Values to Match G-1 Level Swell Data (cont.)

a,b,c

b

Figure 13.4.3-1 Westinghouse ECCS High Pressure Test Facility (G-1 Loop)

b

Figure 13.4.3-2 G-1 Test Vessel and Test Section

b

Figure 13.4.3-3A G-1 Uncovery Test Heater Rod Bundle Cross-Section

b

Figure 13.4.3-3B G-1 Uncovery Test Heater Rod Bundle Cross-Section

b

Figure 13.4.3-4 G-1 Facility Heater Rod

b

Figure 13.4.3-5 G-1 Axial Power Profile

a,c

Figure 13.4.3-6 WCOBRA/TRAC-TF2 Model of the G-1 Test Bundle

a,c

Figure 13.4.3-7 Collapsed Liquid Level and Predicted Cladding Temperatures at the 8- and 10- Foot Elevations, G-1 Test 62

a,c

Figure 13.4.3-8 Void Fraction and Predicted Cladding Temperature at the 10- Foot Elevation, G-1 Test 62

a,c

Figure 13.4.3-9 Comparison of Predicted and Measured Mixture Level Swell for G-1 Bundle Uncovery Tests at Model Nominal YDRAG

a,c

Figure 13.4.3-10 Required YDRAG to Recover Data Versus Bundle Power

a,c

Figure 13.4.3-11 Required YDRAG to Recover Data Versus Pressure

a,c

Figure 13.4.3-12 Required YDRAG to Recover Data Versus Bundle Elevation

13.4.4 Simulation of G-2 Core Uncovery Tests

13.4.4.1 Introduction

The G-2 test facility is designed to provide data for downflow film boiling, reflood heat transfer, and core uncovery over a range of power, flow, temperature, and pressure conditions that simulate PWR large break and small break LOCAs. The core uncovery tests conducted at this facility are particularly relevant to the validation of the WCOBRA/TRAC-TF2 mixture level swell prediction; and are therefore the primary topic of this section.

Additional information on the G-2 Core Uncovery Tests is contained in EPRI NP-1692 (1981).

13.4.4.2 G-2 Facility Description

[

]b

[

]b

[

]b

13.4.4.3 Test Matrix for G-2 Uncovery Tests

[

]a,b,c

13.4.4.4 Test Procedure for G-2 Uncovery Tests

[

]b

[

]b

13.4.4.5 WCOBRA/TRAC-TF2 Model of G-2 Test Facility

Figure 13.4.4-6 shows the WCOBRA/TRAC-TF2 model for the G-2 test bundle. [

]a,b,c

13.4.4.6 Simulation of G-2 Uncovery Tests

[

]a,b,c

13.4.4.7 Discussion of Results

[

]a,c

[

]a,c

13.4.4.8 Summary and Conclusions

[

]a,c

Table 13.4.4-1 Comparison of 17x17-XL PWR Rod and Test Rod Bundle

a,b,c

Table 13.4.4-2 G2 Loop Core Uncovery Test Vessel Flow Areas

b

Table 13.4.4-3 G-2 Core Uncovery Test Matrix

b

Table 13.4.4-4 G-2 Simulation Results Summary at Model Nominal YDRAG

a,b,c

a,b,c

Table 13.4.4-5 YDRAG Values to Match G-2 Level Swell Data

b

Figure 13.4.4-1 G-2 Test Facility Flow Schematic

b

Figure 13.4.4-2 G-2 Test Vessel and Test Section

b

Figure 13.4.4-3 G-2 Rod Bundle, Baffle Cross Section, and Bundle Instrumentation

b

Figure 13.4.4-4 G-2 Facility Heater Rod

b

Figure 13.4.4-5 G-2 Facility Axial Power Profile

a,c

Figure 13.4.4-6 WCOBRA/TRAC-TF2 Model of the G-2 Test Bundle

a,c

Figure 13.4.4-7 Collapsed Liquid Level and Predicted Cladding Temperatures at the 8- and 10- Foot Elevations, G-2 Test 716

a,c

Figure 13.4.4-8 Comparison of Predicted and Measured Mixture Level Swell for G-2 Bundle Uncovery Tests at Model Nominal YDRAG

a,c

Figure 13.4.4-9 Required YDRAG to Recover Data Versus Peak Linear Heat Rate

a,c

[ ]

Figure 13.4.4-10 Required YDRAG to Recover Data Versus Pressure

a,c

Figure 13.4.4-11 Required YDRAG to Recover Data Versus Bundle Elevation

13.4.5 JAERI-TPTF Rod Bundle Tests

13.4.5.1 Introduction

The Two-Phase Flow Test Facility (TPTF) is a separate effect test facility built to study small break LOCA thermal-hydraulic behavior. In particular, the heat transfer and critical heat flux (CHF) point in typical SBLOCA conditions. In these tests, the experiment was continued until a steady-state condition was reached in the uncovered part of the bundle and rods were heated to a high temperature. For these tests, the critical heat flux elevation was obtained.

Additional information on the JAERI-TPTF uncovered bundle heat transfer and critical heat flux elevation tests is contained in JAERI-M 93-238 (Guo, et al., 1993).

The JAERI-TPTF rod bundle tests are CHF elevation tests, but cannot be considered level swell tests since no void fraction or collapsed liquid level information is available for these tests. However, the JAERI-TPTF tests are [

]^{a,c}

13.4.5.2 JAERI-TPTF Facility Description

The TPTF was a high pressure rod bundle thermal-hydraulics loop. The bundle was approximately full height for a typical PWR, and contained 25 heated rods in a 5x5 array.

Figure 13.4.5-1 contains a cross-section of the TPTF test bundle. The 25 heated rods were arranged in a square lattice with a pitch of 0.636 inches, and a rod outer diameter (OD) of 0.483 inches. The bundle had a heated length of 145.7 inches, which contained six spacer grids. Ninety-nine (99) thermocouples to measure rod surface temperature were located at 11 different axial elevations on 9 rods. Both the axial and lateral power profiles were uniform for the critical heat flux tests.

Figure 13.4.5-2 shows a flow diagram of the TPTF. The steam drum produces high-pressure saturated water and steam. The steam and water are pumped separately into a mixer at the inlet of the test section. The steam and water flow rates are measured using orifice flowmeters located upstream of the mixer. The pressure and temperature of the mixed fluid are measured at the test section inlet. This two-phase mixture flows into the test section, is heated by the rods, and then exits and returns to the steam drum.

13.4.5.3 Test Matrix for JAERI-TPTF Simulations

Eighteen critical heat flux experiments were conducted at the TPTF. These experiments spanned pressures from 464 to 1773 psia, mass fluxes from 3.49 to 19.18 lbm/ft^2-sec, and peak linear heat rates from 0.38 to 2.12 kW/ft. [

]^{a,c}

13.4.5.4 Test Procedure for JAERI-TPTF Simulations

These tests were conducted by supplying nearly saturated water to the test section. After a constant flow through the test section was achieved, the power to the bundle was turned on. The system was allowed to reach a quasi steady-state, where the inlet flow into the bundle was equal to the steam mass flow exiting the bundle. The bundle power was selected so that the maximum heater rod surface temperature was no more than 1,200°F.

Data was recorded after the steady-state condition was achieved. The dryout or critical heat flux elevation was defined as the average of the lowest thermocouple elevation where the temperature was 36°F above saturation and the adjacent upstream thermocouple. This exercise was performed for both the 5 instrumented rods in the middle of the assembly, as well as the 4 instrumented rods in the outside of the assembly. An average value for all 9 instrumented rods was also determined.

13.4.5.5 WCOBRA/TRAC-TF2 Model of the JAERI-TPTF

Figure 13.4.5-3 shows the WCOBRA/TRAC-TF2 model of the JAERI-TPTF. [

]^{a,c}

13.4.5.6 Simulation of JAERI-TPTF Tests

[

]a,c

13.4.5.7 Summary and Conclusions

[

]a,c

[

]a,c

Table 13.4.5-1 JAERI-TPTF Rod Bundle Uncovery Test Matrix

Run No.	Pressure (psia)	Rod Power (kW/ft)
321	496	1.07
330	495	1.39
340	494	1.62
30	464	1.72
612	1064	0.87
620	1063	1.25
630	1060	1.54
640	1063	1.86
60	1035	2.12
910	1772	0.85
920	1773	1.25
930	1773	1.52
940	1772	1.82
90	1722	2.00

a,c

Table 13.4.5-2 TPTF Simulation Results Summary		

a,c

Table 13.4.5-3 TPTF Simulation YDRAG Sensitivity Study Results				

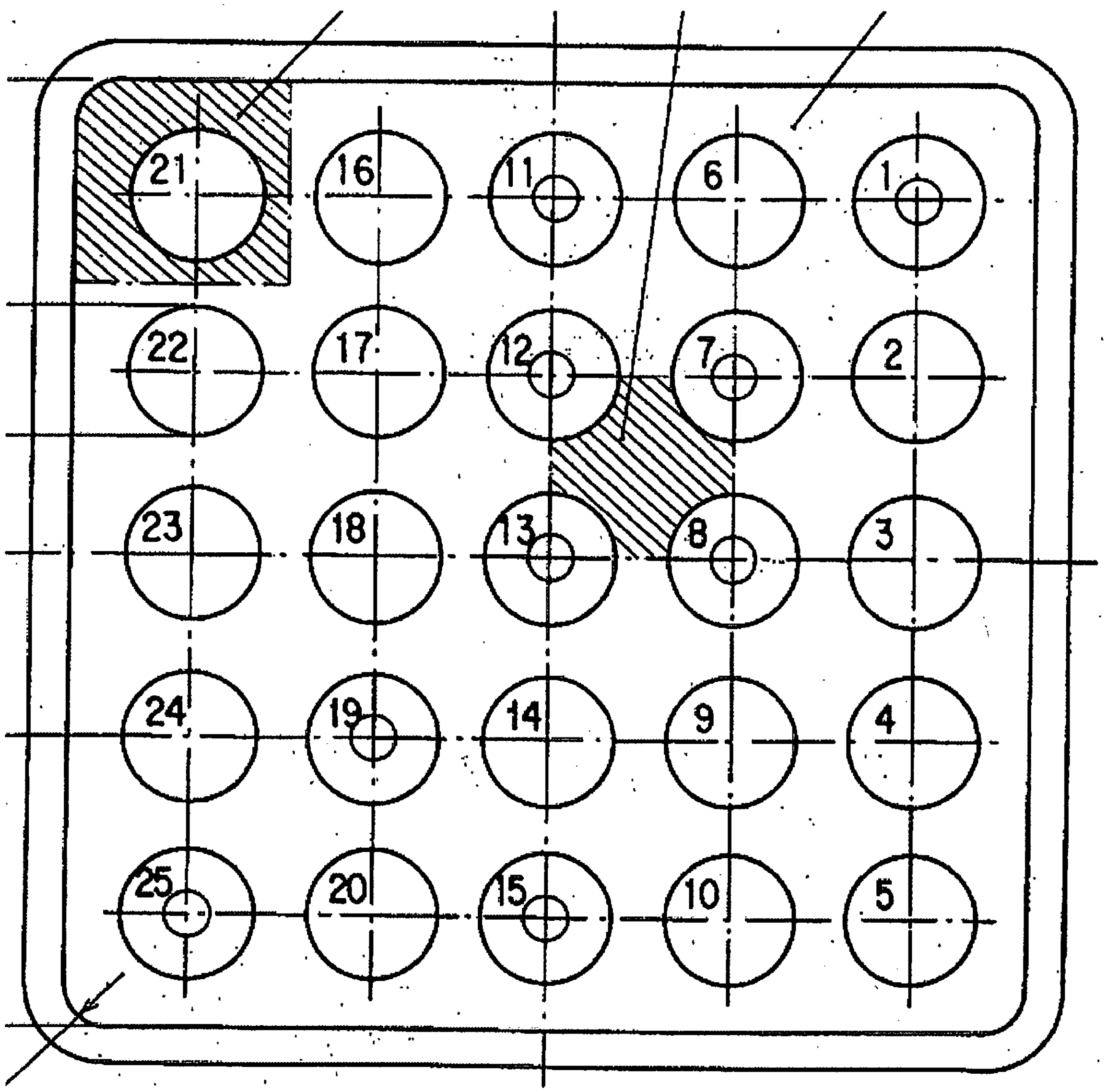

Figure 13.4.5-1 Cross Section of the JAERI-TPTF Test Bundle

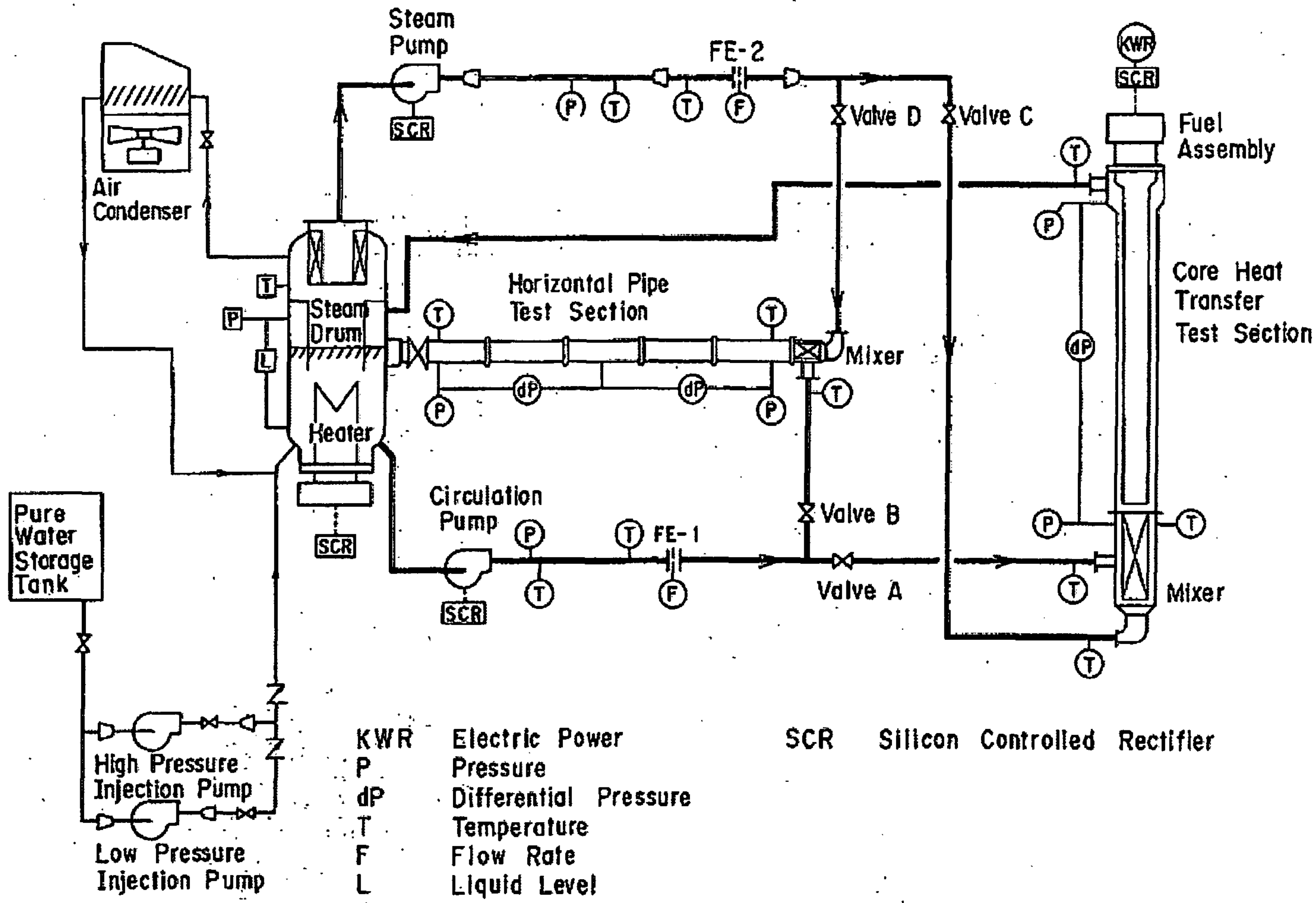

Figure 13.4.5-2 Flow Diagram of the JAERI-TPTF

a,c

Figure 13.4.5-3 WCOBRA/TRAC-TF2 Model of the JAERI-TPTF

a,c

Figure 13.4.5-4 WCOBRA/TRAC-TF2 Predicted Void Fraction Profile, TPTF Test 330

a,c

Figure 13.4.5-5 WCOBRA/TRAC-TF2 Predicted Clad Temperature Profile, TPTF Test 330

a,c

Figure 13.4.5-6 Predicted Versus Measured Critical Heat Flux Elevation

a,c

Figure 13.4.5-7 Predicted Over Measured Critical Heat Flux Elevation Versus Pressure

a,c

Figure 13.4.5-8 Predicted Over Measured Critical Heat Flux Elevation Versus Linear Heat Rate

a,c

Figure 13.4.5-9 Predicted Over Measured Critical Heat Flux Elevation Versus Mass Flux

13.5 SUMMARY AND CONCLUSIONS

[

]a,c

13.6 REFERENCES

1. Anklam, T. M., et al., 1982, "Experimental Investigations of Uncovered Bundle Heat Transfer and Two-Phase Mixture Level Swell Under High Pressure Low Heat Flux Conditions," NUREG/CR-2456.

2. EPRI NP-1692, January 1981, "Heat Transfer Above the two-Phase Mixture Level Under Core Uncovery Conditions in a 336-Rod Bundle," Volumes 1 and 2.

3. Findlay, J. A. and Sozzi, G. L., 1981, "BWR Refill-Reflood Program B Model Qualification Task Plan," NUREG/CR-1899.

4. Guo, Z., et al., December 1993, "Critical Heat Flux for Rod Bundle Under High-Pressure Boiloff Conditions," JAERI-M 93-238.

5. WCAP-9764, 1980, "Documentation of the Westinghouse Core Uncovery Tests and the Small Break Evaluation Model Core Mixture Level Model," Proprietary.

14 SEPARATE EFFECT TESTS USED TO ASSESS CORE HEAT TRANSFER MODEL

14.1 INTRODUCTION

Section 7 in Volume 1 of the WCOBRA/TRAC-TF2 Code Qualification Document (CQD) described the VESSEL component heat transfer package. This package consists of a set of heat transfer correlations and selection logic to determine the appropriate correlation based on the local thermal-hydraulic conditions. The heat transfer package in WCOBRA/TRAC-TF2 produces a continuous boiling curve as a function of wall temperature and local fluid conditions. Figure 14.1-1 shows the heat transfer regime map used by the WCOBRA/TRAC-TF2 vessel component.

Heat transfer is modeled in WCOBRA/TRAC-TF2 as a regime dependent, three step process. Specific models and correlations are used for heat transfer from the wall to vapor field, heat transfer from the wall to the liquid fields, and interfacial heat transfer between the phases. Each of these processes is flow regime dependent and is based on the local hydrodynamic conditions in the computational cell. Section 7 described the wall to fluid heat transfer models, and Section 6 described those for interfacial heat transfer.

The same heat transfer package in WCOBRA/TRAC-TF2 is used for small, intermediate and large break phenomena. No specific logic is included that would result in a difference in small, intermediate and large break heat transfer models.

This section presents the tests used to assess the WCOBRA/TRAC-TF2 heat transfer package against the high ranked core heat transfer phenomena discussed in Section 2.3, Volume 1 and in Table 2-1. This includes [ ]^{a,c}.

Since the core heat transfer package is used for small, intermediate and large break phenomena, the focus of the core heat transfer assessment is heat transfer mode specific, rather than by transient phase. The assessment is broken into three areas: film boiling, single phase vapor and reflood heat transfer. [

]^{a,c} Reflood is considered a special case, which encompasses many of the interactions and entanglements of the core heat transfer PIRT phenomena, and as such will be assessed as a whole.

Single Phase Vapor (SPV)

SPV is predominant during refill and early reflood conditions of a large break, and boiloff/recovery of a small break. The experiments selected for the validation of the WCOBRA/TRAC-TF2 heat transfer package under SPV conditions were chosen from the following test series:

1. Oak Ridge National Laboratory (ORNL) Uncovered Bundle Heat Transfer tests (Anklam et al., 1982).

2. Westinghouse/NRC/EPRI FLECHT-SEASET Reflood Tests (Loftus et al., 1978).

These tests provide reasonable verification of the heat transfer package performance in the high pressure single phase vapor regimes. The tests chosen and their conditions are summarized in Table 14.1-1.

The ranges which these tests cover are compared to the typical PWR ranges in Table 14.1-2. [

]^{a,c}

Dispersed Flow Film Boiling (DFFB)

DFFB is predominant under blowdown and reflood conditions of a large break, and accumulator/safety injection phases of an intermediate break. The experiments selected for the validation of the WCOBRA/TRAC-TF2 heat transfer package under DFFB conditions were chosen from the following test series:

1. Oak Ridge National Laboratory (ORNL) High Pressure Film Boiling Tests (Yoder et al., 1982, Morris et al., 1982, and Mullins et al., 1982).

2. Westinghouse G-1 Intermediate Pressure Blowdown Tests (Cunningham et al., 1974).

3. Westinghouse G-2 Low Pressure Refill Tests (Hochreiter et al., 1976).

[

]^{a,c} The tests chosen and their conditions are summarized in Table 14.1-3.

[

]^{a,c}.

Reflood

The reflood phase of a large break LOCA is characterized by relatively constant, low pressure conditions, with two-phase film boiling and rewet under low flow conditions. As described in Section 2.3.1.2, Volume 1, characteristic features of the reflood transient are the interaction of cold ECCS water with hot fuel rods, and the oscillatory nature of the reflood process. In terms of basic thermal and hydraulic parameters, the reflood process in a typical fuel assembly takes place within the range of conditions depicted in Table 14.1-5.

Pressure, mass velocity, inlet subcooling and steam quality ranges are typically used to characterize the inlet fluid conditions applied to the test assemblies in experiments. Assembly maximum heat rate characterizes the peak power present in the test or fuel assembly, while the average linear heat rate is a measure of the total assembly power. The assembly maximum temperature, while actually a test or predicted result, is important because it identifies whether the tests were in the appropriate heat transfer regime for a sufficient period of time.

[

]^{a,c} The experiments selected for the validation of the WCOBRA/TRAC-TF2 heat transfer package under reflood conditions were chosen from the following test series:

1. Westinghouse/NRC/EPRI FLECHT-SEASET Reflood Tests (Loftus et al., 1978).
2. Westinghouse/NRC FLECHT Low Flooding Rate Tests (Rosal et al., 1975).
3. Westinghouse/NRC FLECHT Skewed Power Reflood Tests (Rosal et al., 1977).
4. Westinghouse/Aerojet FLECHT Supplemental Tests (Cadek et al., 1972).
5. Westinghouse G-2 Reflood Tests (Cunningham et al., 1975).
6. FEBA Reflood Tests (Ihle and Rust, 1984).

The three FLECHT series of tests provide the most comprehensive tests available of heat transfer in rod bundles under constant flooding rate conditions. A broad range of possible assembly conditions, including power distribution, was tested, and detailed fluid and thermal data were obtained. The FEBA tests allow the assessment of a different assembly power distribution from those tested in FLECHT, and the important contribution to heat transfer provided by the fuel assembly grids, since there are tests available with and without grids. The G-2 tests provide data in a bundle of different height, with prototypical mixing vane grids similar to those used in a PWR fuel assembly. The tests chosen and their conditions are summarized in Table 14.1-6.

[

]^{a,c}

[

]a,c

Table 14.1-1 SPV Heat Transfer Test Conditions

Test Series	Test Number	Pressure psia	Vapor Reynolds Number	Steam Cooling Region ft	Power/Rod kW/ft	Comment
ORNL	3.09.10I	650	12,200 – 16,600	9.91-11.88	0.68	
	3.09.10J	620	5,000 – 6,700	9.91-11.88	0.33	
	3.09.10K	580	1,100 – 1,900	7.94-11.88	0.10	
	3.09.10L	1090	13,000 – 17,700	9.91-11.88	0.66	
	3.09.10M	1010	5,100 – 6,500	9.91-11.88	0.31	
	3.09.10N	1030	1,600 – 3,000	7.94-11.88	0.14	
FLECHT SEASET (Steam cooling)	32753	40	18,300 – 20,000	0.0 – 12.0	0.21	The listed rod powers for this test are the peak rod powers.
	36160	39	18,000 – 19,800	0.0 – 12.0	0.16	
	36261	39	14,700 – 16,100	0.0 – 12.0	0.13	
	36362	39	9,100 – 9,900	0.0 – 12.0	0.79	
	36463	40	5,600 – 6,100	0.0 – 12.0	0.48	
	36564	40	4.400 – 4,700	0.0 – 12.0	0.04	
	36766	40	2,800 – 3,000	0.0 – 12.0	0.02	
	36867	39	2,800 – 3,000	0.0 – 12.0	0.02	

Table 14.1-2 Typical Conditions in a PWR During SPV (Blowdown, Refill, Boiloff/Recovery, Reflood)

a,c

Table 14.1-3 DFFB Heat Transfer Test Conditions

Test Series	Test Number	Pressure psia	Mass Flux lbm/s-ft^2	Inlet Temperature °F	Peak Power kW/ft	Comment
ORNL	3.03.6AR	2040	467	513	5.6	
	3.07.9B	1849	146	590	8.3	
	3.07.9C	1805	68.4	559	5.1	
	3.07.9D	1847	10.6	577	6.3	
	3.07.9E	1908	121	579	6.5	
	3.07.9K	635	46.2	415	4.0	
	3.07.9L	1203	108	529	7.0	
	3.07.9M	1242	134	543	7.9	
	3.07.9P	874	107	513	7.4	
	3.07.9Q	947	66.6	502	5.1	
	3.07.9X	872	70.5	514	5.4	
	3.08.6C	1870	214	508	3.4	

b

Table 14.1-4 Typical Conditions in a PWR During DFFB (Blowdown, Refill)

a,c

Table 14.1-5 Typical Conditions in a PWR During Reflood

a,c

Table 14.1-6 Reflood Heat Transfer Test Conditions

Test Series	Test Number	Pressure psia	Flooding Rate in/s	Inlet Subcooling °F	Peak Power kW/ft	Comment
FLECHT SEASET	31805 31203 31701 31504 32013	40 40 40 40 60	0.81 1.51 6.1 0.97 1.04	143 141 140 144 143	0.7 0.7 0.7 0.7 0.7	COSINE POWER SHAPE 17x17 ROD ARRAY
FLECHT LOW FLOODING RATE	05029 05132 04641	40 40 20	0.85 1.0 1.0	141 140 139	0.73 0.95 0.95	COSINE POWER SHAPE 15x15 ROD ARRAY
FLECHT SKEWED	15305 13812 15713 13914 13609	40 41 40 21 21	0.8 1.0 1.0 1.0 1.0	140 83 2 5 141	0.7 0.7 0.7 0.7 0.7	TOP SKEWED POWER SHAPE 15x15 ROD ARRAY

b

a,c

Figure 14.1-1 WCOBRA/TRAC-TF2 Heat Transfer Regime Map (from Figure 7.2-3)

14.2 TEST FACILITIES DESCRIPTION

14.2.1 Test Facilities Used to Assess Single-Phase Vapor (SPV)

14.2.1.1 Oak Ridge National Laboratory Thermal Hydraulic Test Facility (ORNL-THTF) Uncovered Bundle Heat Transfer Tests

A series of steady-state experiments investigating small break LOCA phenomena was performed in the ORNL-THTF high pressure rod bundle thermal-hydraulics loop, as reported in NUREG/CR-2456 (Anklam, et al., 1982). The test facility, test procedure and test conditions are described in more detail in Section 13.4.2 of this report. The uncovered bundle tests provided local conditions for pressure, mass flow, quality, and steam temperature, which were used as input to a driver program containing the WCOBRA/TRAC-TF2 code heat transfer package for assessment. Table 14.1-1 lists the thermal-hydraulic conditions of the six selected ORNL-THTF uncovered bundle tests used to evaluate the WCOBRA/TRAC-TF2 film boiling heat transfer models as part of the heat transfer driver program.

14.2.1.2 FLECHT-SEASET Steam Cooling Tests

The FLECHT-SEASET test series was conducted in order to provide an experimental data base at low flooding rates for simulated Westinghouse 17x17 fuel rods as described by Conway et al. (1977). The data from these tests were evaluated by Lee et al. (1982). The tests and experimental facility are described in more detail in Section 14.2.3.1 of this report. Tests 32753, 36160, 36261, 36362, 36463, 36564, 36766, and 36867 were simulated in order to demonstrate the ability of WCOBRA/TRAC-TF2 to predict the thermal-hydraulic phenomena observed in each test and to verify the ability of the code to predict the single-phase vapor heat transfer observed in the tests. Table 14.1-1 lists the thermal-hydraulic conditions of the eight selected FLECHT-SEASET steam cooling tests used to evaluate the WCOBRA/TRAC-TF2 single-phase vapor heat transfer models.

14.2.2 Test Facilities Used to Assess Dispersed Flow Film Boiling (DFFB) Heat Transfer

14.2.2.1 ORNL-THTF High Pressure Film Boiling Tests

The ORNL-THTF high pressure film boiling tests are one source of data for validating the heat transfer predictions of WCOBRA/TRAC-TF2 in the DFFB regimes of interest for LOCAs. A series of high-pressure steady-state upward DFFB tests in a rod bundle was performed in the ORNL-THTF and is discussed by Yoder (Yoder, et al., 1982). [

]^{a,c} The conditions for these tests are listed in Table 14.2.2.1-1. As seen in the table, these tests were conducted for pressures ranging from 23 bar (635 psia) to 132 bar (1908 psia) at flow rates from 226 kg/s-m^2 (46.2 lbm/s-ft^2) to 713 kg/s-m^2 (146 lbm/s-ft^2). These tests provided local conditions for pressure, mass flow, quality, and steam temperature at the tube exit, which were used as input to a driver program containing the WCOBRA/TRAC-TF2 code heat transfer package for assessment.

Additional ORNL-THTF tests were conducted to investigate heat transfer during dispersed flow film boiling (Morris et al., 1982). These tests simulate dryout and film boiling phenomena at high pressure in a transient condition. The initial conditions for these tests are listed in Table 14.2.2.1-2. To help validate the film boiling heat transfer models of WCOBRA/TRAC-TF2, two of the dispersed flow film boiling tests were simulated using WCOBRA/TRAC-TF2, as well as one of the steady-state tests.

14.2.2.1.1 Facility Description

The test facility is the same as that described in Section 13.4.2.

14.2.2.1.2 Test Procedure

During steady-state operation of the ORNL-THTF, the inlet flow at the bottom of the test section was established and the loop was adjusted to provide the desired inlet fluid temperature and inlet quality. The bundle power was then increased until the dryout (CHF) point was obtained. The steady-state point was assumed to be reached when both pressure and rod surface temperatures stabilized. The results of both rod surface conditions and local equilibrium fluid conditions were then reported as cross-sectional average values for each level. Table 14.2.2.1-1 lists the thermal-hydraulic conditions of the 10 selected ORNL-THTF steady-state film boiling tests used to evaluate the WCOBRA/TRAC-TF2 film boiling heat transfer models as part of the heat transfer driver program.

The following describes the tests used for full experiment simulation.

Steady-State Test – In the steady-state experiment (3.07.9B – Yoder et al., 1982), inlet flow at the bottom of the test section was established and adjusted such that the desired flow rate, temperature, and pressure was reached. The bundle power was increased until the dryout point was at the desired position in the bundle. When the operating pressure and rod surface temperature were stabilized, steady-state was assumed. The test conditions are listed in Table 14.2.2.1-2.

Transient Tests – The first step in the transient experiments (3.08.6C and 3.03.6AR – Mullins et al., 1982) was to establish steady-state conditions prior to the initiation of the transients. The initial conditions for the two selected transient tests are also listed in Table 14.2.2.1-2.

Once steady-state conditions were achieved, the transients were initiated by breaking the outlet rupture disk assembly. The outlet break areas were 0.486 square inches and 0.583 square inches for Tests 3.08.6C and 3.03.6AR, respectively. Following the breaking of the outlet rupture disk, bundle power was ramped up from the initial steady-state levels to near maximum power levels, over a period of time to prolong the film boiling. Then the power was ramped down slowly. The pump was turned off at transient initiation for Test 3.03.6AR, while the pump was left on during the first 20 seconds for Test 3.08.6C.

Figures 14.2.2.1-1 through 14.2.2.1-3 provide the inlet mass flow rates, outlet pressure and test section bundle power for Test 3.03.6AR. Figures 14.2.2.1-4 through 14.2.2.1-6 provide the inlet mass flow rates, outlet pressure and test section bundle power for Test 3.08.6C.

Table 14.2.2.1-1 ORNL-THTF Steady-State DFFB Initial Test Condition

Test	Pressure psia	Mass Flux lbm/s-ft^2	Inlet Quality	Inlet Temperature F	Power kW/ft
3.07.9B	1850	146	-0.107	624.7	8.3
3.07.9C	1806	68.4	-0.179	621.4	5.2
3.07.9D	1849	106	-0.154	624.5	6.3
3.07.9E	1910	121	-0.155	629.0	6.5
3.07.9K	635	46.3	-0.128	492.3	4.1
3.07.9L	334	108	-0.082	567.4	7.1
3.07.9M	1243	135	-0.061	571.4	8.1
3.07.9P	875	107	-0.029	528.4	7.4
3.07.9Q	947	66.6	-0.067	537.9	5.2
3.07.9X	872	70.5	-0.026	528.0	5.4

Table 14.2.2.1-2 ORNL-THTF Initial Test Conditions for WCOBRA/TRAC-TF2 Simulation

a,c

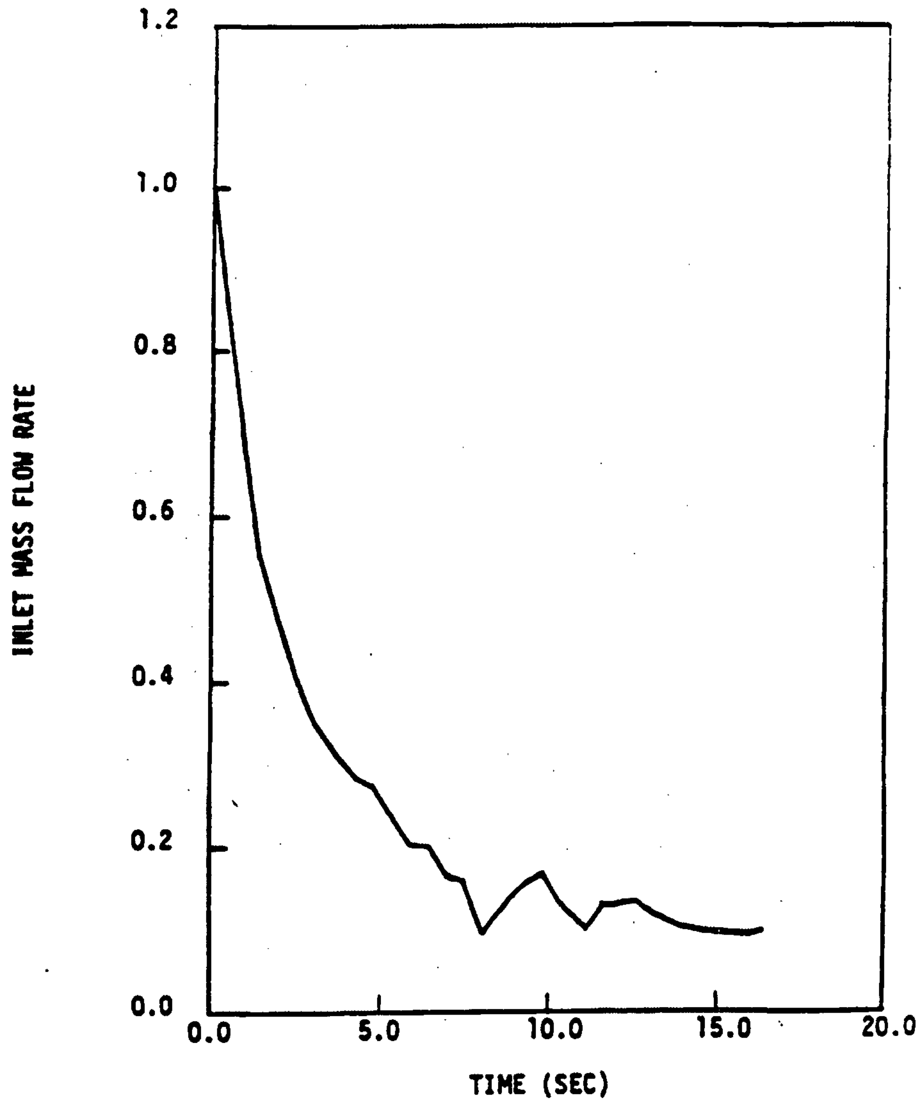

Figure 14.2.2.1-1 **Inlet Mass Flow Rate Forcing Function Normalized to Initial Condition, Test 3.03.6AR**

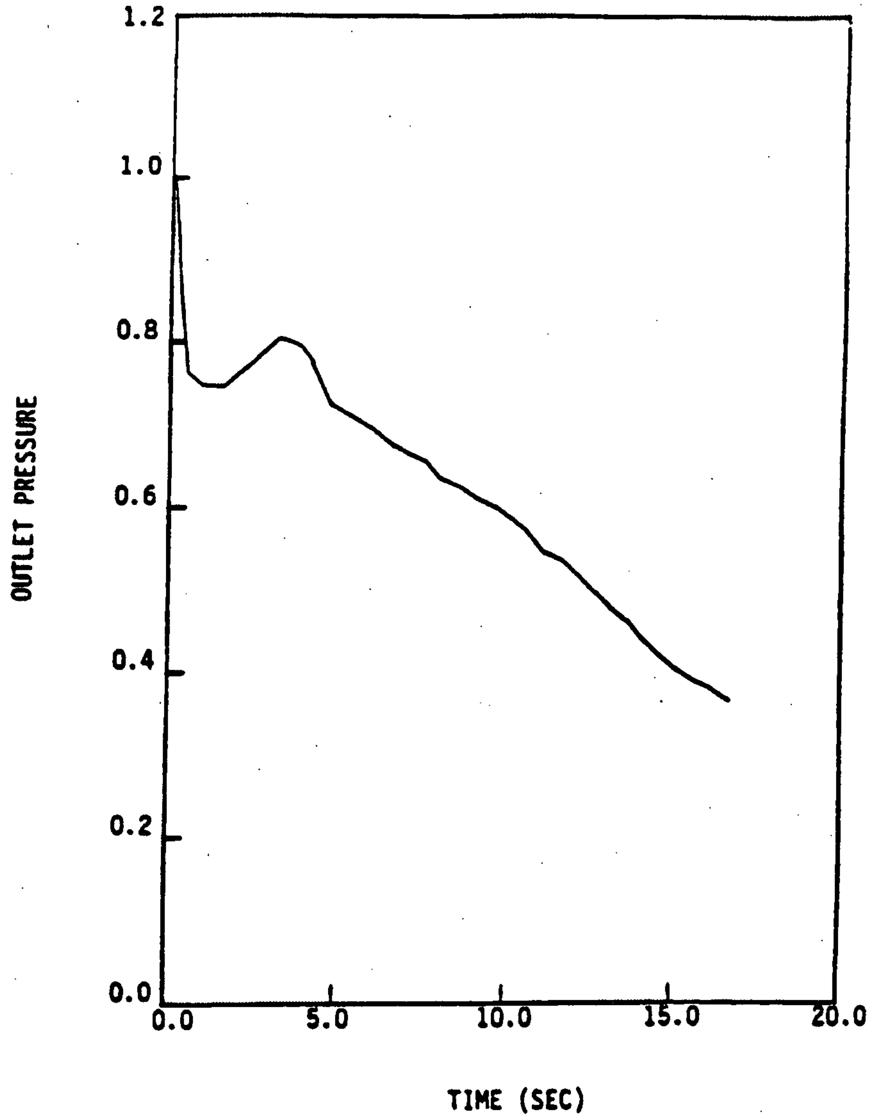

Figure 14.2.2.1-2 Outlet Pressure Forcing Function Normalized to Initial Condition, Test 3.03.6AR

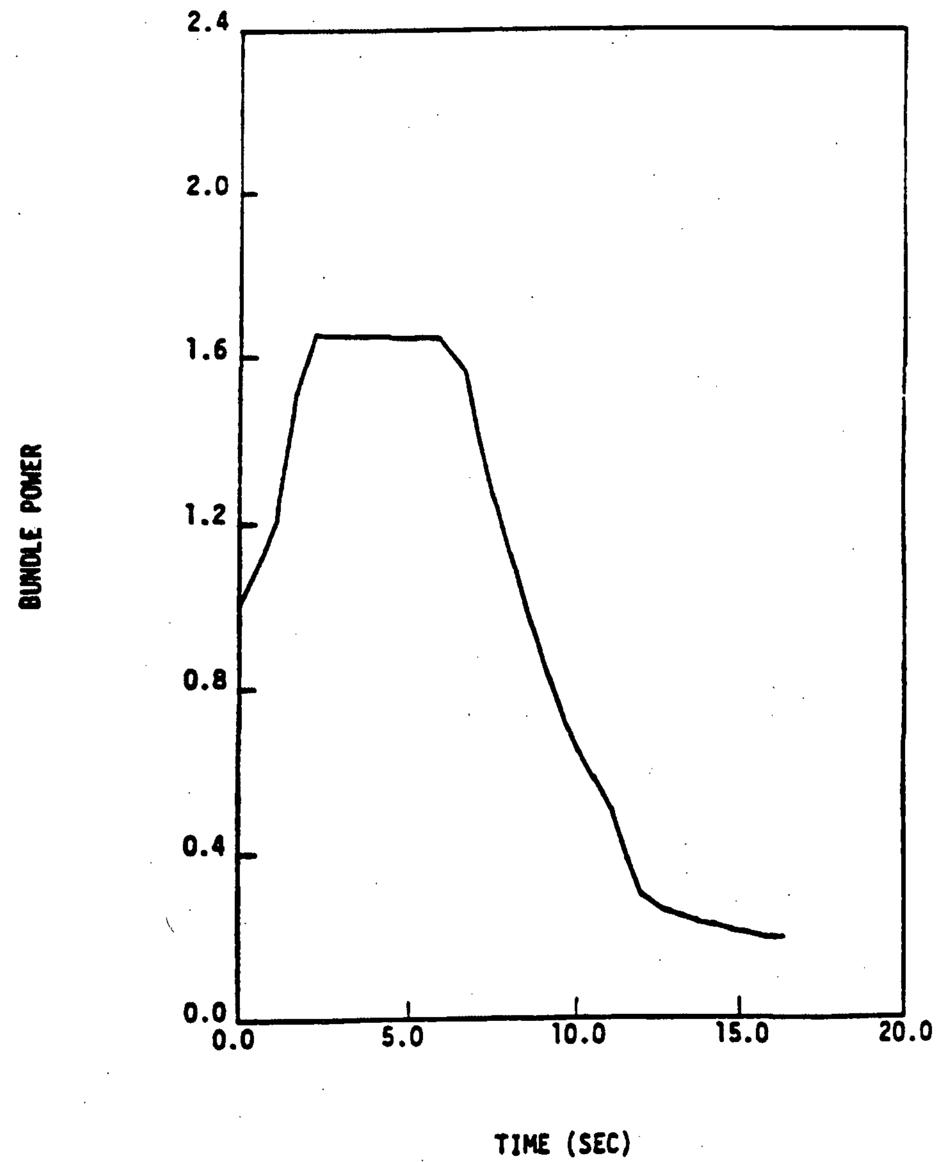

Figure 14.2.2.1-3 Test Section Bundle Power Forcing Function Normalized to Initial Condition, Test 3.03.6AR

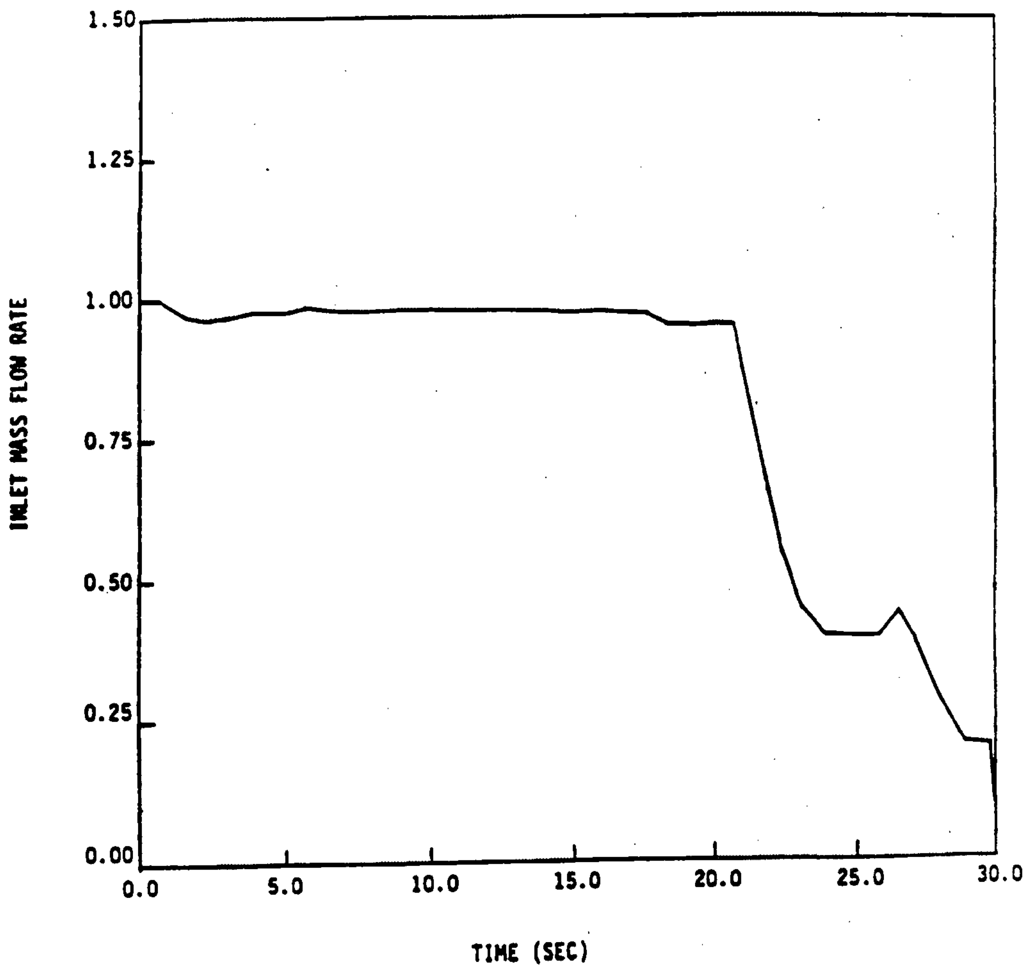

Figure 14.2.2.1-4 Inlet Mass Flow Rate Forcing Function Normalized to Initial Condition, Test 3.08.6C

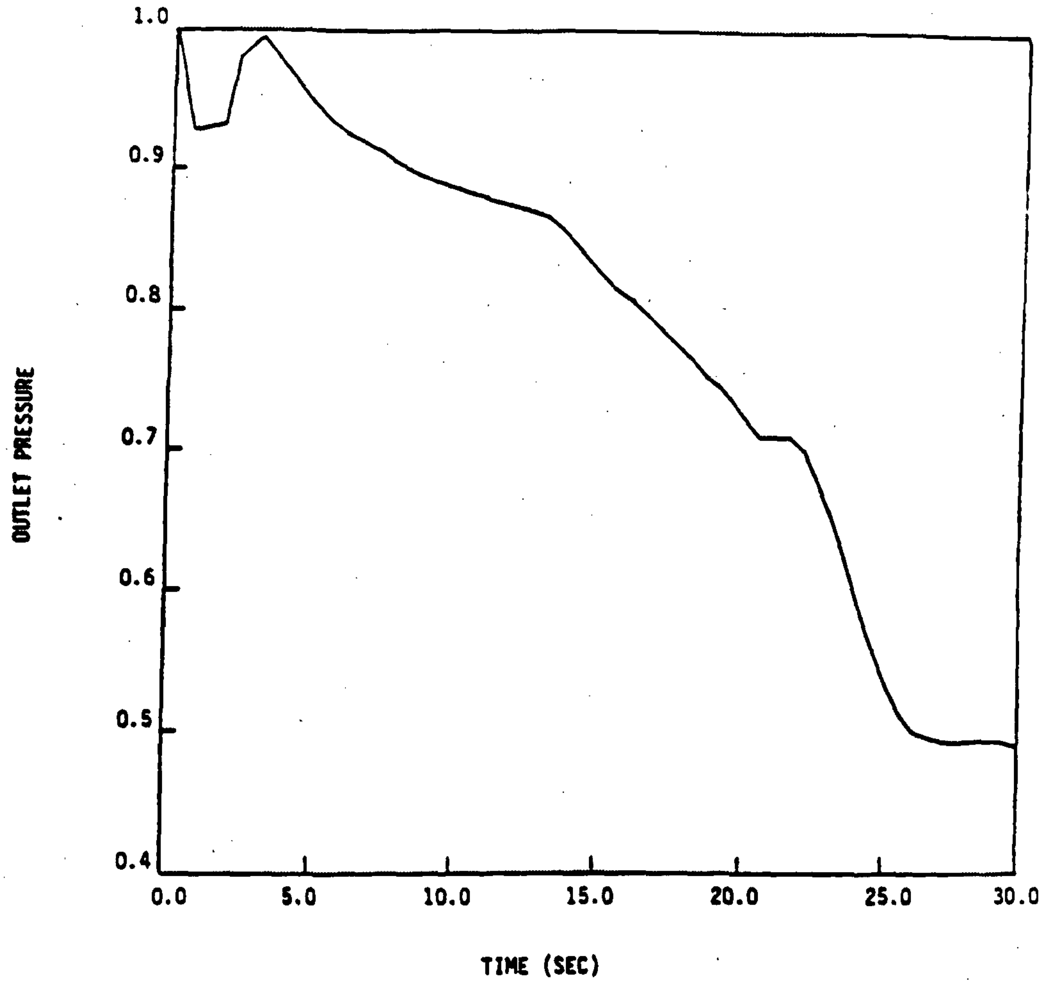

Figure 14.2.2.1-5 Outlet Pressure Forcing Function Normalized to Initial Condition, Test 3.08.6C

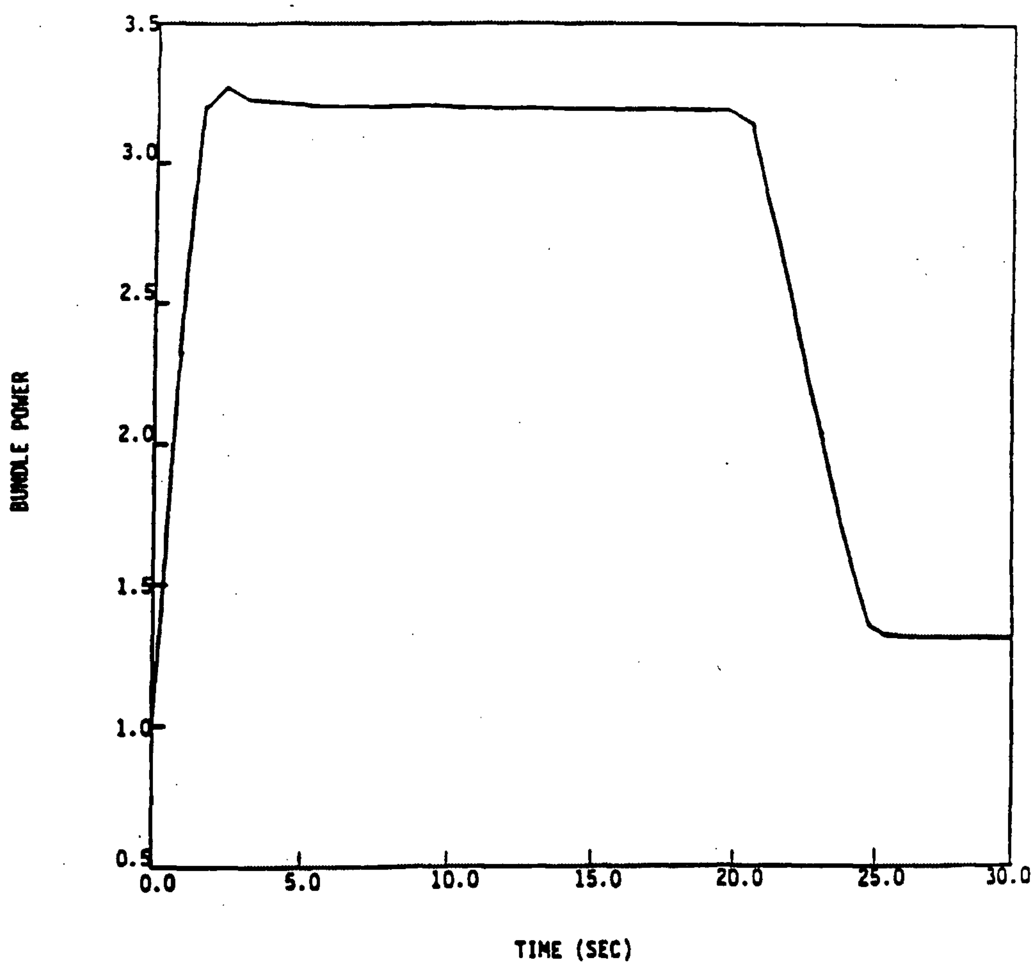

Figure 14.2.2.1-6 Test Section Bundle Power Forcing Function Normalized to Initial Condition, Test 3.08.6C

14.2.2.2 G-1 Intermediate Pressure Blowdown Heat Transfer Experiments

These experiments were designed to provide data which could be used to verify heat transfer models applicable to the analysis of heat transfer during the blowdown portion of a large break Loss-of-Coolant Accident (LOCA) in a Pressurized Water Reactor (PWR). They will be used to demonstrate the adequacy of the film boiling models in WCOBRA/TRAC-TF2.

14.2.2.2.1 Facility Description

The G-1 test facility, Figure 14.2.2.2-1, was designed to simulate thermal-hydraulic conditions calculated for a PWR during the blowdown portion of a LOCA. The facility could be operated at pressures up to 2000 psig and temperatures up to 650°F. The test facility's original purpose was to verify the performance of the Upper Head Injection (UHI) ECCS which was installed in some PWRs. The UHI system injected subcooled water into the top of the core during the blowdown phase of the LOCA. During the same time period, two-phase mixture from the upper plenum and reactor coolant loops was expected to flow into the core and provide additional cooling. Both of these processes were simulated in the test facility.

A detailed description of this facility is contained in Section 13.4.3.2 of this topical. However, a brief summary of the facility description is provided below.

[

]b

14.2.2.2.2 Test Procedure

[

]b

[

]b

Table 14.2.2.2-1 Comparison of PWR Rod and G-1 Test Rod Bundle

a,b,c

)		

Note:
1. For purposes of comparison the cladding values are for 1000°F and the filler values for 2000°F.

Table 14.2.2.2-2 G-1 Initial Test Conditions

b

b

Figure 14.2.2.2-1 Diagram of G-1 Facility (from Cunningham, et al., 1974)

b

Figure14.2.2.2-2 G-1 Test Vessel (from Cunningham, et al., 1974)

b

Figure 14.2.2.2-3 G-1 Heater Rod (from Cunningham, et al., 1974)

b

Figure 14.2.2.2-4 G-1 Heater Rod Axial Power Profile (from Cunningham, et al., 1974)

b

Figure 14.2.2.2-5 G-1 Bundle Cross Section and Instrumentation (from Cunningham, et al., 1974)

14.2.2.3 G-2 Low Pressure Refill Heat Transfer Experiments

Low pressure Upper Head Injection (UHI) refill tests conducted at the Westinghouse G-2 test facility were simulated using the WCOBRA/TRAC-TF2 computer code. Comparisons of the WCOBRA/TRAC-TF2 results to the refill test experimental data can be used to help assess the capability of WCOBRA/TRAC-TF2 to accurately predict top-down quench phenomena, low pressure film boiling, and countercurrent film boiling heat transfer.

14.2.2.3.1 Facility Description

[

]b

A detailed description of this facility is contained in Section 13.4.4.2 of this topical. However, a brief summary of the facility description is provided below.

[

]b

14.2.2.3.2 Test Procedure

[

]b Figure 14.2.2.3-6 shows the low pressure UHI refill test sequence of events. Table 14.2.2.3-2 summarizes the test conditions of the tests which were simulated with WCOBRA/TRAC-TF2.

Table 14.2.2.3-1 Comparison of 17x17 PWR Fuel Rod and G-2 Test Rod

a,b,c

Table 14.2.2.3-2 G-2 Refill Initial Test Conditions

a,b,c

b

[redacted]

Figure 14.2.2.3-1 G-2 Test Facility Flow Schematic (from Cunningham, et al., 1975)

b

Figure 14.2.2.3-2 G-2 Loop Heater Rod (from Cunningham, et al., 1975)

b

Figure 14.2.2.3-3 G-2 Loop Heater Rod Axial Power Profile (from Cunningham, et al., 1975)

b

Figure 14.2.2.3-4 Test Rod Bundle, Cross Section and Instrumentation (from Cunningham, et al., 1975)

b

Figure 14.2.2.3-5 G-2 Loop Ground Plate (from Cunningham, et al., 1975)

b

Figure 14.2.2.3-6 Low Pressure UHI Refill Test Sequence of Events (from Hochreiter, et al., 1976)

14.2.3 Test Facilities Used to Assess Reflood Heat Transfer

14.2.3.1 FLECHT-SEASET Reflood Tests

The FLECHT-SEASET test series was conducted in order to provide an experimental data base at low flooding rates for simulated Westinghouse 17x17 fuel rods. The tests and experimental facility are described by Conway et al. (1977) and the data from these tests were evaluated by Lee et al. (1982). Tests 31203, 31504, 31701, 31805, and 32013 were simulated in order to demonstrate the ability of WCOBRA/TRAC-TF2 to predict the thermal-hydraulic phenomena observed in each test and to verify the ability of the code to predict the parametric trends found in the tests. The test conditions for these experiments are shown in Table 14.2.3.1-1. Each of these tests had a peak rod power of 0.7 kW/ft and a uniform radial power shape.

14.2.3.1.1 Facility Description

A diagram of the FLECHT-SEASET test bundle is shown in Figure 14.2.3.1-1. The test section consisted of 161 electrical heater rods (93 non-instrumented and 68 instrumented) arranged in a square pitch with dimensions comparable to 17x17 PWR fuel rod arrays. The rod diameter was 0.374 inches and the rod pitch was 0.496 inches. The bundle also contained 16 control rod guide tubes of 0.484-inch diameter and eight solid filler rods. The triangular filler rods reduced the excess flow area to within 5 percent of the power/flow area ratio of a PWR fuel assembly. The test section was enclosed by a cylindrical stainless steel housing and was connected to an upper and lower plenum. The housing, with an inside diameter of 7.625 inches, was insulated from the outside air to reduce the heat loss to the environment. The bundle flow area was 24.1 square inches. The upper ends of both the housing and test rods were bolted to the top of the test assembly. The lower ends were allowed to hang free permitting axial movement. Horizontal movement and/or bowing of the heater rods was restricted by grid spacers located at 20.5-inch intervals, starting at the beginning of the heated length.

The electrical heater rods were constructed of a spiral-wound heating element embedded in a boron-nitride insulator. A chopped cosine power profile with a peak/average ratio of 1.66 was approximated by a seven-step power profile. The length of each power step and the peak-to-average power factors are shown in Figure 14.2.3.1-2 along with the location of six grid spacers. (Grids at the top and bottom of the bundle are not shown.)

Type K thermocouples were mounted in 68 of the heater rods and in four of the thimble tubes. Differential pressure cells were located every 12 inches along the test section and provided data used in determining mass balance and the bundle void fraction. Steam probes were placed in the bundle and in the test section outlet. The probes were located in the thimble tubes and were designed to separate moisture from the high temperature steam and then aspirate the steam across a thermocouple.

14.2.3.1.2 Test Procedure

The tests were conducted by first pressurizing the test section to the desired system pressure by valving steam from a boiler into the system and the exhaust line control valve. Water was then injected into the test section lower plenum until it reached the beginning of the heated length of the bundle heater rods. Power was next applied to the bundle and the rods were allowed to heatup. When the temperature of any two bundle thermocouples exceeded the pre-selected value of 1600°F, the bundle was reflooded at a specified rate and power was decreased to match the ANS 1971 + 20 percent decay heat rate.

Table 14.2.3.1-1 Test Conditions for FLECHT-SEASET Tests			
Test No.	**Forced Injection Rate in/s**	**Upper Plenum Pressure psia**	**Injection Water Temperature °F**
31805	0.81	40	124
31504	0.97	40	123
32013	1.04	60	150
31203	1.51	40	126
31701	6.1	40	127

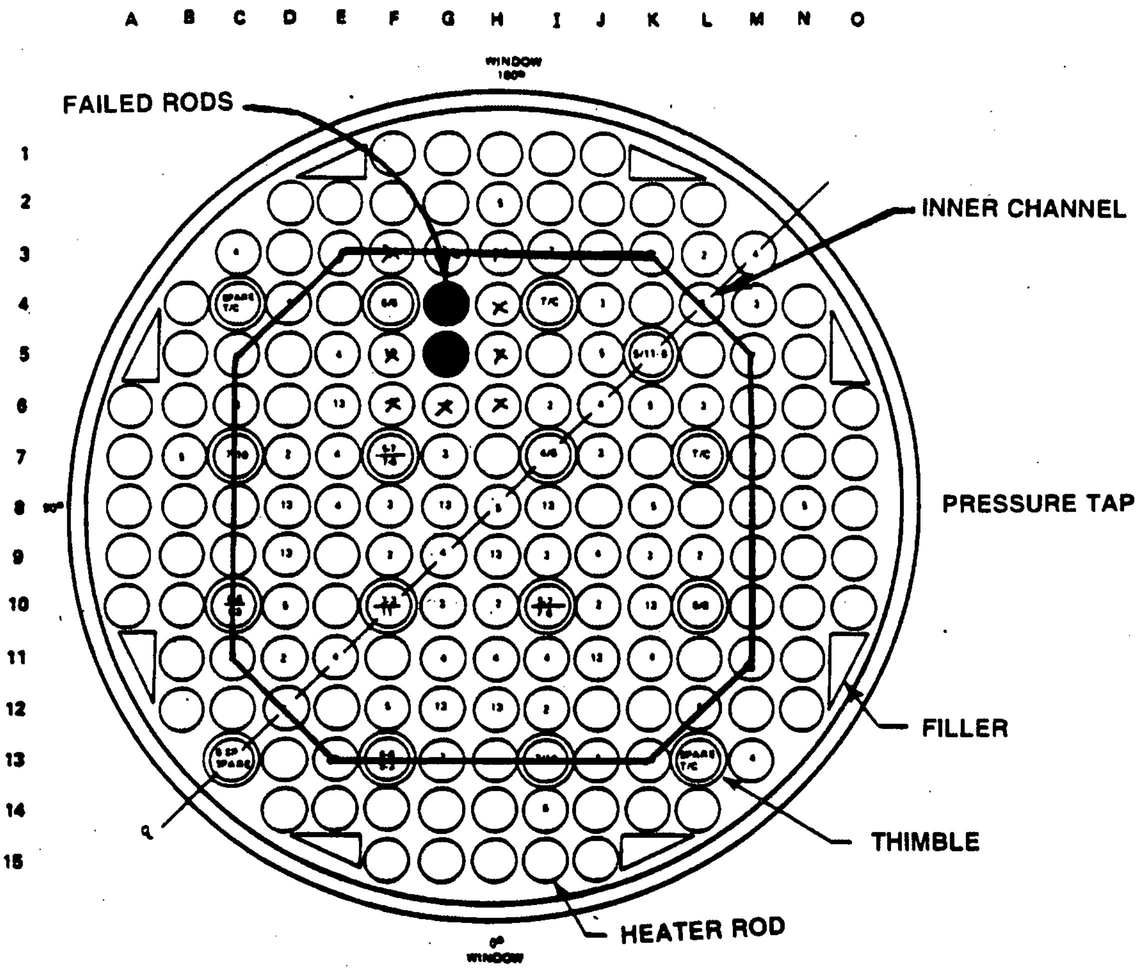

BUNDLE STATISTICS

HOUSING INSIDE DIAMETER	194.0 mm (7.625 in.)
HOUSING WALL THICKNESS	5.08 mm (0.200 in.)
ROD DIAMETER	9.50 mm (0.374 in.)
THIMBLE DIAMETER	12.0 mm (0.474 in.)
ROD PITCH	12.6 mm (0.496 in.)
CROSS-SECTIONAL FLOW AREA	15571 mm^2 (24.136 in.^{2})
FILLER DIMENSIONS	18.8 x 8.43 mm (0.741 x 0.332 in.)
161 HEATER RODS	— —
16 THIMBLES	— —
8 FILLERS	— —

Figure 14.2.3.1-1 FLECHT-SEASET Rod Bundle Cross Section (from Loftus, et al., 1981)

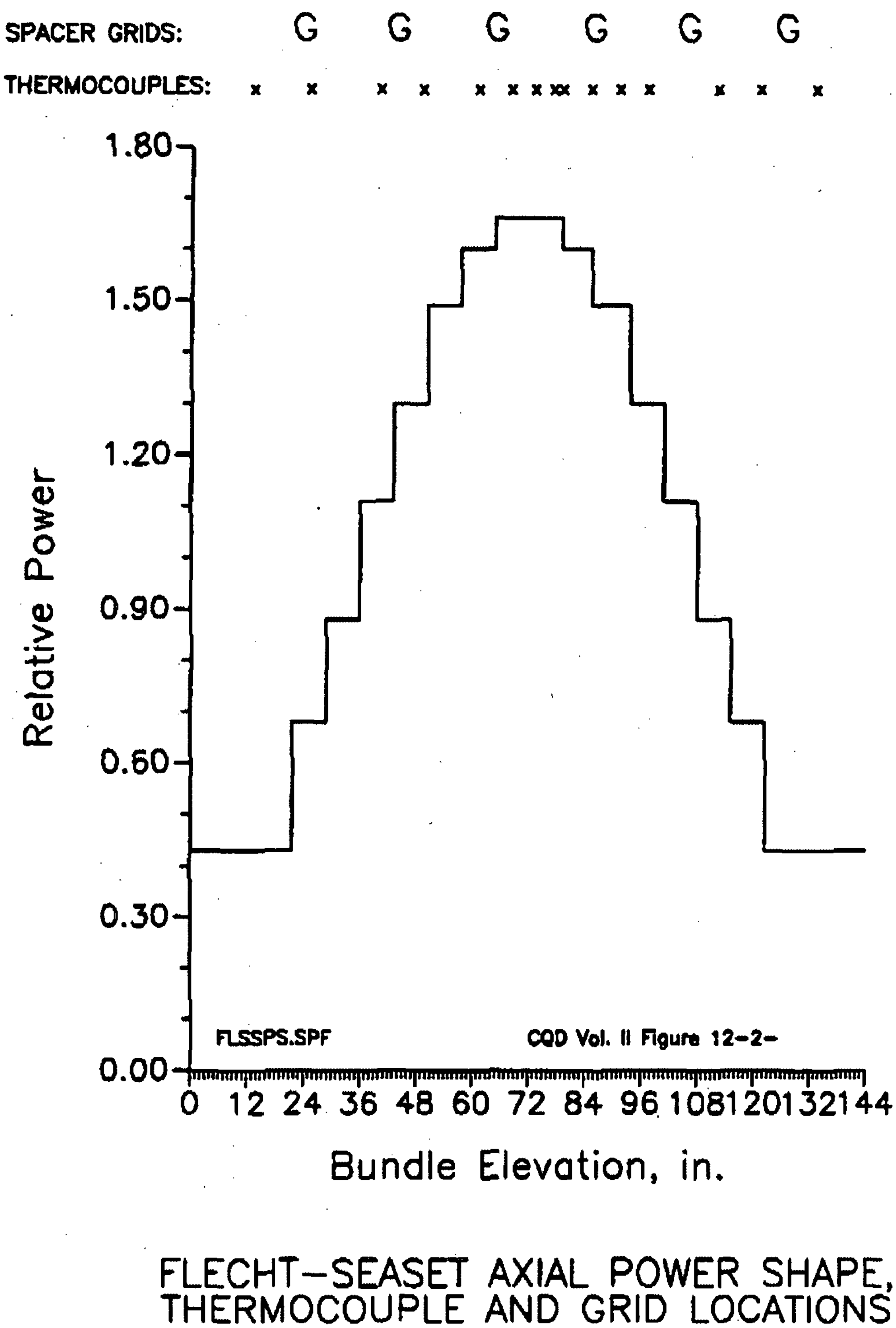

Figure 14.2.3.1-2 FLECHT-SEASET Axial Power Shape Profile and Grid Locations

14.2.3.2 FLECHT Low Flooding Rate Tests

The FLECHT Low Flooding Rate Cosine Power Shape Test series was conducted to provide experimental data for Westinghouse 15x15 fuel. The tests and the experimental facility are described by Rosal et al. (1975). Tests 05029, 05132, and 04641 were simulated to demonstrate the ability of WCOBRA/TRAC-TF2 to predict the thermal-hydraulic phenomena observed in these experiments. The test conditions for these tests are shown in Table 14.2.3.2-1. These tests had a cosine axial power shape with a peak to average power ratio of 1.66.

14.2.3.2.1 Facility Description

A diagram of the FLECHT test bundle is shown in Figure 14.2.3.2-1. The test section consisted of 91 electrical heater rods arranged in a square pitch with dimensions comparable to 15x15 PWR fuel rod arrays. The rod diameter was 0.422 inches and the rod pitch was 0.563 inches. The test bundle also contained eight control rod guide tubes and one instrument tube in a 10x10 square array. The test section was enclosed by a square, 0.7-inch thick carbon steel housing, and was connected to upper and lower plenums. The housing had internal dimensions of 5.889 inches x 5.889 inches, and was insulated from the outside air to reduce heat loss to the environment. Horizontal movement and/or bowing of the heater rods was restricted by eight grid spacers located at 20.5-inch intervals, starting at the beginning of the heated length.

The electrical heater rods were constructed of a spiral-wound heating element embedded in a boron-nitride insulator. A chopped cosine power profile with a peak/average ratio of 1.66 was approximated by a seven-step power profile. The length of each power step and the peak to average power factors are shown in Figure 14.2.3.2-2 along with the location of the grid spacers.

The bundle was assembled with 6 heater rods instrumented with 8 thermocouples, 15 rods with 5 thermocouples, 22 rods with 3 thermocouples and 48 un-instrumented rods.

Test section instrumentation also included fluid and wall thermocouples in the upper and lower plenums, differential pressure transducers which measured pressure drops every two feet along the heated length of the rod bundle, and an overall pressure drop across the entire bundle. A static pressure transducer connected to the upper plenum monitored the test section pressure.

14.2.3.2.2 Test Procedure

The tests were conducted by first pressurizing the test section to the desired system pressure by valving steam from a boiler into the system and the exhaust line control valve. Water was then injected into the test section lower plenum until it reached the beginning of the heated length of the bundle heater rods. Power was next applied to the bundle and the rods were allowed to heatup. When the temperature of any two bundle thermocouples exceeded a pre-selected value, the bundle reflood was initiated and power was decreased to match the ANS 1971 + 20 percent decay heat rate.

Table 14.2.3.2-1 Test Conditions for FLECHT Low Flooding Rate Tests				
Test No.	**Forced Injection Rate in/s**	**Upper Plenum Pressure psia**	**Injection Water Temperature °F**	**Peak Rod Power kW/ft**
05029	0.85	40	126	0.73
05132	1.0	40	127	0.95
04641	1.0	20	89	0.95

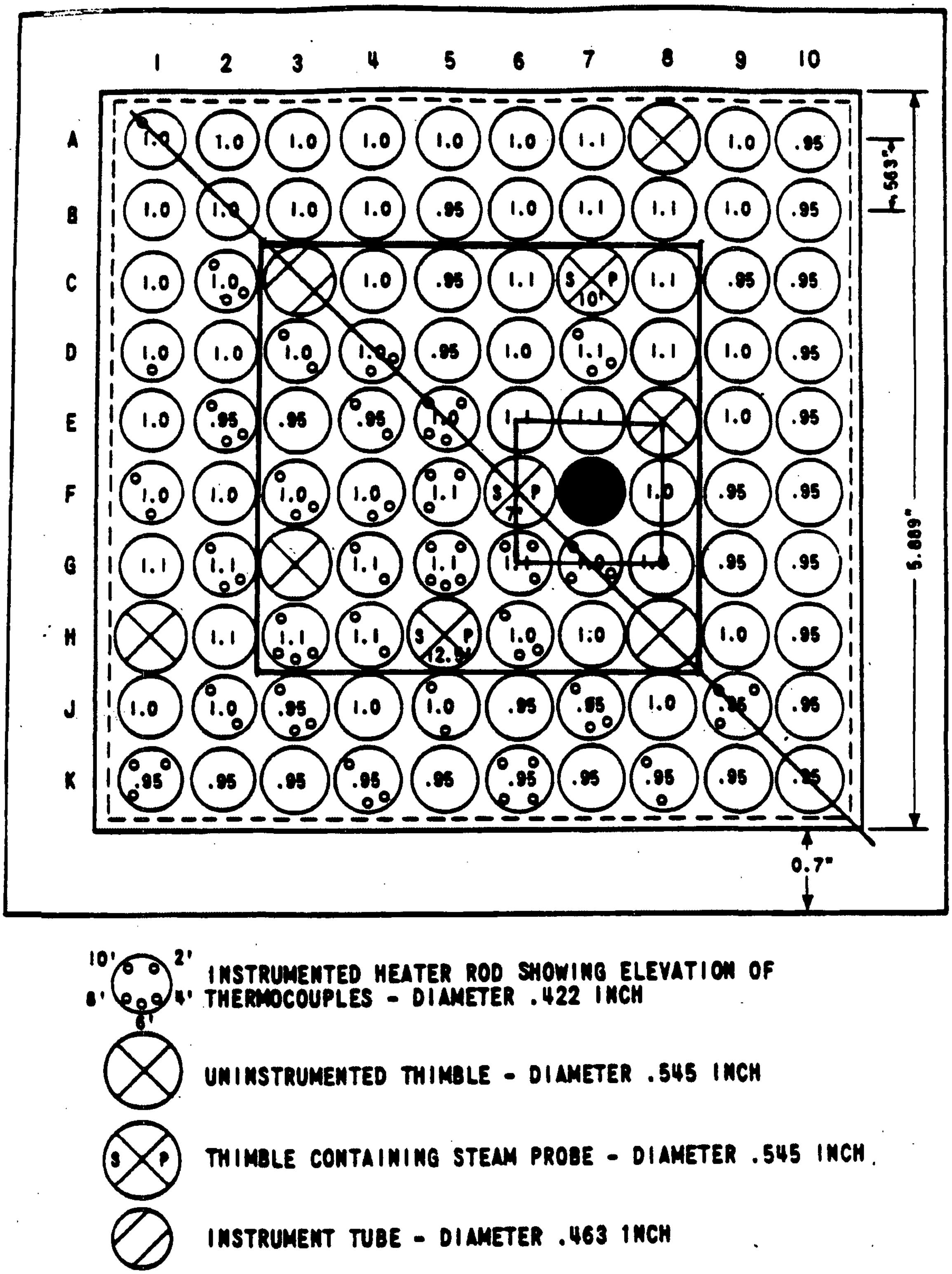

Figure 14.2.3.2-1 FLECHT Rod Bundle Cross Section (from Rosal, et al., 1975)

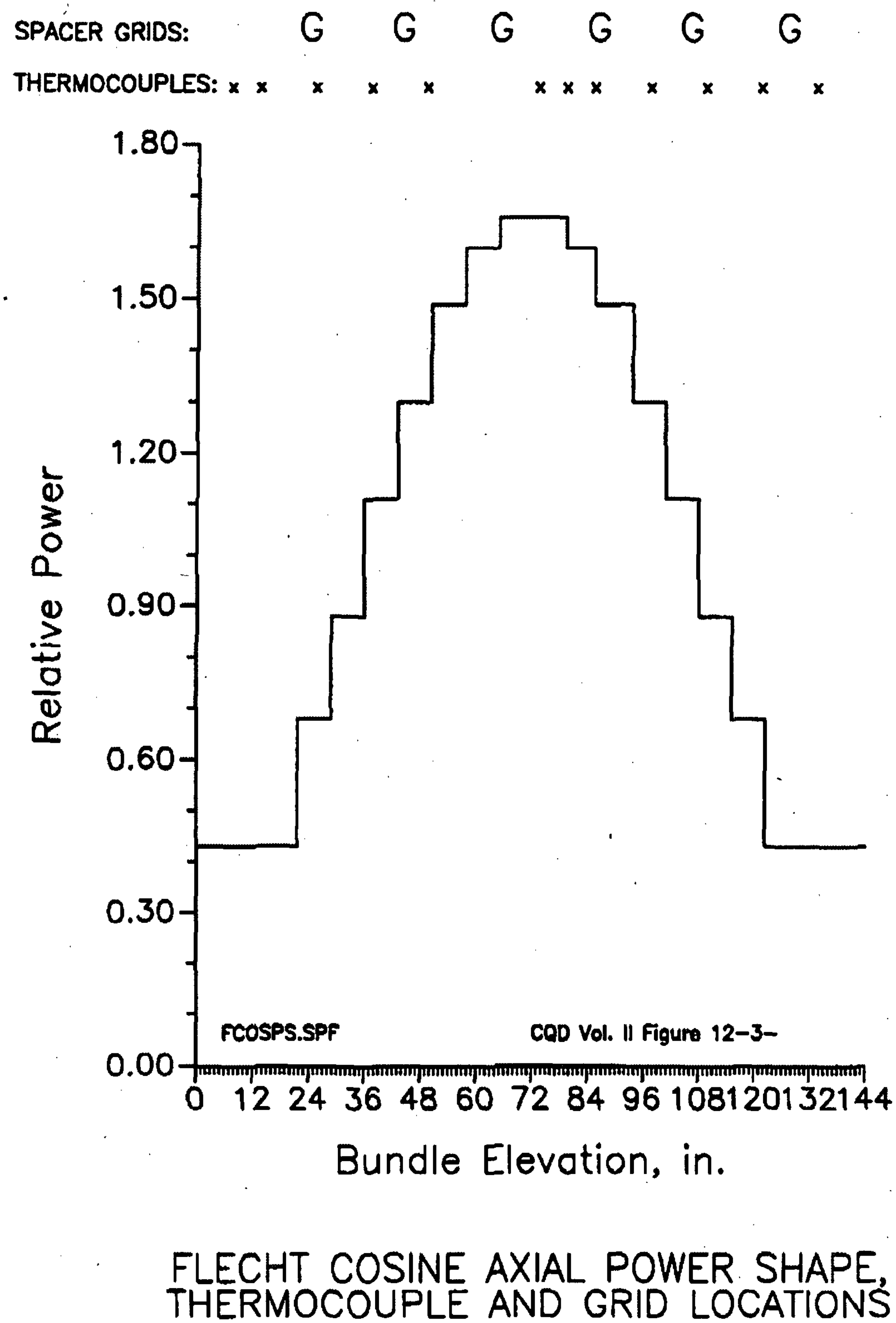

Figure 14.2.3.2-2 FLECHT Cosine Axial Power Shape Profile and Grid Locations

14.2.3.3 FLECHT Top-Skewed Power Tests

The FLECHT skewed power tests were run to provide experimental data at low flooding rates for simulated Westinghouse 15x15 fuel with a top-skewed axial power shape. These tests are described by Rosal et al. (1977). Tests 15305, 13812, 15713, 13914, and 13609 were simulated to demonstrate the ability of WCOBRA/TRAC-TF2 to predict the thermal-hydraulic phenomena observed in these experiments. Table 14.2.3.3-1 lists the conditions for each of these tests. These tests were simulated in order to demonstrate the ability of WCOBRA/TRAC-TF2 to predict the correct thermal-hydraulic response during reflood in a rod bundle with a top-skewed power shape.

14.2.3.3.1 Facility Description

A diagram of the FLECHT top-skewed power shape test bundle is shown in Figure 14.2.3.3-1. The test section consisted of 105 electrical heater rods arranged to simulate a quarter section of a 15x15 PWR fuel assembly. The rod diameter was 0.422 inches and the rod pitch was 0.563 inches. The test bundle also contained 7 simulated control rod thimble tubes and 12 solid filler rods. The triangular filler rods reduced the excess flow area to within 5 percent of the power/flow area ratio of a PWR fuel assembly. The test section was enclosed by a 0.188-inch thick cylindrical stainless steel housing that was connected to the upper and lower plenums. The housing, with an inside diameter of 7.0 inches, was insulated on the exterior to reduce heat loss to the environment. Horizontal movement and/or bowing of the heater rods was restricted by eight grid spacers located at 20.5-inch intervals starting at the beginning of the heated length.

The electrical heater rods were constructed of a spiral-wound heating element embedded in a boron-nitride insulator. The top-skewed power shape was peaked at 9.75 feet and had a maximum peak-to-average power ratio of 1.35. The power shape profile is shown in Figure 14.2.3.3-2.

Heater rod thermocouples were located at 14 elevations in the bundle including 4 thermocouple elevations downstream at the peak power location. Differential pressure transducers were spaced 12 inches apart along the test section. Steam probes were located in thimble tubes in the bundle and also in the test section outlet.

14.2.3.3.2 Test Procedure

The tests were conducted by first pressurizing the test section to the desired system pressure by valving steam from a boiler into the system and the exhaust line control valve. Water was then injected into the test section lower plenum until it reached the beginning of the heated length of the bundle heater rods. Power was next applied to the bundle and the rods were allowed to heatup. When the temperature of any two bundle thermocouples exceeded the pre-selected value of 1600°F, the bundle was reflooded at a specified rate and power was decreased to match the ANS 1971 + 20 percent decay heat rate.

Table 14.2.3.3-1 Test Conditions for FLECHT Top-Skewed Power Tests				
Test No.	**Forced Injection Rate in/s**	**Upper Plenum Pressure psia**	**Injection Water Temperature °F**	**Peak Rod Power kW/ft**
15305	0.8	40	127	0.7
13812	1.0	41	184	0.7
15713	1.0	40	265	0.7
13914	1.0	21	223	0.7
13609	1.0	21	87	0.7

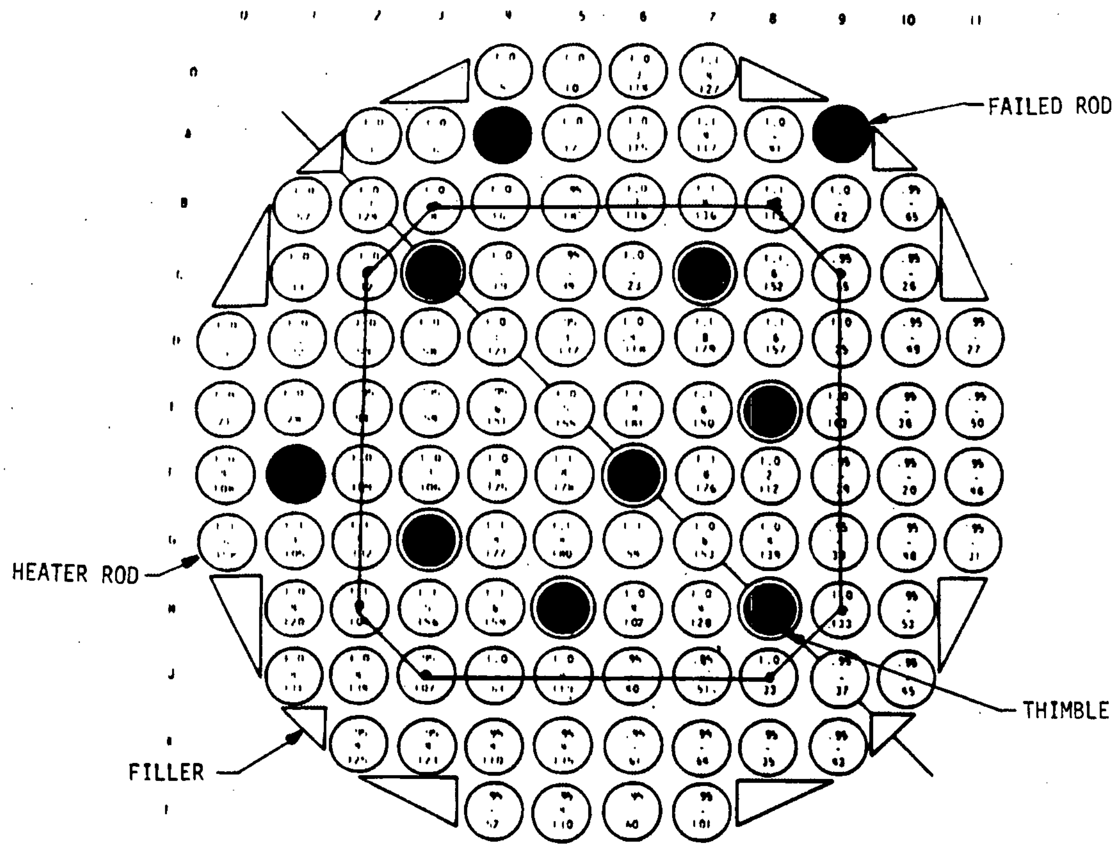

Figure 14.2.3.3-1 FLECHT Top-Skewed Power Shape Test Bundle (from Rosal, et al., 1977)

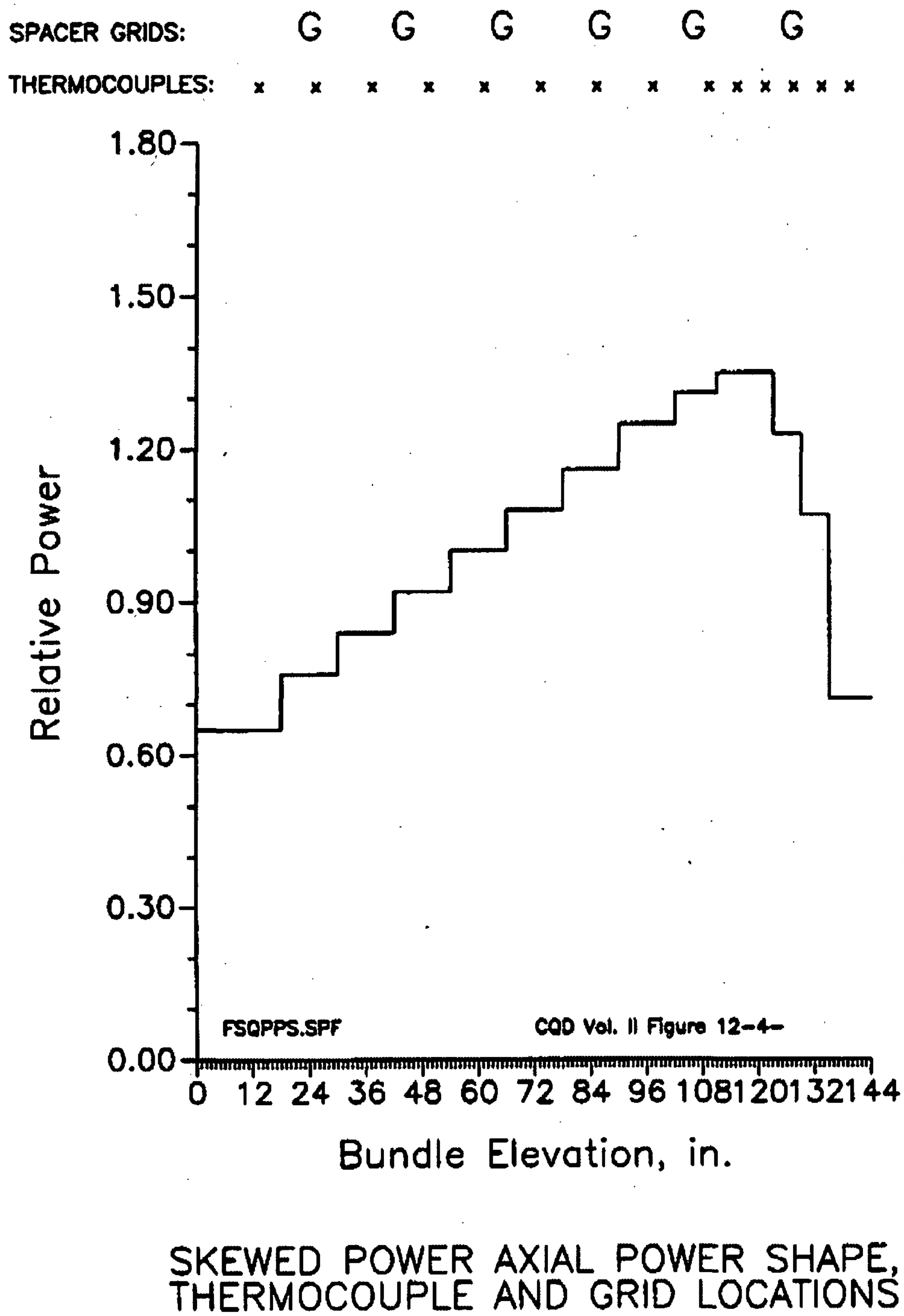

Figure 14.2.3.3-2 FLECHT Top-Skewed Axial Power Shape

14.2.3.4 FLECHT Supplemental Tests

The FLECHT Supplemental Test series was conducted to provide experimental data for Westinghouse 15x15 fuel. The tests and the experimental facility are described by (Cadek et al., 1972). Test 0791 was simulated to demonstrate the ability of WCOBRA/TRAC-TF2 to predict the thermal-hydraulic phenomena observed in this reflood experiment with a very low flooding rate. The test conditions for this test are shown in Table 14.2.3.4-1.

14.2.3.4.1 Facility Description

[

]b

14.2.3.4.2 Test Procedure

[

]b

Table 14.2.3.4-1 Test Conditions for FLECHT Supplemental Test

b

b

Figure 14.2.3.4-1 FLECHT Rod Bundle Cross Section (from Cadek et al., 1972)

b

Figure 14.2.3.4-2 FLECHT Heater Rod Schematic Diagram

b

Figure 14.2.3.4-3 FLECHT Axial Power Shape Profile and Grid Locations

14.2.3.5 G-2 Reflood Experiments

The low pressure, forced reflood tests performed at the Westinghouse G-2 test facility were simulated using the WCOBRA/TRAC-TF2 computer code. Comparisons of the WCOBRA/TRAC-TF2 results to the reflood test data can be used to help assess the capability of WCOBRA/TRAC-TF2 to accurately predict rod bundle reflood heat transfer behavior including spacer grid effects on dispersed flow film boiling heat transfer. [

]b

14.2.3.5.1 Facility Description

The facility is the same as that described in Section 14.2.2.3.

14.2.3.5.2 Test Procedure

[

]b

Table 14.2.3.5-1 G-2 Reflood Tests and Conditions

b

14.2.3.6 FEBA

The FEBA (Flooding Experiments with Blocked Arrays) tests were a series of forced reflood tests conducted by the Karlsruhe Nuclear Research Center in West Germany and reported by Ihle and Rust (1984). The main purpose of these experiments was to investigate the effects of grid spacers and flow blockages on reflood heat transfer. However, FEBA tests also provided many typical results of a reflood transient.

In order to further verify WCOBRA/TRAC-TF2, four FEBA tests were simulated. [

]^{a,b,c} Table 14.2.3.6-1 summarizes the conditions for each test.

14.2.3.6.1 Facility Description

The FEBA test facility was originally designed to simulate typical forced reflood conditions in a KWU PWR core. [

]^{b}

14.2.3.6.2 Test Procedure

[

]^{b}

Table 14.2.3.6-1 Conditions for FEBA Tests

b

b

Figure 14.2.3.6-1 FEBA Test Bundle Cross Section (from Ihle and Rust, 1984)

b

Figure 14.2.3.6-2 FEBA Power Shape and Grid Elevation (from Ihle and Rust, 1984)

14.3 REFERENCES

1. Anklam, T. M., et al., 1982, "Experimental Investigations of Uncovered Bundle Heat Transfer and Two-Phase Mixture Level Swell Under High Pressure Low Heat Flux Conditions," NUREG/CR-2456.

2. Cadek, F. F., et al., October 1972, "PWR FLECHT Final Report Supplement," WCAP-7931.

3. Conway, C. E. et al., 1977, "PWR FLECHT Separate Effects and System Effects Test (SEASET) Program Plan," NRC/EPRI/Westinghouse-1.

4. Cunningham, J. P., et al., 1974, "ECCS Heat Transfer Experiments with Upper Head Injection, Volume 1: Test Facility, Procedures and Data," WCAP-8400.

5. Cunningham, J. P., Gray, A. D., Mendler, O. J., and Steer, R. W., 1975, "G-2 Facility Forced Flooding Tests with a 17x17 Rod Array – Volume 1: Test Facility, Procedures, and Data," WCAP-8551.

6. Hochreiter, L. E., et al., 1976, "G-2, 17x17 Refill Heat Transfer Test and Analysis," WCAP-8793.

7. Ihle, P., and Rust, K., 1984, "FEBA – Flooding Experiments with Blocked Arrays, Data Report 1, Test Series I through IV," Kernforschungszentrum Karlsruhe.

8. Lee, N., Wong, S., Yeh, H. C., and Hochreiter, L. E., 1982, "PWR FLECHT SEASET Unblocked Bundle, Forced and Gravity Reflood Task Data Evaluation and Analysis Report," NUREG/CR-2256, WCAP-9891.

9. Loftus, M. J. et al., 1981, "PWR FLECHT-SEASET Unblocked Bundle, Forced and Gravity Reflood Task Data Report," Volumes 1 and 2, NUREG/CR-1532, (WCAP-9699).

10. Morris D. G., et al., 1982, "An Analysis of Transient Film Boiling of High-Pressure Water in a Rod Bundle," NUREG/CR-2469.

11. Mullins, C. B., et al., 1982, "Thermal-Hydraulic Test Facility Experimental Data Report for Test 3.03.6AR and Test 308.6C – Transient Film Boiling in Upflow," NUREG/CR-2525, Volumes 2 and 5.

12. Rosal, E. R., Hochreiter, L. E., McGuire, M. F., and Krepinevich, M. C., 1975, "FLECHT Low Flooding Rate Cosine Test Series Data Report," WCAP-8651.

13. Rosal, E. R., Conway, C. E., and Krepinevich, M. C., 1977, "FLECHT Low Flooding Rate Skewed Test Series Data Report," WCAP-9108.

14. Yoder, et al., 1982, "Dispersed Flow Film Boiling in Rod Bundle Geometry-Steady State Heat Transfer Data and Correlation Comparisons," NUREG/CR-2435, ORNL-5822.